Glacier Inventory Compilation and Glacier Change Assessment in the Kullu District, Northern India

Geo 511 Master Thesis

September 2014

Department of Geography

University of Zurich

Ursina Stoll

09-719-113

Supervisors:

Dr. Holger Frey

PD Dr. Christian Huggel

Faculty Member:

Prof. Dr. Andreas Vieli

Ursina Stoll

Dorfstrasse 29

8218 Osterfingen

ustoll@outlook.com

Summary

Glacier variations are a worldwide phenomena related to the ongoing Climate Change. Although the Himalayas are the most glaciated regions after poles, their conditions are only sparsely documented. This study is embedded in the Indian Himalayas Climate Adaption Program (IHCAP), which is funded by the Swiss Agency for Development and Cooperation (SDC), and investigates in detail the glaciers of the Kullu District in the Western Himalayas. A mapping of all glaciers in the Kullu District based on multispectral remote sensing data was conducted for 2002 and 2013. The inventory of 2002 was compiled from a scene of Landsat 7 ETM+, for 2013 from a scene of Landsat 8 OLI.

Frey et al. (2012) performed a glacier inventory of the western Himalayas. Parts of their inventory were used as basis and reference for the inventory of 2002.

Seven topographic parameters of the two inventories were generated using a void-filled version of the Shuttle Radar Topography Mission (SRTM) digital elevation model (DEM) that was specially generated for this study (named SRTM DEM US). This was done in order to minimize the influence of the unsatisfactorily interpolated voids, which showed up in the publicly available versions. In addition to the topographic parameters, the clean ice portion and the resulting relative percentage of debris-cover was determined. The inventory for the year 2002 contains 697 glaciers larger than 0.02 km^2 which cover an area of 590.04 km^2 and thereof 12.43% are covered with debris. For 2013, 627 glaciers with a total area of 581.78 km^2 and a debris-cover of only 2.3% are recorded.

Beside the topographic parameters, the ice thickness distribution of the year 2002 was determined with a model from Linsbauer et al. (2012) and a volume of 27.82 km^3 was examined.

The approximated volume change between the two points in time was generated by the elevation difference between the SRTM DEM US (2000) and a co-registered version of

ASTER Global DEM 2 (GDEM2) ($\approx$2009) on the one the hand; this resulted in a decrease of –3.73 km³. One the other hand, a GlabTop model output generated with the co-registered ASTER GDEM2 was used and delivered a decrease of –2.62 km³.

Based on the two compiled inventories for 2002 and 2013 a change assessment had been done, that considered the area and the debris-cover change of the glaciers in the Kullu District. The points that are essential to consider in order to compile glacier inventories for change assessments were summarized as recommendation for further investigations.

Zusammenfassung

Gletscherveränderungen sind ein weltweites Phänomen und stehen im direkten Zusammenhang mit dem Klimawandel. Obwohl der Himalaya nach den Polen die meist vergletscherte Region der Welt ist, sind die Gletscher dort nur sehr lückenhaft erforscht und dokumentiert. Diese Masterarbeit ist in ein grösseres Projekt eingebettet, welches sich mit der Anpassung des indischen Himalayas an die neuen Klimabedingungen auseinandersetzt (Indian Himalayas Climate Adaption Program) und durch die Eidgenössische Direktion für Entwicklung und Zusammenarbeit finanziert wird. Das Projekt untersucht die Gletscher im Kullu District und im westlichen Himalaya genauer.

Die Kartierung aller Gletscher im Kullu District wurde ausgearbeitet für die Jahre 2002 und 2013 und basiert auf multispektralen Fernerkundungsdaten. Die Daten für das Inventar von 2002 stammen von einer Landsat 7 ETM+ Szene, jene für das Inventar 2013 von einer Landsat 8 OLI Szene.

Frey et al. (2012) haben für den westlichen Himalaya bereits ein Inventar erstellt und Teile davon wurden als Basis für das Inventar von 2002 dieser Studie verwendet.

Für die zwei Inventare wurden sieben topographische Parameter generiert. Dazu wurde speziell für diese Studie eine Version des digitalen Höhenmodells der Shuttle Radar Topography Mission generiert, bei der alle Partien ohne Datenwerte („Löcher") mit Höheninformationen versehen worden sind und die als Grundlage für die weiteren Berechnungen diente (SRTM DEM US genannt).

Zusätzlich zu den topographischen Parametern wurde die prozentuale Schuttbedeckung, respektive die Fläche des sauberen Eises bestimmt.

Das Inventar für das Jahr 2002 beinhaltet 697 Gletscher, die grösser als 0.02 km^2 sind und diese bedecken eine Fläche von 590.04 km^2. Davon sind 12.43% schuttbedeckt. Für das Jahr 2013 sind es 627 Gletscher grösser als 0.02 km^2 mit einer Fläche von 581.78 km^2, wovon nur noch 2.3% schuttbedeckt sind.

Weiter wurde die Eisdickenverteilung für das Jahr 2002 mit einem Modell von Linsbauer et al. (2012) bestimmt. Das Volumen betrug 27.82 km³. Die geschätzte Volumenabnahme zwischen den zwei Zeitpunkten wurde zum einen angenähert durch die Differenz zwischen den zwei digitalen Höhenmodellen SRTM DEM US und einer ko-registrierten Version vom Advanced Spaceborne Thermal Emission and Reflection Radiometer (ASTER); dadurch wurde eine Abnahme von –3.73 km³ verzeichnet. Zum anderen wurde die Volumenabnahme geschätzt durch ein Modellergebnis von GlabTop, das mit demselben ko-registrierten digitalen Höhenmodell wie die Subtraktion durchgeführt wurde. Dieser Ansatz führte zu einer Volumenabnahme von –2.62 km³.

Basierend auf den zwei Inventaren für 2002 und 2013 wurden die Veränderungen genauer untersucht, vor allem auch in Bezug auf die Fläche und den Schuttbedeckungsanteil der Gletscher im Kullu District.

Die wichtigen Punkte, die zu berücksichtigen sind bei der Ausarbeitung von Gletscherinventaren, welche für solche Veränderungsanalysen gedacht sind, wurden zum Schluss zusammengefasst als Empfehlung für weitere Untersuchungen.

Acknowledgements

First I would like to thank Holger Frey for his kind support, the various inputs and problem solving ideas during my master thesis. Christian Huggel I would like to thank for all his exciting lectures during my academic studies and for giving me the opportunity to write this thesis within the framework of the ongoing research in the Kullu District.

Next to my supervisors, Andreas Linsbauer was an essential help in understanding and succeeding to run GlabTop. Additional to Holger and Andreas I would like to thank also Nadine Salzmann and Simon Allan for their information at first hand from India.

A special thank goes to my fellow students in the g10 room for all the countless coffee breaks, the mental support, the motivating words and their support in the time of my health complaints. And I am very grateful to Christoph Rohner for his technical inputs and advices.

To my family I am especially grateful for their everlasting support during my studies and in general. Marius Reist I would like to thank as well for his successful diversions in the year I was occupied with my master thesis.

Finally, many thanks to everyone who reviewed a part of this thesis: Pascale Polich, Simon Etter, Dimitri Kink, Carmen Benko, Gabriela Gschwend, Marianne, Nicolas and Neil Rafferty and my mother Brigitte Stoll-Stamm.

Contents

Abbreviations

ASTER	Advanced Spaceborne Thermal Emission and Reflection Radiometer
CGIAR	Consultative Group on International Agricultural Research
DDF	Degree Day Factor
DEM	Digital Elevation Model
DEZA	Direktion für Entwicklung und Zusammenarbeit
ELA	Equilibrium Line Altitude
ENVI	Exelis Visual Information Solutions
ETM	Enhanced Thematic Mapper
ETM+	Enhanced Thematic Mapper Plus
GDEM	Global Digital Elevation Model
GHNP	Great Himalaxan National Park
GIS	Geographic Informationsystem
GlabTop	Glacierbed Topography
GLIMS	Global Land Ice Measurements from Space
GLOF	Glacier Lake Outburst Flood
GPCC	Global Program Climate Change
GPR	Ground Penetrating Radar
HK	Himalayan Karakoram
ICESat	Ice, Cloud and land Elevation Satellite
IDW	Inverse Distance Weighting

IHCAP	Indian Himalayas Climate Adaption Program
IHR	Indian Himalayan Region
IID	Individual Identification
InSAR	Interferometric Synthetic Aperture Radar
LP DAAC	Land Processes Distributed Active Archive Center
MSS	Multispectral Scanner
OLI	Operational Land Imager
RBV	Return Beam Vidicon
RGB	Red-Green-Blue
RQ	Research Question
SDC	Swiss Agency for Development and Cooperation
SLC-off	Scan Line Corrector Failure
SRTM	Shuttle Radar Topography Mission
TM	Thematic Mapper
USGS	Geological Survey of the United States
UTM	Universal Transverse Mercator

1. Introduction

1.1 Motivation

Glacier changes due to the changes in climate are a current topic in natural sciences. Efforts are being expanded to investigate the responsible parameters and the consequences of such glacier changes (Marzeion et al., 2014). The Himalayas with its highly glaciated mountains are an interesting area related to investigate climate change. The knowledge and the data coverage of the glaciers in the Himalayas, however, is relatively sparse, due to the remote areas, the complex and steep topography, the complex political situation and the therefore difficult physical access (Bolch et al., 2012). The Himalayas are a densely populated region and exhibit a high vulnerability to transformations due to glacier changes. The glaciers can act as natural buffers to hydrological seasonality. They can store precipitation temporarily in snow and ice and release it as meltwater during summer and early autumn (Bolch et al., 2012). Therefore, the meltwater of snow and ice is important in sustaining the seasonal water availability (Immerzeel et al., 2010; Moors et al., 2011). It provides a water resource for the population in the valleys but also plays an important role for the runoff of lowland rivers (Bolch et al., 2012). The influence of the monsoon on the regional precipitation and climate regime results in a even more heterogeneous and complex but nevertheless interesting situation in the Himalayas.

1.2 Context of project

The current Master thesis is carried out within the framework of the Indian Himalayas Climate Adaption Program (IHCAP) which is a project under the Global Program Climate Change (GPCC) of the Swiss Agency for Development and Cooperation (SDC). University of Zurich, University of Berne, University of Fribourg and Meteodat GmbH are involved in the

Introduction

IHCAP as the Swiss consortium and work together with the Indian communities and research institutions. The program builds on capacity and knowledge enhancement related to the following three pillars (IHCAP, 2013).

→   scientific and technical knowledge cooperation between Indian and Swiss scientific institutions

→   strengthening institutions for adaptation measures among vulnerable communities

→   mainstreaming adaptation policies for improved action in the Indian Himalayan Region (IHR)

The IHR has to meet the challenges of climate change, due to its dependency on climate sensitive areas and natural resources for sustaining livelihoods. The climate change is a threat to social and economic development. Therefore, the program assists people of the mountain regions, who are vulnerable to changes in the climate. Furthermore, it responds to the increasing stress on natural resources and supports the actions on climate change of the federal and state government (IHCAP, 2013). In addition to the support and teaching of scientific and technical knowledge, a case study of the Kullu District is performed in the context of the IHCAP. The overall objectives of the Kullu hazard and risk study is the improvement of the understanding of the hydrogeomorphic processes, their triggers and evolution. This knowledge is essential to define the hazard and potential risks the Kullu District and its villages are facing.

1.3   Goals

The following research questions (RQ) are tried to be answered in this thesis:

RQ 1: Is it possible to compile an improved void-filled SRTM DEM version for the region of the Kullu District?

RQ 2: Compilation of glacier inventories for 2002 and 2013: What must be considered compiling glacier inventories of two different years for a change assessment?

RQ 3: How did the glaciers in the Kullu District change in the examined time span (2002-2013) concerning their area and also their debris-cover extent?

RQ 4: What were the volume and the ice thickness distribution changes of the glaciers in the Kullu District between the years 2002 and 2013?

1.4   Structure of the thesis

The presented study can roughly be divided into seven sections. After a short description of the background of the thesis, the project in which it is embedded, as well as the resulting research questions are outlined. The following chapter 2 introduces the study site. Chapter 3 introduces the different data and its sources as well as the properties, used in the studies. The semi-automatic methods to develop a glacier inventory and the model GlabTop, which estimates the volume and the thickness distribution of the glacial ice, are presented in chapter 4. The results of the compilation of the inventories, the void-filled SRTM DEM, the volume and ice thickness distribution and the change assessment between the investigated years are portrayed in chapter 5. The critical discussion of all the results takes place in the chapter 6, where the findings of the study are interpreted in a broader context. There, the difficulties and problems which appeared during the study are mentioned as well. In the chapter 7 the research questions are answered and an outlook for potential further improvements is given.

2. Study Region

2.1 The Himalayan-Karakoram region

The glacier coverage of the Himalayan Karakoram region (HK) is the largest one after the polar regions (Bolch et al., 2012) but little is known of his present state (Cogley, 2011). This is because of the remoteness, the rough topography and the complex political situation in the HK region which all do not simplify the physical access to the study sites (Bolch et al., 2012). The location of the HK region is shown in Figure 2.1.

The climatic situation of the HK region is influenced by the monsoon and the westerlies; in Figure 2.1a the influencing wind systems are shown. In Figure 2.1b the mean precipitation is shown, but due to the heterogeneous topography of the HK region the local climate is highly variable.
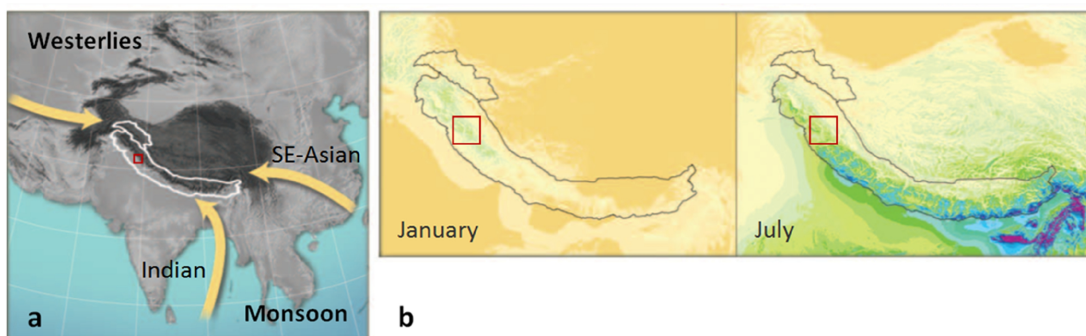
Figure 2.1: Overview of the study region (HK), the red square locates the region of the Kullu District, in (a) the main wind systems are shown and (b) depict the mean precipitation in January and July. After Bolch et al. (2012).

Furthermore the stream flows of the large river systems in the HK region are as well influenced by the climatic situation due to the meltwater from the glaciers and as the seasonal snow. A large number of people depend on this water sources, especially in the dry season and in the mountain valleys (Bolch et al., 2012; Immerzeel et al., 2010).

The estimated glacier changes in the HK region are relatively heterogeneous and show large regional differences (Bolch et al., 2012; Molden, 2012). These differences depict on the one hand the large range of affecting factors of the response of glaciers to the climate change; and on the other hand, the influence of the used methods of change detection (Molden, 2012). Different studies investigate the glacier mass changes of the Himalayan glaciers, the contribution to sea level rise and are discussed in section 6.5 and compared to the results of this study.

2.2   The Kullu District

The Kullu District is part of the state Himachal Pradesh in northern India and situated in the HK region. The district is divided into four tehsils (Kullu, Manali, Banjar and Nirmand), this are governmental units, also known as counties. About 300'000 people live in total 172 villages (census 2011) (Soot, 2013). Thereby, Kullu and Manali are towns of touristic attraction (IHCAP, 2013).

The Kullu District is situated south of the main Himalayan divide and is located within the monsoonal rain- and snowshed (Figure 2.1a). Rainfall during the monsoon period constitutes 39% of the annual rainfall and the precipitation intensifies from south west to north east. The amount of annual precipitation varies from 934.9 mm (Bhuntar, 1089 m a.s.l.) to 1431.0 mm (Manali, 1950 m a.s.l.) (Soot, 2013). Kullu District serves as the principal catchment area of the Beas River, due to its high summer and winter precipitation. The Beas itself is an important feeder of the Indus rivers system (Dutta et al., 2012). The glaciers of the Kullu District are not only a tourist attraction, but also an important water reservoir as well as the origin of the Himalayan Rivers. Because of these various aspects the consequences of the climate change have the potential of harming the region and their population

Elevations in the Kullu District range from about 1'000 m a.s.l. to over 6'000 m a.s.l.. The Kullu District has a broad main valley with gentle landscape features (Kuniyal et al., 2004).

But it is also characterized by deeply incised river valleys and high mountain ridges as well as massifs of very high, glaciated mountain peaks (Gardner, 2002).

The average temperature in Kullu town ranges from 22.4°C in January to 40.1°C in June. The rainy season is from July to August. During this period, the average temperature is 36.1°C (Kuniyal et al., 2004).
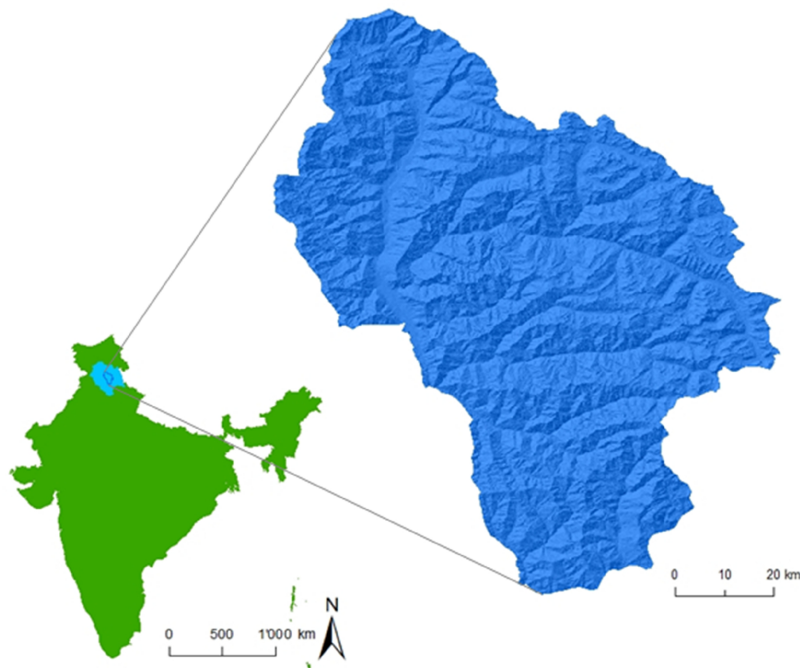
Figure 2.2: The map of India (green) and Himachal Pradesh (light blue) is shown. The outlines of the Kullu District (dark blue) located in Himachal Pradesh are also shown at larger scale and with the ASTER GDEM2 hillshade in the background. ("Global Administrative Areas. Boundaries without limits," 2012).

For the Kullu Case Study, four hotspots have been selected for further investigations. For the development of the glacier inventories and the glacier change assessment performed in this study, three hotspots are of interest. The focus of the investigations lied on the first three hotspots,. The fourth hotspot lies in the Seraj area in the south of the district, and was of no further interest for this study, due to the lack of glaciers. The hotspots are shortly described in the following sections.
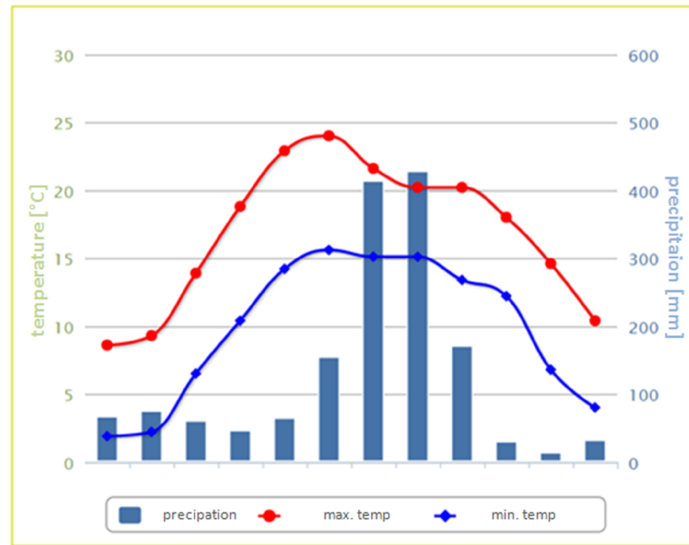
Figure 2.3: Climate diagram Shimla, Himachal Pradesh ("Klimadaten Simla / Himachal Pradesh," n.d.).
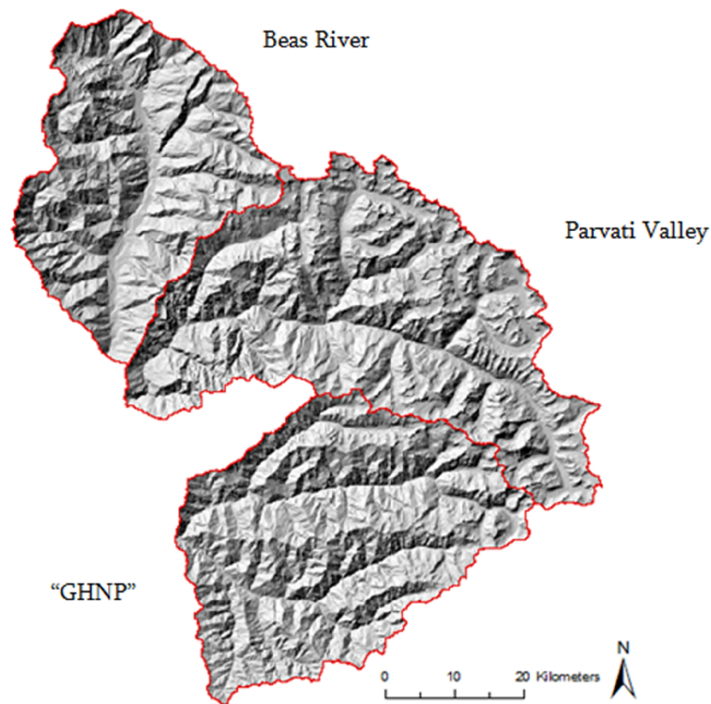
Figure 2.4: Hotspots of the Kullu Case Study, with hillshade of the SRTM DEM US. The outlines of the Hotspot called "GHNP" do not correspond to the outlines of the Great Himalayan National Park (GHNP), they are shown in Figure 2.5.

Study Region

Catchment of the Beas River

The Beas River flows through the towns Manali and Kullu (Kuniyal et al., 2004). Until March the upper part of the Beas valley receives its precipitation from western disturbances. Half of the Beas valley (to the south of Katrain) lies in the rain shadow and receives much fewer precipitation than the northern part (Kuniyal et al., 2004).

The Beas is the major river of the Kullu District and has many main tributaries; such as the Manalsu, Chhakinal, Phojal, Sarwari, Parbati and Sainj. The Beas originates from the Rothang crest in the Pir Panjal range (Kuniyal et al., 2004).

Parbati Valley

The narrow Parbati valley with its steep rocky hills reaching up to 6260 m a.s.l. beyond the Pin Parbati pass (Kuniyal et al., 2004). The northwest highest point in the Parbati valley is Deo Tiba at 6001 m a.s.l. which acts as water divide between the Parbati and the Beas valley. The Parbati River flows through the town Manikaran and feeds the Beas river at Bhuntar (Kuniyal et al., 2004).

Great Himalayan National Park

The Great Himalayan National Park (GHNP) was initially constituted in 1984 and formally declared as National Park in 1999. It extends over an area of 754.4 km². In 1992, a buffer zone of 5km around the park was established and the creation of the Sainj Wildlife Sanctuary as well as the Tirthan Wildlife Sanctuary was initiated. Both sanctuaries were added to the GHNP in 2010. Containing these additional areas the park covers an area of 1171 km² (GHNP, 2014). The GHNP is dominated by high mountain ridges which reach up to 5800 m a.s.l and is divided by three streams, the Tirthan, Sainj and Jiwa Nala (Baviskar, 2003).

The temperate and alpine climate lead to four seasons: spring (April-June), rainy summer (July-September), autumn (October-November) and winter (December-March). The precipitation during the monsoon season is abundant, during the rest of the year it is

relatively moderate. The temperature varies between -10°C and 40°C, whereby in January the temperature reaches its minimum, in June its maximum (GHNP, 2014).
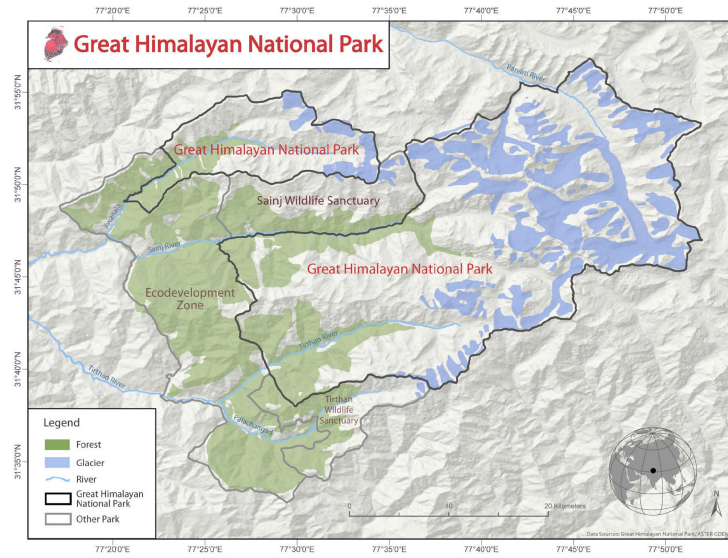
Figure 2.5: Map of the Great Himalayan National Park and the adjacent sanctuaries *(GHNP, 2014).*

3. Data

3.1 Satellite imagery

Remote sensing uses instruments and methods to measure the properties of an object without direct physical contact to it. It measures the emanating energy from earth surface using sensors fixed on aircrafts or satellite platforms (Richards, 2013). Thereby, it is possible to get information of remote regions, which are difficult to access physically. A multi-temporal collection of satellite images allows the detection of changes on the earth surface. Remote sensing is useful to make statements concerning the temporal and spatial distribution as well as the characteristics of objects or landscape elements, such as glaciers (Frey, 2011).

Despite the numerous remote sensing satellites, only Landsat was used in the current study, due to the free availability of an already orthorectified dataset of the study area. The data was downloaded from the USGS Global Visualization Viewer archive (http://glovis.usgs.org). The Landsat mission started in 1972 with Landsat 1. In February 2013 the newest Landsat 8 was launched. The following sensors were on board of the different Landsat satellites: the Return Beam Vidicon (RBV), the Multispectral Scanner (MSS), the Thematic Mapper (TM), the Enhanced Thematic Mapper (ETM), the Enhanced Thematic Mapper Plus (ETM+) (Lillesand et al., 2008), the Operational Land Imager (OLI) and the Thermal Infrared Sensor (TIRS) (USGS, 2014a). Landsat is especially useful to detect ground features by combining multiple spectral bands (Rosenfeld, 1984) – the topic of band ratios is treated in detail later on (section 4.2.1). For the inventory of 2002, scenes from the Landsat Mission 7 were used, collected with the ETM+ sensor, with a resolution of 30 m (Lillesand et al., 2008). The second inventory was based on the newest Landsat data from Mission 8 collected with the OLI sensor with 30m resolution.

It is important to take the differences between the Landsat 7 and 8 into account. The resolution and the wavelength of the several bands of the sensors are different. Table 3.1 and Table 3.2 show the band designation of the two Landsat satellites. It seems obvious that the

band combination for Landsat 8 to create a Red-Green-Blue (RGB) composite differs from Landsat 7, because Landsat 8 has additional bands. For example the Natural Color Composite of bands 3, 2 and 1 (Landsat 7) becomes bands 4, 3 and 2 (Landsat 8) (marked grey in the table) and the false-color composite of bands 4, 3 and 2 (Landsat 7) becomes to bands 5, 4 and 2 (Landsat 8).

Table 3.1: Wavelength and resolution of the several bands of the ETM+ sensor (USGS, 2014a).

Enhanced Thematic Mapper Plus (ETM+) Landsat 7	Wavelength (μm)	Resolution (m)
Band 1	0.45-0.52	30
Band 2	0.52-0.60	30
Band 3	0.63-0.69	30
Band 4	0.77-0.90	30
Band 5	1.55-1.75	30
Band 6	10.40-12.50	60
Band 7	2.09-2.35	30
Band 8	0.52-0.90	15

Table 3.2: Wavelength and resolution of the OLI and TIRS sensor (USGS, 2014a).

Operational Land Imager (OLI), Thermal Infrared Sensor (TIRS) Landsat 8	Wavelength (μm)	Resolution (m)
Band 1 Coastal aerosol	0.43-0.45	30
Band 2 Blue	0.45-51	30
Band 3 Green	0.53-0.59	30
Band 4 Red	064-0.67	30
Band 5 NIR	0.85-0.88	30
Band 6 SWIR 1	1.57-1.65	30
Band 7 SWIR 2	2.11-2.29	30
Band 8 Panchromatic	0.5-0.68	15
Band 9 Cirrus	1.36-1.38	30
Band 10 TIRS 1	10.6-11.19	100
Band 11 TIRS 2	11.5-12.51	100

Landsat has the disadvantage of operating in electromagnetic bandwidths that cannot penetrate clouds; unlike Radar (Radio Detection and Ranging) (Rosenfeld, 1984). Images with heavy cloud coverage are therefore not suitable for glacier mapping. Another limiting factor is snow coverage. Due to the semi-automatic method of glacier mapping presented later on (section 4.2), the imagery has to show as few snow covered areas as possible, because the method cannot distinguish between clean ice and snow. Concerning these limitations the satellite imagery were selected to do the inventories. As the inventory of 2002 was carved out of the inventory done by Frey et al. (2012), the same satellite scenes were used. These were collected on the second of August in 2002. The best suitable scene in 2013 was collected on

27th October 2013. The image from 2013 showed more seasonal snow than the images from 2002, but the selected scene was the best suited for this year. In Table 3.3 the details of the used satellite data are listed. Another spectral challenge was the deep cast shadows due to steep terrain. To deal with this problem it was important to select an appropriate parameter to reduce the time consuming manual correction (Paul and Kääb, 2005).

Table 3.3: List of used satellite data.

Platform and Sensor	ID (P=path, R=row)	Date (dd/mm/yyyy)
Landsat 7 ETM+	P:147 R:037	02/08/2002
Landsat 7 ETM+	P:147 R:038	02/08/2002
Landsat 8 OLI	P:147 R:038	27/10/2013

The scenes of the USGS archive are all in Universal Transverse Mercator (UTM) projection and the Kullu District is covered by the UTM zone 43N (WGS_1984_UTM_zone_43N).

3.2   Digital elevation models (DEMs)

In this thesis digital elevation models (DEMs) are important in three aspects: Firstly, to generate the drainage divides of the glaciers; secondly, to derive the topographic parameters of the individual glaciers (e.g. elevation, slope inclination) and thirdly, GlabTop models the ice thickness distribution based on a DEM (Linsbauer et al., 2012). For the region of the Kullu District, there is no local DEM publicly available, however two DEM's covering almost the entire world in a relatively accurate resolution exist and can be used as a compromise for glacier mapping. To compile a glacier inventory – with reliable glacier parameters – it is essential, that the DEM has been acquired within the same time period, at least the same decade as the satellite scene of the inventory is based on. In addition to that, the spatial resolution of the DEM and the satellite imagery should also be comparable (Paul et al., 2009).

These conditions are met by the following presented DEMs. The second version of the Advanced Spaceborn Thermal Emission and Reflection Radiometer Global Digital Elevation Model (ASTER GDEM2) and the Shuttle Radar Topography Mission Digital Elevation Model (SRTM DEM) are both freely available elevation models which are already orthorectified and georeferenced. In the following sections 3.2.1 and 3.2.2, both DEMs are shortly described, as well as their differences, advantages and disadvantages are mentioned.

3.2.1 ASTER GDEM2

The ASTER is one of five instruments on the platform Terra which was launched in the year 1999 by the United States National Aeronautics and Space Administration (NASA) in collaboration with the Ministry of Economy, Trade and Industry (METI) (Abrams et al., 2010; Toutin, 2008). The objectives for this mission were the generation of high spatially resolved earth imagery in 14 spectral bands on a global, regional and local scale. The ASTER GDEM is compiled of various along-track stereo images with a spatial resolution of one arc second (30 m) and covers the earth from 83° N to 83° S. Unlike the SRTM DEM (see section 3.2.2) the ASTER GDEM covers the arctic regions (Tachikawa et al., 2011). The first version, GDEM1, was published in June 2009, produced out of various images until August 2008, unfortunately some of the elevation data was incorrect. Therefore, a second version was released in the same format but with a better quality two years later in October 2011. The second version is composed of stereo images from 2005 until 2009. The improved quality derives from the additionally used stereo images to reduce the elevation errors and as well from the improved algorithms (Urai et al., 2012). An advantage of a DEM generation out of a high number of scenes is the reduced probability of large errors and artifacts. The disadvantage on the other hand is the lack of an exact recording date (Frey, 2011). Depending on the surface cover and the validation team Tachikawa et al. (2011) found a vertical error of the range from –0.8m to + 8m.

Data

The ASTER GDEM2 (Figure 3.1) can be downloaded free of charge for example from the homepage of the Land Processes Distributed Active Archive Center (LP DAAC) from USGS (LP DAAC, 2014). The ASTER GDEM2 was used to fill the voids of the hereafter mentioned SRTM DEM.
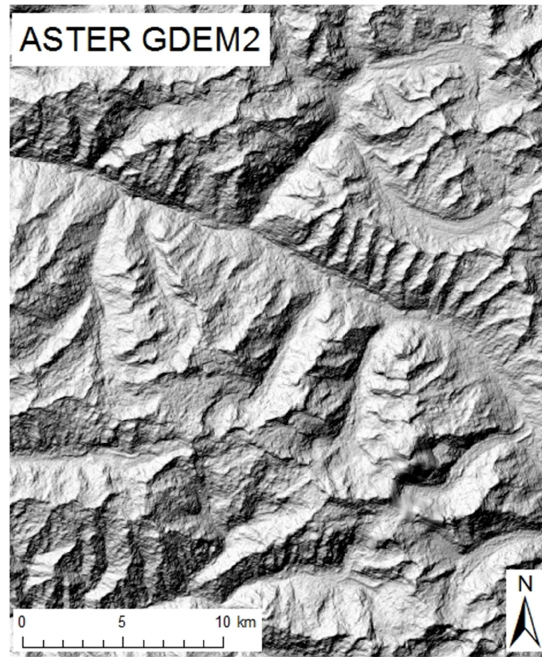
Figure 3.1: ASTER GDEM2 30 m resolution (see Figure 3.3 for location).

3.2.2 SRTM

Another DEM with worldwide coverage and free access is generated based on data collected during the SRTM. This was a joint endeavor of NASA, the National Geospatial-Intelligence Agency and the German and Italian Space Agencies (Farr et al., 2007). The data was acquired by radar interferometry (InSAR) between the 11th and 22th February 2000 and covers the earth surface from 60° N to 56° S with a C-band radar. In contrast to the ASTER GDEMs the polar regions are not covered (Frey and Paul, 2012).

The SRTM DEM is available in a 30m spatial resolution (1 arc second) for the imagery of the United States of America and in a 90m spatial resolution (3 arc seconds) for the other covered

parts of the world's surface (Rabus et al., 2003). Due to effects of the radar systems rugged terrain and the high mountain areas, as well as water bodies are prone to errors. Layover is one of them. This means that the radar signal that is reflected from the top of a vertical feature reaches the antenna before the signal from the base of the feature. This makes vertical features appear to lean toward the nadir. This impact is most extreme at steep incident angles and short ranges (Lillesand et al., 2008) and is seen in Figure 3.2 c) in pyramid 1. Another effect is radar shadow, which is caused by the angle of view and the terrain slope. Slopes facing away from the antenna will return a weak or even no signal at all. In Figure 3.2 d) the slope of pyramid 4 is steeper than the incident angle of the radar pulse and therefore receives no illumination and appears completely black. There is a trade-off between the relief-displacement and shadowing. Radar images acquired at steep incident angles have severe layover and foreshortening, but little shadowing. Vice versa the shadowing effect is greater and the relief displacement becomes weaker at flatter incident angles (Lillesand et al., 2008). Another inaccuracy of the SRTM is produced due to the penetration depth of the radar, which enters a few centimeters in the snow coverage depending on the moisture. The thereby calculated earth surface does not match with the actual surface.

The overall accuracy shows a horizontal error of ± 20m and a vertical error of ± 16 m for 90% of all the data (Frey, 2011; Lillesand et al., 2008; Rabus et al., 2003).

The aforementioned effects can cause voids and errors in the elevation data. The region of the western Himalayas is highly affected by such data voids. 31.7% of the investigated hotspot area in the Kullu District is affected by voids in the original SRTM DEM file (Figure 3.3 andFigure 3.6). Therefore the Consultative Group for International Agriculture Research (CGIAR) compiled a void-free version of the SRTM DEM (SRTM3v4), which is also available online in 5°x5° tiles (CGIAR-CSI, 2008)

Data
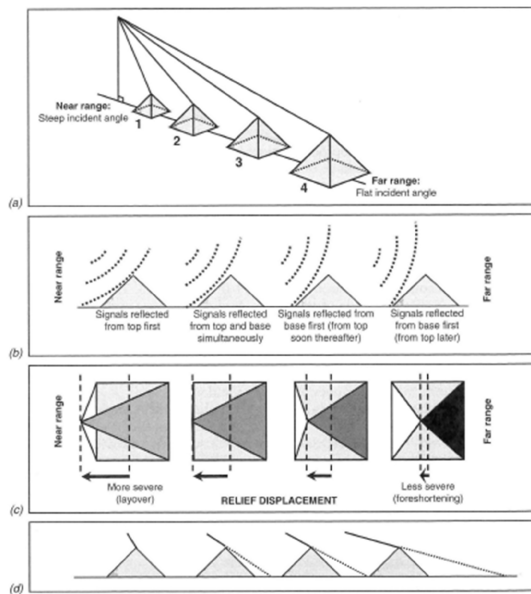
Figure 3.2: Relief displacement and shadowing in radar images. (a) Relationship between range and incident angle. (b) Relationship between terrain slope and wavefront of incident radiation. (c) Appearance of resulting image, showing brightness and geometric characteristics. (d) increased length of shadows at flat incident angles. Note absence of shadows at pyramid 1 , and lengthy shadow at pyramid 4. (Lillesand et al., 2008).
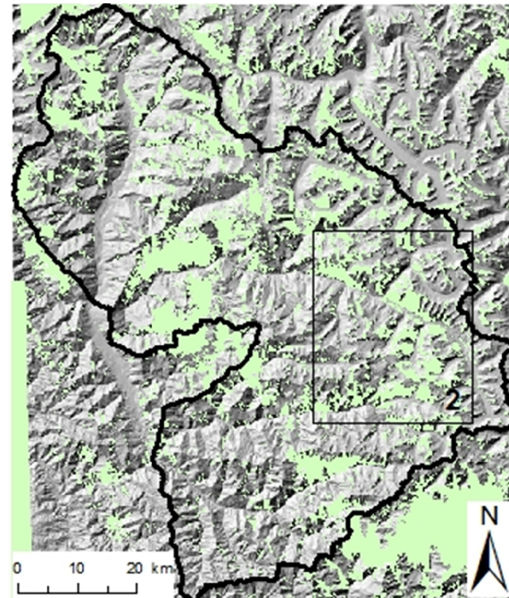
Figure 3.3: SRTM DEM with voids (green). The outlines of the investigated hotspots of the Kullu District as well as the outline of the next figures are shown.

The terrain data was interpolated in the data voids from information of other elevation datasets (Reuter et al., 2007). For further details concerning the interpolating approaches see Reuter et al., (2007) and CGIAR-CSI (2008). However Burns & Nolin (2014) confirm, that the declaration of the alternatively used DEMs to interpolate the voids is not really clear. In the region of the western Himalayas, the void-filled version of CGIAR still shows large artifacts which are mostly congruent with the data voids of the original SRTM version. These artifacts are caused by erroneous interpolation of the data voids (Frey et al., 2012). The interpolated regions appear systematically too low and therefore the hillshade view looks similar to a landscape with crater-like depressions (Figure 3.4).
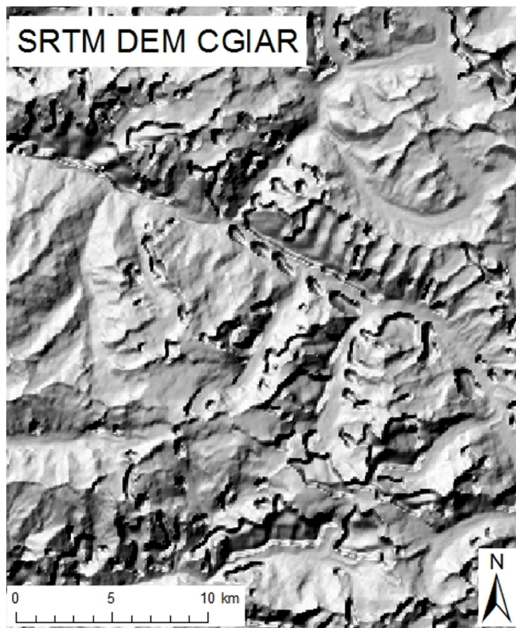
Figure 3.4: SRTM DEM, void-filled version from CGIAR (see Figure 3.3 for location).
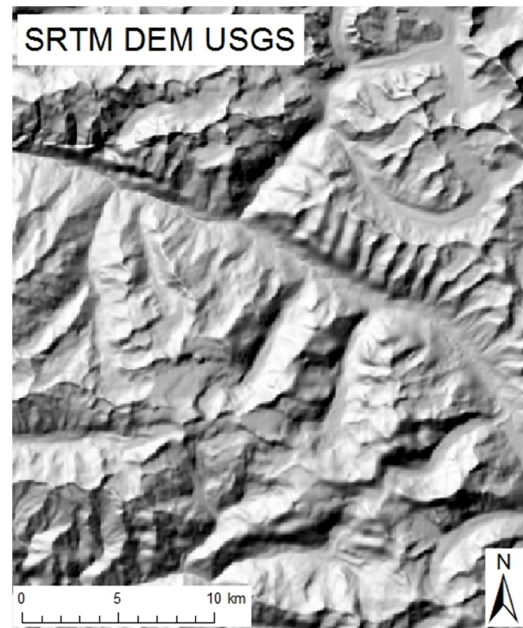
Figure 3.5: SRTM DEM, void-filled version from USGS (see Figure 3.3 for location).
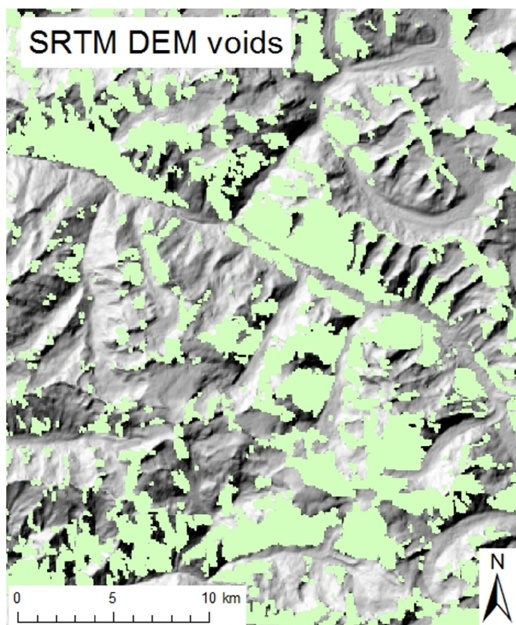
Figure 3.6: SRTM DEM with voids (green) (see Figure 3.3 for location).
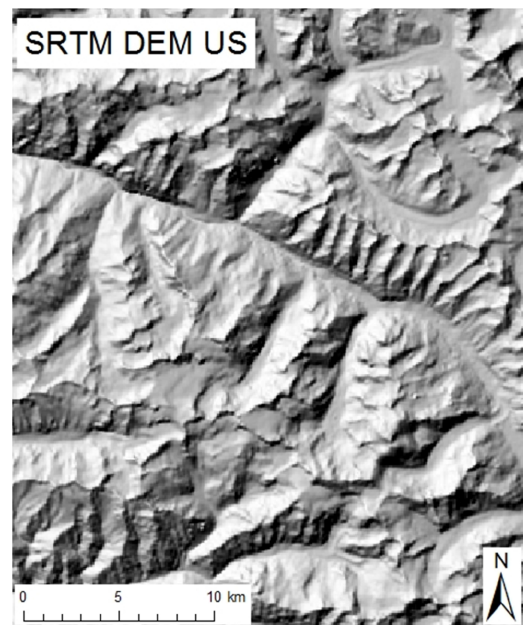
Figure 3.7: SRTM DEM with voids filled with data from ASTER GDEM2 (SRTM DEM US) (see Figure 3.3 for location).

A different void-filled version of the SRTM DEM is also available from the USGS Earth Explorer USGS (2014b) and does not show such wrongly interpolated data voids (Figure 3.5). The version of USGS was published on the 1th of October 2012. But the interpolation algorithm and the used data for the interpolation of the voids are not clearly documented.

The third void-filled version of the SRTM DEM was compiled as part of this study; simply by filling all the voids (Figure 3.6) with the elevation data out of ASTER GDEM2 (see section 4.1). This third version was produced in order to analyze the differences to the available versions of CGIAR and USGS. The three void-filled versions were later compared and evaluated. The comparison with the version of CGIAR showed a much better quality of the newly complied version and a good accordance with the version of USGS (see section 5.1). In the following, the version of the SRTM DEM, filled the voids with elevation data from ASTER GDEM2 is called "SRTM DEM US" (Figure 3.7).

3.3   Glacier inventory of 2002

Frey et al. (2012) produced a glacier inventory for the whole western Himalaya, whereby the state around the year 2000 was mapped. Therefore different satellite scenes from various years around 2000 were used. Also the region of the Kullu District was covered by a scene of the year 2002 (Frey et al., 2012) and served as basis for the development of the glacier inventory of the year 2002 for the Kullu District compiled in this study. This previous inventory of Frey et al. (2012) was revised and adapted to the inventory of 2013. The dataset of Frey et al. (2012) from the GLIMS database (NSIDC, 2014). In section 4.2.2 it is described which focus the inventory was revised with.

3.4   Branch lines and GPR dataset

To model and estimate the ice thickness distribution of the glaciers, a model called GlabTop was used. In order to calculate the ice thickness distribution, the branch lines of the glaciers were required as input dataset (Linsbauer et al., 2012). Fortunately, a dataset of the region

around the Kullu District was available from Linsbauer, pers. communication (2014). This dataset was then reviewed and adjusted to the outlines of the inventories developed in this study. Details concerning the digitalization of such branch lines are mentioned in Paul and Linsbauer (2012). In Figure 3.8 one can see such branchlines for the Chhota Shigri and some neighboring glaciers (blue lines).
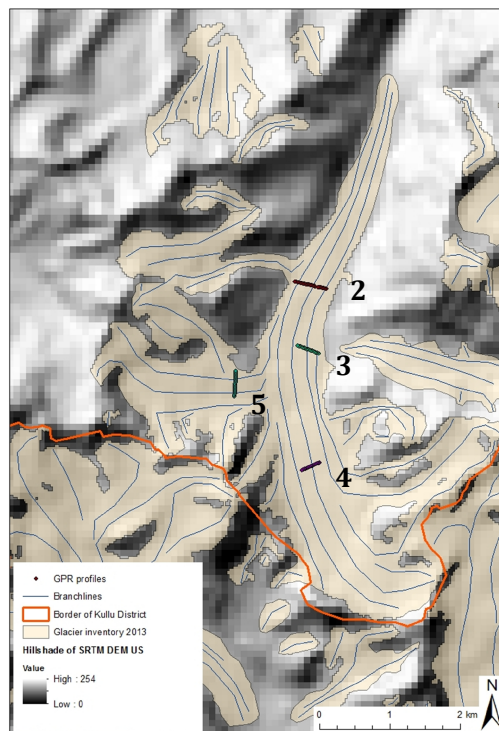
Figure 3.8: Chhota Shigri glacier with the GPR profiles used for the GlabTop validation and the branch lines (blue lines). Profile 1 was not available.

To validate the outputs of the GlabTop volume and ice thickness distribution a dataset of four ground penetrating radar (GPR) profiles of the Chhota Shigri was used (Figure 3.8). This GPR profiles were collected in the context of a study concerning the mass-balance and the dynamic behavior of Chhota Shigri in October 2009 by Azam et al. (2012). Chhota Shigri is a glacier right at the border to the Kullu District. Even though it does not lie within the study area it was considered to be reasonable to use this data, as it was the only possibility to validate the model outputs.

4. Methods

4.1   Compilation of an improved SRTM DEM

In the context of this study an improved void-filled SRTM DEM was generated (section 3.2.2), because the version of CGIAR shows various errors in the region of the Western Himalayas. Thereby, the aim was to generate even more accurate void-filled DEM than the version of USGS.

Three 5 by 5 degree tiles of the SRTM DEM with voids were downloaded from the USGS archive (http://earthexplorer.usgs.gov/, accessed 14.05.2014) to cover the region of Kullu (UTM zone 43N). In this ID included are as well the coordinates of the left lower corner of the tile.

Table 4.1: List of used SRTM DEM tiles.

Entity ID	Coordinates
SRTM3N31E077V1	31°N 77°E
SRTM3N32E076V1	32°N 76°E
SRTM3N32E077V1	32°N 77°E

These voids were then filled with the data of the ASTER GDEM2, according to the procedure Kääb (2005) used already some years before replacing the voids of SRTM with the first version of ASTER DEM. Therefore the ASTER data was resampled to the same spatial resolution as the SRTM (90m). Using a conditional function in ArcGIS, the voids were filled with raster data from the ASTER GDEM2, wherever the SRTM DEM has no data. As an output of this function, the void-filled SRTM DEM US was produced.

4.2 Glacier mapping

In the following sections, the development of the glacier inventories is explained. This process is divided into the following steps: the mapping of the clean ice (4.2.1), the mapping of the debris-covered ice parts (4.2.2) and the delineation of the ice dividing to separate the individual glaciers (4.2.3). The last step describes the derivation of the topographic parameters of the glaciers (4.2.4). The process is described in detail by the means of the inventory of 2013. Frey et al. (2012) delivered the data of their inventory from the Western Himalayas from 2002, which served as a basis for the inventory of the year 2002 seeing as it was not necessary to apply the whole approach. The essential adjustments of the inventory from Frey et al. (2012) are mentioned in section 4.2.2.

4.2.1 Mapping of clean ice (raw map)

Based on imagery from Landsat 8 OLI scenes (Landsat ETM+ for 2002), the glaciers of the study area were mapped using ratio images. The ratio images were computed from the raw digital numbers of two different bands. Hall et al. (1987) observed that the ratio of Landsat bands TM4 (NIR: 0.76-0.90 μm) and TM5 (SWIR: 1.55-1.75 μm) are useful to enhance the reflectivity differences on glaciers. The ratio image enhances snow and ice features due to the different spectral response of snow and ice between band 4 (high digital numbers) and 5 (low digital numbers). The ratio of band 3 (RED: 0.63-0.69 μm) and band 5 (SWIR: 1.55-1.75 μm) produces similar results (Andreassen et al., 2008; Racoviteanu et al., 2008b). Glacier ice appears light grey and snow appears white in the Landsat TM3 and 4 and almost black in TM5. By calculating a ratio out of these two bands, a ratio image, which highlights all snow and ice covered areas is received. Andreassen et al. (2008) discovered that the ratio of TM3 and TM5 works slightly better for shadows and thin debris-cover (Andreassen et al., 2008; Paul and Kääb, 2005). Landsat TM and ETM+ have the same spectral bands, thus, based on the mentioned findings, it was decided to work with the ratio ETM3/ETM5 (Figure 4.1b). As a consequence of the different spectral properties of the bands of Landsat 8, as mentioned in

the previous section 3.1, the corresponding bands for the ratio image are OLI4 (RED: 0.64-0.67) and OLI6 (SWIR: 1.57-1.65) instead of TM3/TM5 respectively ETM3/ETM5 which were used for the inventory of 2002.
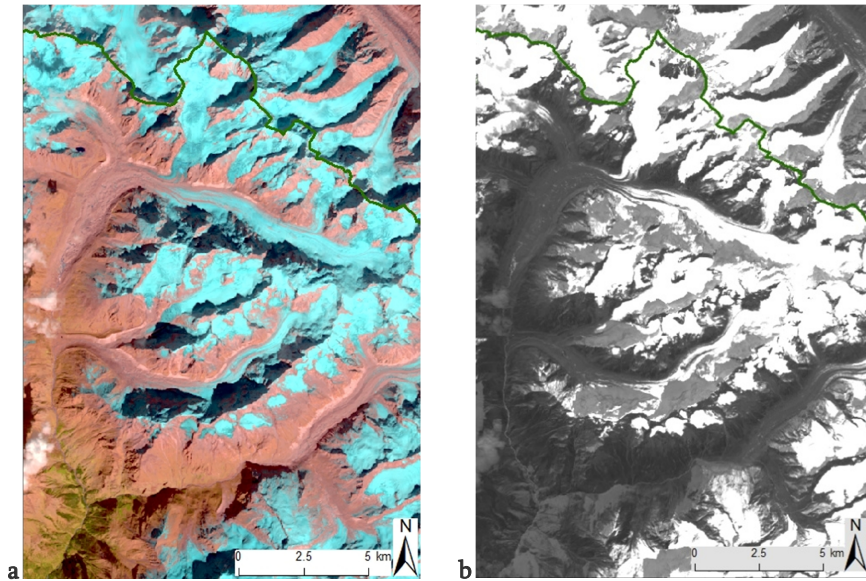
Figure 4.1: (a) False color image of Landsat 8 OLI 2013 and (b) ratio image out of OLI4/OLI6, in green the borders of the Kullu District are shown (see Figure 5.1 outline 3 for location of this figures).

The limitation of this ratio method is the similar reflection properties of water bodies and areas which are covered in snow and ice. In addition, the debris-covered ice is not mapped, due to spectral similarities of the surrounding terrain (Andreassen et al., 2008). This is a common problem with automated methods, based on multispectral data.

The resulting clean ice (and snow) map was then compared to a false-color composite (ETM+ bands, 5, 4, 3; OLI bands, 6, 5, 4 as RGB) of the Landsat image to optimize the threshold value (Figure 4.1 a). This threshold value defined which pixels of the ratio image were classified as clean ice/snow and which were not. The false-color composite was generated in Exelis Visual Information Solutions (ENVI). The optimal threshold was selected interactively by the comparison of different threshold values in the sensitive regions (shadow) in order to

minimize the workload of further processing (Paul and Andreassen, 2009). Due to this interactive process, the selection of the threshold was, to some degree subjective.

Figure 4.2 shows three different threshold values applied to the ratio image of OLI4/OLI6. It becomes obvious that there is a huge influence of the threshold on the mapped area. By applying this threshold value to the ratio image an enhanced map of the snow and ice covered areas was created. For the mapping of the glaciers in the year 2013 the value 1.7 was chosen. The inventory of 2002 by Frey et al (2012) was based on threshold values between 1.9 and 2.1, depending on the part of the Western Himalaya. This means that pixels were finally classified as ice or snow if the pixels had values larger than the threshold: (ETM3/ETM5) > 1.9-2.1 respectively (OLI4/OLI6) > 1.7.
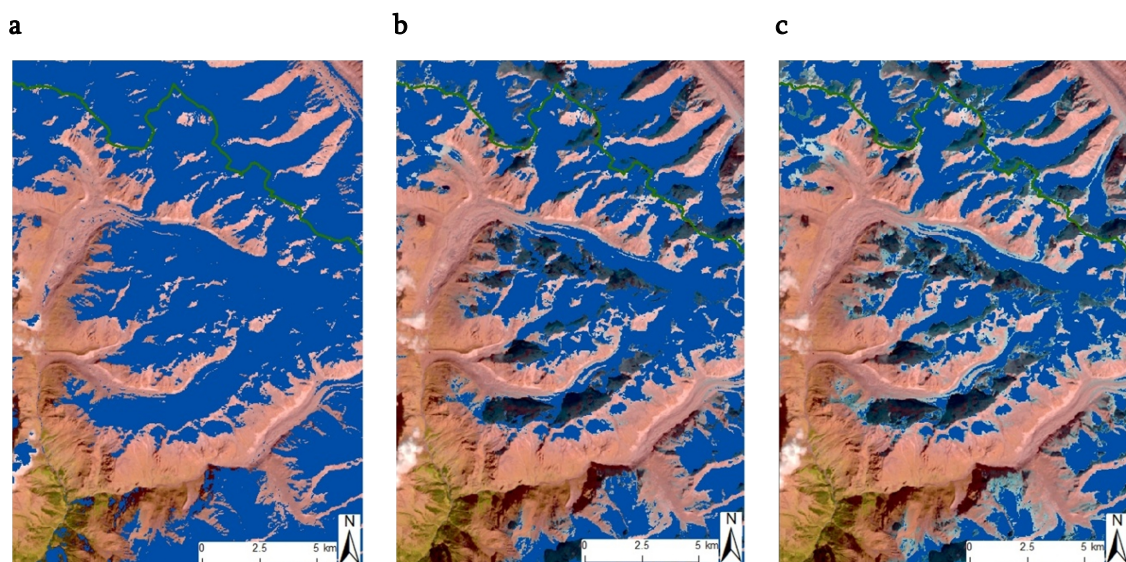
Figure 4.2: Different threshold values applied to the ratio image of OLI4/OLI6 in front of the false color image of Landsat 8 OLI, (a) threshold 2.4, (b) threshold 1.7 and (c) threshold 1 (see Figure 5.1 outline 3 for location of this figures).

In a next step, a median filter (3 by 3 kernel) was applied to the classified binary image in order to remove isolated pixels and fill up isolated gaps (Andreassen et al., 2008; Paul et al., 2002). According to Paul et al. (2002) the number of pixels added and subtracted to a single glacier by this median filter lies in a similar range. The median-filtered glacier map was then

converted from the raster format to a feature format within ArcGIS in order to receive the glacier polygons in the Kullu District.

As mentioned at the beginning, the inventory of 2013 was compiled completely independently, whereas the inventory of 2002 was derived out of the inventory of Frey et al. (2012), which was used as a basis. The above mentioned steps, the ratio images, the threshold values and the median filter were only performed for the year 2013. For the inventory of 2002 these steps were already done by Frey et al. (2012). But the dataset of 2002 had to be adapted to the inventory of 2013.

4.2.2   Manual corrections (Level 0, Level 1)

The glacier map, produced out of the processes, described above, in ArcGIS, had to be inspected visually in order to eliminate errors, caused by wrongly mapped areas. Thereby, the lack of mapped glacier parts, due to debris-covered ice or regions in cast shadow or with cloud cover on the images, as well as the subtraction of wrongly mapped snow patches had to be conducted. The thick debris-cover of the glaciers is a characteristic element of the Himalayas because of ice avalanches and rock falls on the glacier surfaces from the steep surrounding slopes (Racoviteanu et al., 2008b; Shroder et al., 2000). Adding this debris-cover means a time-consuming manual work. However, this step is essential because of the huge debris-covered area, and the debris-cover having a non-negligible importance for the understanding of the glacier retreat in future (e.g. Scherler et al., 2011).

The median filtered glacier map, produced in section 4.2.1, was defined as a raw map. First, the raw map was corrected, whereby the glacier areas under light cloud cover and in the shadow were added and the snowfields, incorrectly defined as glacier, were subtracted. This corrected glacier was then called Level 0. In Figure 4.3 the different processing steps, which are treated hereinafter, are showed. The Figure 4.5 at the end of the section 4.2.3 shows the map sections of each level.

The snowfields were detected by the comparison of the satellite scene of the year 2013 with scenes from earlier years, which show less seasonal snow, and were afterwards deleted.

Additionally to satellite scenes from earlier years Google Earth imagery, with a high temporal resolution was used to look at the conditions in the Kullu District in the last years. Thereby it was possible to see where in the dark shadow glacier ice was present and where it was not. The glacier parts covered by debris were then detected and added to level 0 outlines. Finally the unique difference between Level 0 and 1 was distinguished to be only the debris-covered ice.

The inventory of Frey et al. (2012) for the year 2002 was also corrected manually. Many of the thresholds are subjective, therefore it would be important that the two inventories are made by the same person, with the same interpretation. Because Frey et al. (2012) did the inventory for a larger territory, their manual corrections had a smaller degree of refinement. The inventory of 2002 was examined with the satellite scene and compared to the inventory of 2013 as well adapting necessary outlines.

Level 0
- **Glaciers without debris-covered parts**
  - + glacier parts in shadow
  - + glacier parts under clouds
  - - Seasonal snow

Level 1
- **Glaciers with debris covered parts**
  - + debris covered glacier parts

Level 2
- **Individual glaciers**
  - Intersection with basins, get out of the drainage divides

Level 3
- **Topographical parameters**
  - Max, min, mean, median elevation; mean slope; mean aspect (°), mean aspect (e.g. NW); debris cover (%)

Figure 4.3: Flowchart of the processing steps of the different inventory levels.

4.2.3   Delineation of ice divides (Level 2)

To generate Level 2, the glaciers had to be separated along their drainage divides to get the extent of their individual glacier area. The ice divides define the glacier basins in a hydrologic sense, the glaciers were split off where they drain in another direction (Racoviteanu et al., 2009). Many different approaches exist in order to do this division automatically or semi-automatically. A semi-automatic approach, described by Bolch et al. (2010) was tested in this study, however as shown in Figure 4.4 the result was not satisfying. Moreover, the drainage divides should be adapted to the former divides, if inventories already exist for the mapped region (Paul and Andreassen, 2009).

The accumulation zones around the mountain ridges are not correctly mapped with this method. Therefore the basins generated by Frey et al. (2012) were taken and revised. Frey et al. (2012) also tried the semi-automatic method used by Bolch et al. (2010), and applied a buffer of 700m around the glaciers first. After an unsatisfying result they decided to revise the basins manually. The basins of Frey et al. (2012) were adjusted to Level 1 (2002 and 2013). For this adjustment a hill shaded view of the DEMs (SRTM DEM US and ASTER GDEM2) and a flow direction raster were used as reference. The problem of these references is that they are based also on the DEM and therefore show the same weak points in the accumulation areas, as the drainage basins generated with the method of Bolch et al. (2010). Therefore, the satellite image, where ridges were recognizable due to illumination differences, was used primarily in order to determine the divides in the critical regions.
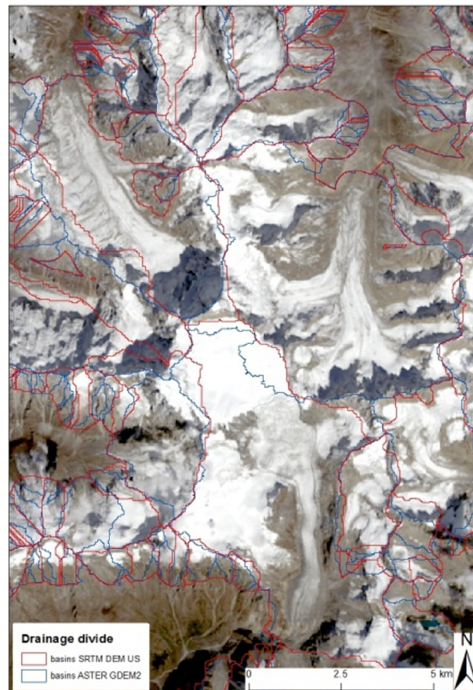
Figure 4.4: Drainage divides out of SRTM DEM US (red) and ASTER GDEM2 (blue).

To have some further information concerning approaches to get drainage divides, Racoviteanu et al. (2009) give a short review of different semi-automatic algorithms. This paper summarizes the results of the 2008 GLIMS workshop. The different approaches revised in the paper are described in detail by Tobias Bolch et al. (2010), Manley (1980) and Paul & Kääb (2005). Another relatively new approach to get drainage divides is described by Kienholz et al. (2013). This approach is also based on hydrological modeling tools but works in contrast to previous automated approaches with multiple pour points to take into account the fact that because of the convex surface of the glacier not all of the ice converges to the same point. The algorithm merges the different flow sheds of the individual glaciers they belong to (Kienholz et al., 2013).
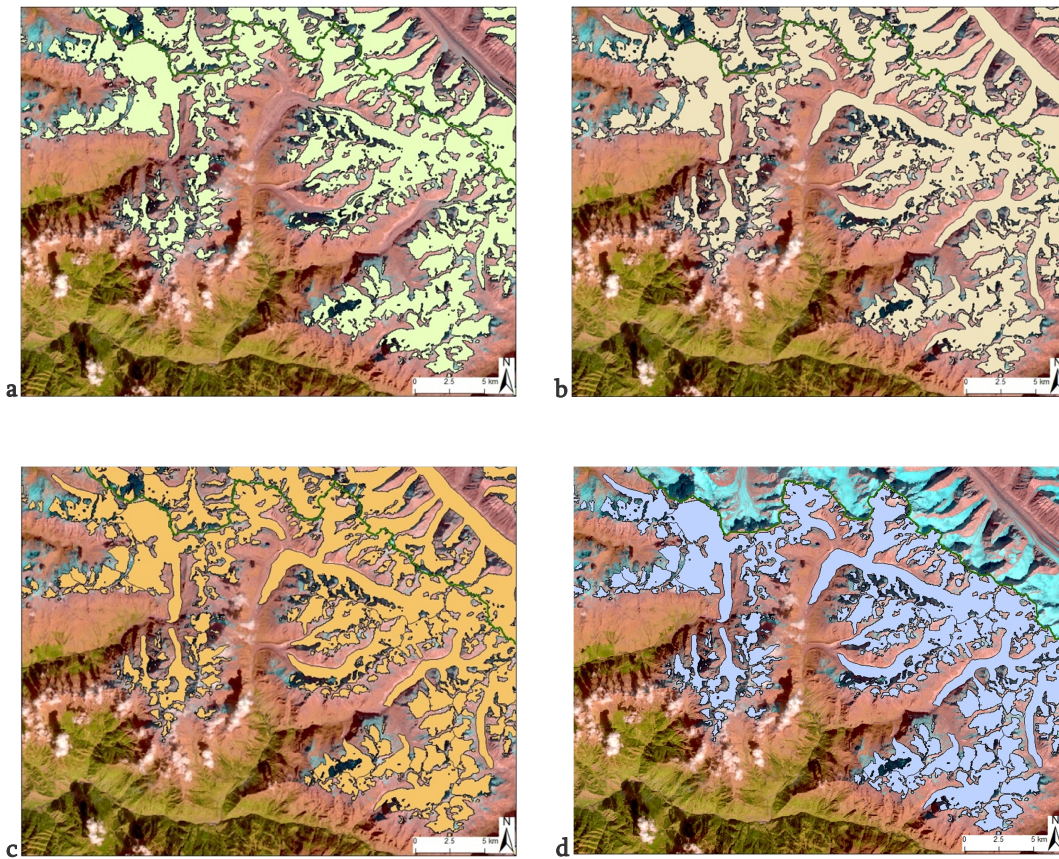
Figure 4.5: Different levels of processing (a) level 0, (b) level 1, (c) level 2 greater than 0.02 km² and (d) level 3 only Kullu District. (see Figure 5.1 outline 1 for location of figures).

The glacier basins, produced with this process were then used to cut the Level 1 shapefiles into individual glaciers. Due to the high probability to misclassify small snowpatches outside of the glacier, all glacier polygons smaller than 0.02 km² were excluded from the inventory. With this threshold this effect could be prevented to some degree. This step generates the next Level 2.

For 2002 the adapted polygons were first merged to uncut glacier shapefiles and afterwards cut again with the revised basin dataset of this study. This was essential to be sure that both inventories had the same glacier divides.

4.2.4 Topographic glacier parameters (Level 3)

After intersecting the drainage divides with the glacier polygons, glacier-specific topographic parameters were calculated. With this step, the Level 3 of the inventories was generated.

The two dimensional parameters area and perimeter were automatically generated for each glacier polygon. Three-dimensional parameters have to be calculated by combining the two dimensional outlines with a DEM and DEM-derived parameters (Kääb et al., 2002). Thus further topographic parameters such as minimum, maximum, mean and median elevation were derived by dint of the zonal statistic tool in ArcGIS. Slope and aspect were obtained as an average over the glacier (mean slope, mean aspect) as well as the debris-covered parts of a glacier (Paul et al., 2002 and Kääb et al., 2002). To derive these parameters, the improved void-filled SRTM DEM US was used. The different parameters listed in the attribute table and their derivation are shortly explained and defined hereafter and shown in Table 4.2.

Identification code

In order to identify the glaciers in the two inventories, each glacier received his individual identification code called "IID". The glaciers of the 2002 inventory were numbered consecutively with the aid of points assigned within the glacier polygons. These points and thereby numbering of the glaciers was then transcribed to the inventory of 2013. Because of certain differences between the two inventories, the points had to be adapted. Some were deleted and a few were added because of glacier fragmentation (or incorrectly mapped snow covered areas). With this procedure it was ensured that the same glaciers have the same IID in both glacier inventories (2002 and 2013). This was an important base for further calculations.

Area and perimeter

As soon as the individual glacier entities were defined, the area and perimeter was automatically generated in ArcGIS and stored in the attribute table. The area was recorded in

square kilometers and Paul et al. (2009) recommend an accuracy of three digits after the decimal point in order to facilitate sorting the glaciers into logarithmic size classes subsequent analysis. They got sorted into the seven different size classes 1-7 (1: <0.05, 2: 0.05-0.1, 3: 0.1-0.5, 4: 0.5-1, 5: 1-5, 6: 5-10, 7: >10 km²).

Elevation (max, min, mean, median)

Using the elevation information from the DEM US and the glacier IID, the highest, mean, median and the lowest elevation were derived. The mean elevation, determined from zone statistics, represents the sum of all elevation values, divided by the number of all cells used for the sum. The median elevation is therefore the hypsographic 1:1 area ratio, it divides the area in half (Paul et al., 2009).

Mean aspect (degree/sector)

The calculation of the mean aspect required further processing steps. The aspect grid out of the DEM US showed values between 0 and 359.99°, which prevented a direct calculation of the mean aspect. If the glacier contains - for example - two values of 20° and 340°, the expected mean would be 0°/360° but the calculated mean is (20°+340°)/2=180°. In order to avoid this phenomenon out of the sine and the cosine of the aspect grid, the arctangent was calculated. This allows the calculation of the correct mean aspect value of the individual glaciers. To additionally receive the information of the cardinal direction, the degree values can be converted to the sectors 1 to 8 (N, NE, E, SE, S, SW, W, NW) (Frank Paul, 2006, Evans, 2006).

Mean slope

The mean slope of the glaciers was calculated throughout zonal statistics. The input datasets for this calculation were the slope grid out of the DEM US and the outlines of the glaciers. The slope is independent from the glacier length because it refers to the single cells of the DEM US (Manley, 1980).

Percentage of debris respectively clean ice

For the derivation of the debris-covered part per glacier, it was essential to compare different input layers; this was more time consuming. With zonal statistics of the grid of the Level 0 as raster input and the dataset of Level 3 as zone, the debris-covered part, respectively the area of clean ice was derived. In the attribute table the amount of debris-covered glacier area on the total glacier area as well as the amount of the clean ice area was stored.

Mean thickness

The mean ice thickness of the individual glaciers was calculated with zonal statistics out of the ice thickness grid and the glacier outlines. The mean thickness grid was one of the outputs of the GlabTop model (section 4.3.1).

Table 4.2: Glacier parameters in the attribute table of the inventories.

Name	Item	Unit
Code	IID	
Area	area	km^2
Perimeter	perimeter	km
Minimum elevation	min_elev	m a.s.l.
Maximum elevation	max_elev	m a.s.l.
Median elevation	med_elev	m a.s.l.
Mean elevation	mean_elev	m a.s.l.
Mean slope	mean_slope	°
Mean aspect (degree)	mean_aspect_d	°
Mean aspect (sector)	mean_aspect_s	1-8
debris-cover	mean_debr	%
clean ice	mean_ice	%
mean Thickness	mean_thick	m
size class	size_class	1-7

4.3   Different approaches of modeling the glacier thickness and volume

The knowledge of the glacier ice volume is crucial for the assessment of the amount of water stored as ice in glaciers. The ice thickness distribution respectively the knowledge of the glacier bed topography is important for making a statement concerning the future retreat of the glaciers. To forecasting the amount of water supplied to the rivers and the potential contribution to sea-level rise, meteorological data and information about the energy balance would be required as well. Due to the increase in global mean temperature, the environment in high mountain area changes which leads to a glacier change. Such changes, which will intensify in the future and have impacts on different scales (from global, regional to local) and include, e.g. retreating glaciers, newly built glacier lakes in front or above the shrinking glaciers, rock falls (Frey et al., 2010; Kulkarni et al., 2005; Watson and Haeberli, 2004). On a global scale, the changes of glacier geometry and volume affect the sea level rise. On a regional scale, the water supply will be impacted, due to changes in runoff. On a local scale, the changes have an influence on the frequency and intensity of natural hazards (Linsbauer et al., 2009).

There are different approaches to estimate the ice volume of a glacier. Some of them were evaluated by Frey et al. (2013) for Himalaya-Karakoram region. In addition to the here applied GlabTop method (section 4.3.1), there exists also the "volume-area scaling method" described e.g. of Chen & Ohmura, 1990 or Bahr et al., 1997. Haeberli & Hoelzle (1995) developed a method to estimate the ice volume based on the average surface slope of glacier also referred to as "slope dependent thickness estimation".

Linsbauer et al. (2012) developed the approach used in this study- called GlabTop -, to estimate the ice thickness distribution of glaciers, based on the considerations of Haeberli & Hoelzle (1995). In this approach, the ice-thickness is calculated at several points along the flowlines of major glacier branches (so called branch lines) and interpolated between these points and the glacier margin (Paul and Linsbauer, 2012). In addition to the branch lines, the

method of Linsbauer et al. (2012) requires a DEM and the glacier outlines as input data. Frey et al. (2013) modified the GlabTop approach with a less time consuming automatically point selection instead of the digitalization of the branchlines to GlabTop2. .

Farinotti et al. (2009) developed as well a method facing the ice-thickness distribution based on glacier mass turnover and on the principles of the flow dynamics. The approach of Farinotti et al. (2009) was improved by Huss & Farinotti (2012) where the input parameters were minimized to glacier outlines and a DEM.

In this study the GlabTop method of Linsbauer et al. (2012)was applied and the other approachs mentioned before were only listed for the sake of completeness.

4.3.1 GlabTop

Based on the findings of Frey et al. (2013), the GlabTop model of Linsbauer et al. (2012) was used to estimate glacier volumes in the Kullu District in this study. In the following section, the method of the GlabTop model is explained in detail. As already mentioned above, the model is based on the physical dependence of the ice thickness from the slope. By assuming an ideal plasticity and neglecting basal sliding of the ice body with a larger horizontal than vertical extent (about 10 times) (Paul and Linsbauer, 2012), the ice thickness d along the central flowline depends mainly on the slope α and the basal shear stress τ (Cuffey and Paterson, 2010; Haeberli and Hoelzle, 1995).

$$d = \frac{\tau}{\rho g f \, \sin\alpha} \qquad\qquad (1)$$

Where ρ is the density of ice (900kg/m³), g is the gravitation (9.81 m/s²), f the shape factor (0.8) and α the slope [°, $\alpha \neq 0$] is. The shape factor relates to the ratio between the cross-sectional area of a glacier and its perimeter and relates to the friction with the valley walls. According to Cuffey & Paterson (2010) the most valley glaciers have a shape factor of 0.6 to 0.8. GlabTop uses constantly a shape factor of 0.8.

Methods

The basal shear stress τ is calculated based on the aid of a glacier-specific empirical relation examined by Maisch & Haeberli (1982), which relates the shear stress τ to the elevation range Δh of a glacier (difference between the lowest and the highest point of the glacier), using a quadratic regression to all points (Haeberli and Hoelzle, 1995):

$$\tau = 0.005 + 1.598\Delta h - 0.435\Delta h^2 \qquad (2)$$

It has to be noted that in contrast to the first equation, the basal shear stress τ in equation (2) is in bar (10^5 Pa) and Δh in km.

Implementation in GIS

To implement GlabTop in a Geographic Information System (GIS) the previously mentioned input parameters are needed: a DEM, glacier outlines and branch lines (Linsbauer et al., 2009; Paul and Linsbauer, 2012). For details concerning the digitalization of branch lines see Frank Paul & Linsbauer (2012). After loading the input parameters into the model, GlabTop calculates the topography of the glacier bed (DEM without glaciers) in the following steps (Paul and Linsbauer, 2012):

Calculation of the basal shear stress τ and the slope α: Based on equation (2), a unique basal shear stress τ is calculated for every glacier, as well as the required Δh is derived from the DEM (A). To receive the mean slope of the whole glacier, the DEM is smoothed by a focal mean filter (B), in order to reduce the influence of surface structures of the glacier (e.g. crevasses, moraines) on the local slope (*sin α*; Figure 4.6b). The model uses three different filters depending on the slope inclination (<5°, 7x7 kernel; 5°-20°, 5x5 kernel; >20°, 3x3 kernel).

Figure 4.6: (a) schematic summary of the basic processing steps for glacier bed interpolation in a flowchart (squares denote datasets and circles denote GIS-based calculations), with eq, equation; IDW, inverse distance weighting; bl, branch line. (b) This schematic perspective view illustrates the basic parameters used for glacier bed modeling *(edited according to Frank Paul & Linsbauer, 2012)*

Calculation of glacier thickness for the base points: The branch lines are converted to a 100 m raster cell and segmented to sectors of 50 m elevation range, using the DEM (C). The mean slope ($sin\,\alpha$) is calculated from the smoothed glacier surface for every branch line sector and assigned to the base point (D). Using Equation (1), the ice thickness is calculated for every base point (E) using the shear stress out of (A) and the mean slope out of (D).

Spatial densification of the base points along the branch lines (IDW): To get continuous thickness values along the complete branch lines an interpolation with the TopoToRaster algorithm was applied to all base points (F). Out of the resulting interpolated grid with thickness values for the entire glacier, the cells under the branch lines were selected and reconverted to a vector format. This results in a continuous (25 m spacing) dataset of depth values, that can be used for special interpolation.

Interpolation of the ice thickness distribution (topogrid): In order to interpolate the thickness values over the entire glaciers to a continuous grid, the thickness values out of (E) and (F) as well as the glacier outlines with an assumed elevation of 0 were used for a "topogrid

interpolation". Subtracting this thickness grid from the original DEM yields the DEM without glaciers, hence the DEM of the glacier bed topography.

GlabTop has various model outputs. Probably the most important ones are the ice thickness grid for every glacier and the DEM of the non glacierised topography. Further derivations are the mean thickness and the total volume of a glacier and the locations of future lakes in overdeependings under the glacier (Linsbauer et al., 2009). The detection of the overdeependings is a result of a hydrologic analysis of the DEM of the glacier bed topography in GIS with the tool "fill". The output of this analysis is important to investigate future hazard potential, especially in locations where the future lakes are located underneath rock walls or hanging glaciers, which could easily trigger chain reactions (e.g. rock or ice fall in the lake which leads to a flood wave) (Frey et al., 2010; Haeberli and Hohmann, 2008). Additionally, the DEM of the glacier bed topography can be used to model the flow path of potential flood waves and to model discharge changes in glacierised catchments. (Linsbauer et al., 2009)

Accuracy of the GlabTop approach

Sources of uncertainty of the ice thickness estimation are, among other things, the parameters of Equation (1), such as shape factor, surface slope and basal shear stress, but also the interpolation method (Linsbauer et al., 2012).

As mentioned above (beginning of section 4.3.1), the shape factor can vary from 0.7 (ablation area) to 0.9 (accumulation area) (Maisch and Haeberli, 1982) but nevertheless, GlabTop uses a constant value of 0.8. The shape factor has a typical uncertainty of $\pm$ 12.5%. The uncertainty of the slope value results from local artefacts in the DEM, which causes a typical inaccuracy up to $\pm$ 10%. The uncertainty range of the basal shear stress of around $\pm$ 30% has a major influence on the ice thickness estimation (Linsbauer et al., 2012). The GlabTop model was tested with this different uncertainty values by Linsbauer et al. (2012) using GPR profiles of valley glaciers in Switzerland.

Linsbauer et al. (2012) replaced the inverse distance weighting (IDW) interpolation method (Paul and Linsbauer, 2012) with the "TopoToRaster"-algorithm (in GlabTop), in order to gain

a stronger smoothing of the subglacial topography with fewer artefacts. The mean ice thickness was modeled slightly thicker using the TopoToRaster method, than with IDW. Linsbauer et al. (2012) compared the results of these two different interpolation methods with GPR measurements on three Swiss valley glaciers. The outputs of the two methods (TopoToRaster and IDW) agree very well with each other. The ice thickness differences between the modeled GlabTop outputs and the GPR profiles are often remarkably large, but lie within the 30% uncertainty range. One reason for this quite significant uncertainty, concerning the mean ice thickness and volume estimation, is that GPR profiles often cover the crevasse-free, flat and therefore thick glacier parts with compressing flows. As a consequence, the GPR profiles are not representative for the entire glaciers. Assuming a worst case scenario, depending on the variable input parameters τ, α, f, the ice thickness' can be underestimated by 42% or overestimated by 62% (Linsbauer et al., 2012). But the distribution of the ice thickness, the glacier bed topography and the overdeependings mainly depend on the slope, which is represented correctly by GlabTop (Linsbauer et al., 2012).

As a preparation for applying GlabTop to smaller regions on a local scale, it makes sense to adapt the input parameters to the local conditions. First of all, a correct digitalization of the branch lines is particularly essential and the shape factor as well as the slope can be adapted to the local conditions. Additionally, a change in the interpolation method or the filter/threshold, in order to smooth the DEM, can lead to better results (Paul and Linsbauer, 2012).

The interpretation of overdeepenings must be done carefully, especially at the glacier margins. The GlabTop outputs sometimes show overdeepenings at these points, which are originated likely out of differences between the glacier outlines and the glacier margins in the DEM. This difference has an impact on the derived glacier bed. For example, if the outline of a glacier lies outside of the margins of the DEM, GlabTop models an overdeepening between the two glacier margins (Paul and Linsbauer, 2012).

The results of the different modeling were afterwards validated with the aid of the GPR profiles of the Chhota Shigri.

5. Results

As Introduction to the following results the Figure 5.1 serves as an overview of the Kullu District. The satellite image of the year 2002, which served as basis for the compilation of the inventory of the year 2002, is shown as background. The borders of the Kullu District are marked in black and the three rectangles in the north eastern part of the district indicate the outlines of the various figures in this study, zoomed in, regarding at different topics. Rectangle 1 refers to figures in section 4.2.3, 5.3 and 5.4. Rectangle 2 refers to the differences between the DEMs in section 5.1 and 5.3. Rectangle 3 refers to the figures in section 4.2.1.
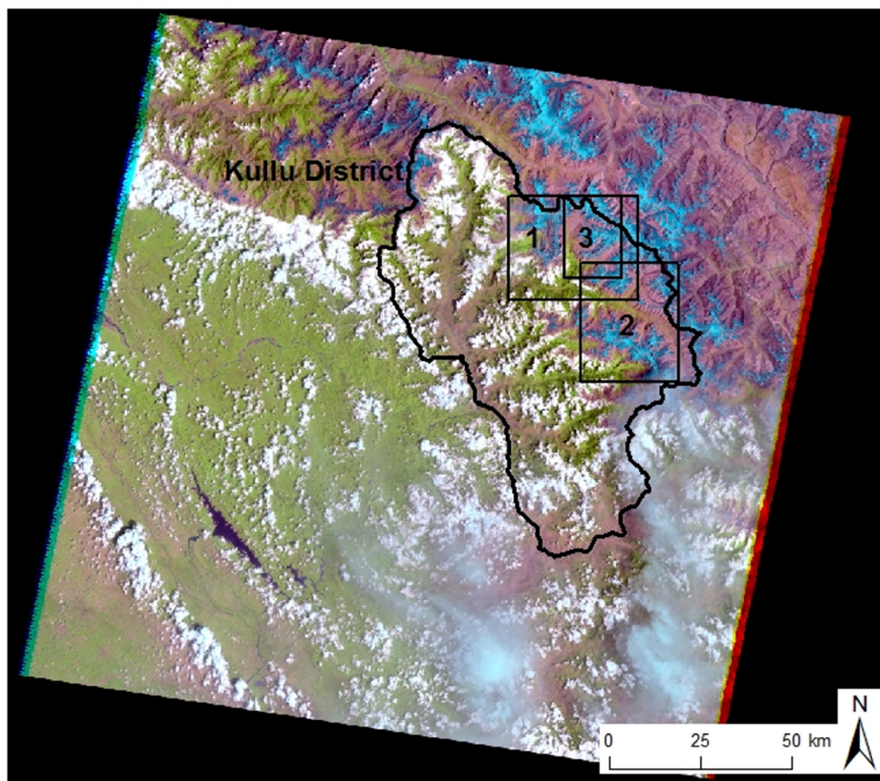
Figure 5.1: Borders of the Kullu District, false-color satellite image of 2002 and the rectangles 1, 2 and 3 indicating different locations of various figures in this study.

5.1   Improved SRTM DEM

After the compilation of the new void-filled SRTM DEM US (described in section 3.2.2), the differences between the existing void-filled SRTM DEMs and the ASTER GDEM2 were investigated in order to make a statement on their relative accuracy and their suitability for glacier mapping. The three DEMs were compared to each other at a resolution of 90 meter, using hillshade views (Figure 3.4, Figure 3.5 and Figure 3.7) and difference images of the direct subtractions (Figure 5.2 and Figure 5.3). This shows the spatial distribution of the differences, the quality of the void-filled zones and the horizontal shifts (Figure 5.2 ASTER GDEM2) of the DEMs to each other. Figure 5.2 and Figure 5.3a/b show the differences resulting from the direct DEM subtractions in the region of the Parbati Valley (outline 2; Figure 5.1).

In the current study, the differences between the ASTER GDEM2 and the SRTM DEMs in general and their suitability for glacier mapping are not further discussed in detail, see e.g. Frey and Paul (2012) or Rexer and Hirt (2014). In the following comparison, the focus was set on the quality of the void-filled version of SRTM DEM, generated in the context of this study.

After subtracting ASTER GDEM2 from the improved SRTM DEM US, the relief of the region is visible (Figure 5.2). The mean of the pixels is –9.21, means that the surface of the SRTM on average is lower than the surface of the ASTER GDEM2 (in m a.s.l.). The grayish spots correspond to the voids of the original SRTM DEM, as they were filled with data of the ASTER GDEM2; the difference of the two DEMs is zero. The surfaces of the glaciers show yellow to blue colors. The arrows in Figure 5.2 indicate the zones with conspicuous blue color, which are interpreted in the discussion as a potential surface lowering. The SRTM DEM US indicates larger elevations than the ASTER GDEM2 in the blue colored regions. In return the ASTER GDEM2 states larger elevations than the SRTM DEM US in red colored areas.
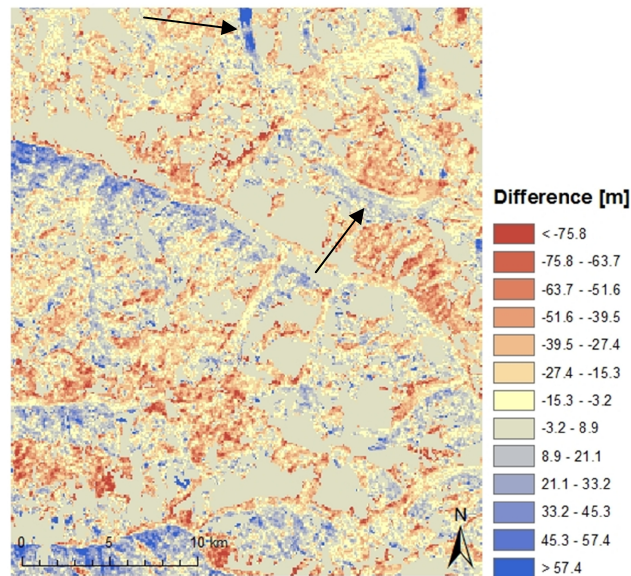
Figure 5.2: Differences of the SRTM DEM US – ASTER GDEM2 in the region of the Parbati Valley

By subtracting the SRTM DEM CGIAR of the improved SRTM DEM US, the major differences produced during the void correction become visible (Figure 5.3a). The positive values of the voids (blue) imply a much lower surface of the version of CGIAR than the void filling of the SRTM DEM US (SRTM voids filled with ASTER GDEM2 data). The low surface within the voids can also be observed in the hillshade of the SRTM DEM CGIAR (Figure 3.4). These errors in the dataset (crater like landscape) were already mentioned in the section 3.2.2 and they result in huge differences up to several hundred meters between the two DEMs. Figure 5.3b) shows the subtraction of the SRTM DEM USGS from the STRM DEM US. In the areas of the voids, large deviation from the raw SRTM DEM can be observed. Even though some parts with dark blue or red zones (much lower or much higher surface in the void filling) are also detected. The comparisons made here are only relative, because none of these DEMs can be seen as a correct reference. In Table 5.1 the statistic values of the three mentioned DEM difference images are listed and among others the large difference between the SRTM DEM US and CGIAR can be seen.
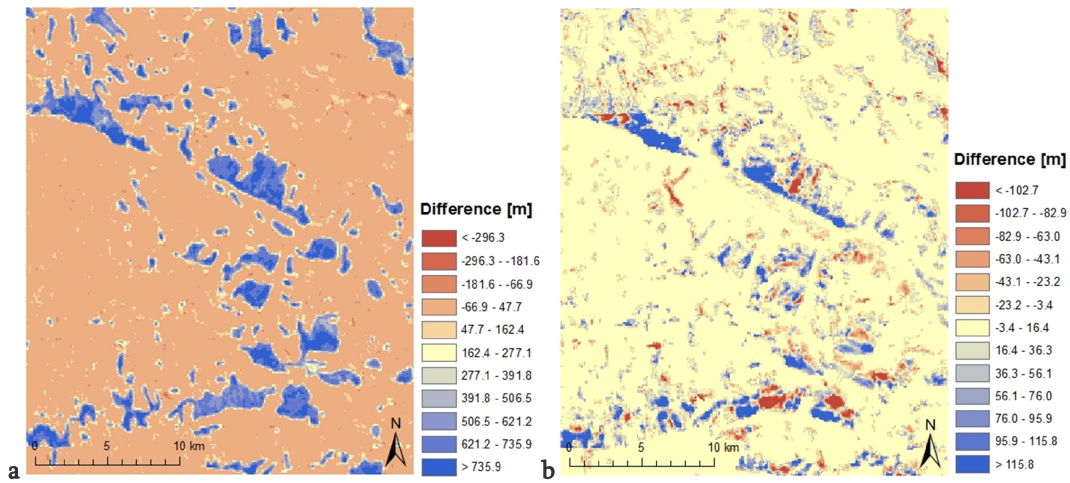
Figure 5.3: Difference images of (a) the SRTM DEM US - SRTM DEM CGIAR and (b) the SRTM DEM US - SRTM DEM USGS in the region of the Parbati Valley.

Table 5.1: Statistic values of the DEM differences.

	SRTM DEM US - ASTER GDEM2	SRTM DEM US – SRTM DEM CGIAR	SRTM DEM US - SRTM DEM USGS
min	-259	-380	-370
max	268	1'075	677
mean	-9.21	105.12	6.52
Std dev	24.22	229.38	39.74

Out of the different SRTM DEMs (US, CGIAR and USGS) the ice thickness was modeled with the GlabTop model and compared to the GPR profiles, taken at the Chhota Shigri in 2009 by Azam et al. (2012).

Figure 5.4 shows the modeled ice thickness along the profile 3, produced with the different DEMs (see Figure 3.8 for the location of profile 3). The violet line represents the GPR profile of Azam et al. (2012) as the ground truth. The ice thickness of the GlabTop output calculated with ASTER GDEM2 (blue) (30 m resolution) shows a relative unsatisfactory result. The GlabTop modeling with ASTER GDEM2 is not discussed in further detail and is just shown

for the sake of completeness. The comparison in Figure 5.4 shows nearly equal ice thickness for the version with CGIAR and USGS but a quite different one for the version with the SRTM DEM US. The modeled ice thickness with the SRTM DEM CGIAR and USGS differs by an average of 51.64 m respectively 52.75 m from the GPR profile. The ice thickness modeled with the SRTM DEM US, however, deviates only by an average of 7.87 m from the GPR profile.
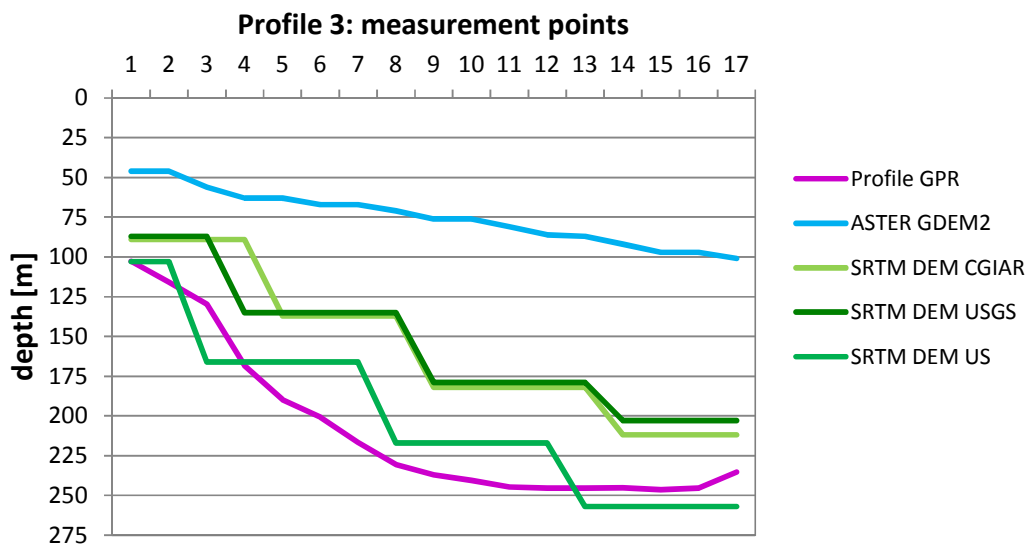
Figure 5.4: Ice thickness outputs from GlabTop modeling with different DEMs compared with the ground truth of the GPR profile 3 at Chhota Shigri Glacier.

Similar to Figure 5.4 the GlabTop the ice thickness was calculated with the different DEMs for the other three GPR profiles (appendix). To sum up, from the total four GPR profiles, SRTM DEM US for three profiles shows the most similar ice thickness output compared to the ground truth. The Table 5.2 shows the statistic values of all four profiles together and demonstrates the suitability of the SRTM DEM US.

Table 5.2: Statistic values of the differences between the measured GPR ice thickness and the the modeled ice thickness, depending on the input DEM.

	GPR-ASTER diff	GPR-CGIAR diff	GPR-USGS diff	GPR-US diff
tot. min	-2.45	5.1	15.8	-36.2
tot. max	164.60	143.17	255.9	127.17
tot. mean	91.23	73.01	102.59	53.56
tot. std dev	10.76	4.52	10.35	5.46

5.2   Inventories

5.2.1   Glacier per size class and aspect sector

After the automated glacier mapping and the manual corrections, the separation of the glacier at their individual drainage divides and the generation of the topographic glacier parameters etc. for the years 2002 and 2013 all levels from 0 to 3 (end product) were generated (described in section 4.2). In this section, the level 3 of both inventories is described and presented in detail.

For the year 2002, in total 697 glaciers larger than 0.02 km² were mapped. They covered an area of 590.04 km². All polygons smaller than 0.02 km² were neglected. For the year 2013 627 glaciers were mapped, which cover an area of 581.78 km². The glaciers and their parameters were divided in different size classes or grouped in their ordinal direction, the aspect sectors. The boundaries of the size classes are chose according to Paul et al. (2011), the categories "reflect well the general characteristic of most glacierised mountain ranges, with abundant small glaciers present in regions with a few larger ones". The following number and percentage values can be seen in the Figure 5.5 and Figure 5.6 and also in two additional tables in the appendix.

Results

Figure 5.5 shows the part of the total number or area per size class for the years 2002 and 2013. The asymmetry between the number and the area of the glaciers in the smallest size class is visible.
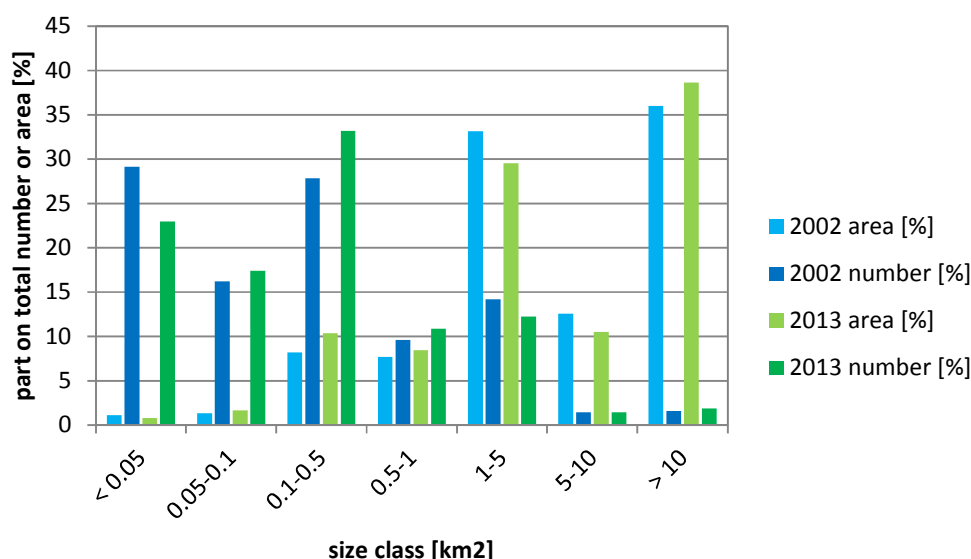
Figure 5.5: Part on total number of glaciers or area per size class in 2002 and 2013.

The majority of the glaciers were smaller than 1 km^2; in the year 2002 577 (82.78%) and in the year 2013 529 (84.37%) glaciers. In the year 2002, all glaciers smaller than 1 km^2 covered 107.94 km^2 (18.29%), and in the year 2013, they had a total area of 124.07 km^2 (21.33%).

In the following, the percentage changes between the years 2002 and 2013 are compared per size class. Firstly, the number of glaciers and afterwards the area they covered per size class is examined.

The percentage of the glacier <u>number</u> per size class < 0.05 km^2 decreased from 2002 to 2013 (−6.16%), while the size classes 0.05-0.1 km^2 (+1.17%), 0.1-0.5 km^2 (+5.34%) and 0.5-1 km^2 (+1.23%) grew. The size class 1-5 km^2 decreased slightly (−1.92%), while size class 5-10 km^2 (+0.001%) and >10 km^2 (+0.34%) remained about the same.

Concerning the percentage of the glacier <u>area</u> per size class, the class <0.05 km^2 (−0.31%) and 0.05-0.1 km^2 (+0.33%) remained more or less at the same level. The size class 0.1-0.5 km^2

(+2.21%) increased, as well as the class 0.5-1 km^2 (+0.81) albeit considerably lower. In the size class 1-5 km^2 the percentage of the glacier area decreased from 2002 to 2013 (–3.59%) as well as in the size class 5-10 km^2 (–2.09%). The size class > 10 km^2 recorded a surprising increase (+2.65%), because one glacier of the second largest size class changed to the largest one from the year 2002 to 2013.

As above introduced, the number and the area of the glaciers is hereafter also examined per aspect sectors. A clear statement concerning the distribution of the glacier number, depending on the aspect sectors for the years 2002 and 2013, is rather difficult (Figure 5.6). Generally, there were more glaciers in the northern and western sectors.
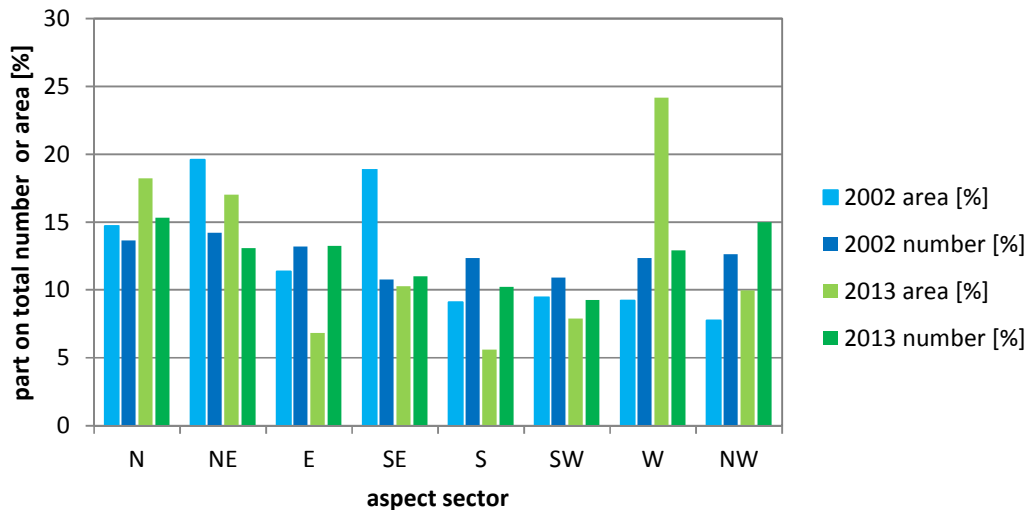
Figure 5.6: Part on total number of glaciers or area per aspect sector in 2002 and 2013.

Concerning the area of the glaciers for 2002, there was a maximum in the north-eastern (115.6 km^2, 19.5%), followed by the south-eastern sector (111.2 km^2, 18.4%). A minimum was situated in the north-western sector (45.7 km^2, 7.7%). In the year 2013, the western sector showed a clear peak of percentage area (140.7 km^2, 24.18%) but also the northern (106.0 km^2, 18.2%) and the north-eastern sectors (98.9 km^2, 17.0%) showed a high percentage of the glacier area. In the year 2013 the glacier coverage was smallest in the southern sector (32.6 km^2, 5.6%).

One has to keep in mind, that the pictured increases or decreases per size classes and aspect sectors respectively are percentage and not absolute glacier areas. Whereas all values with unit km² are changes of the absolute glacier area and are shown later in section 5.4.

5.2.2 Hypsography

An investigation of the spatial distribution of the glaciers on a vertical scale can be seen in the Figure 5.7. This figure shows the glaciated area in km² per 100 m elevation band from 3,500 to 6,500 m a.s.l.. The dark and light blue lines illustrate the total glaciated areas in the year 2002 respectively 2013. The dark and light green lines represent the areas covered by clean ice only (without debris-covered parts) of both years, 2002 respectively 2013. Additionally, the dark and light brown lines constitute the debris-covered areas in the two years. In both years, 2002 and 2013, the maximum of the glaciated area was situated at an elevation of 5,100 m a.s.l.; the area was bigger in 2002 (69.95 km²) than in 2013 (67.44 km²). The total glaciated areas varied between the two investigated years at elevation bands from 4'800 m a.s.l. to 5'200 m a.s.l (on average 2.78 km² per elevation band). The vertical distribution above 5'200 m a.s.l. did not change considerably between 2002 and 2013 (on average 0.43 km² of decrease per 100 m elevation band).

The area of the clean ice was almost identical in the years 2002 and 2013 (dark and light green). A difference over the elevation range from 4'400 m a.s.l. and 4'700 m a.s.l., was only detected where the area in 2013 was larger than 2002 (on average 2.14 km² per 100 m elevation band). Over the elevation range from 5'100 m a.s.l. to 5'300 m a.s.l., the area decreased from 2002 to 2013 around 0.8 km² per elevation band.

The dark and light brown curves show the distribution of the debris-covered area in the two years. A relatively large difference between the two curves can be observed. Furthermore, the area of debris-covered ice was larger in the year 2002.

The debris-cover between 3'500 m a.s.l. and 4'300 m a.s.l. stayed quite the same in both years. Between 4'300 m a.s.l. and 5'200 m a.s.l., the area in the year 2002 (dark brown) was larger (on average 2.26 km² per 100 m elevation band) than in 2013 (light brown).
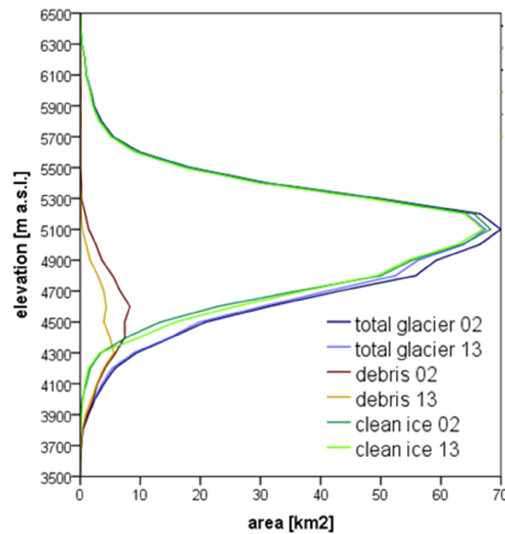
Figure 5.7: Hypsometry of all glaciers in the Kullu study region. The area of the total glaciers in blue, the debris-covered glacier parts in brown and the clean ice glacier parts in green colors.

The curves of both years show a slight peak at the elevation of 4,600 m a.s.l. and a slight depression just beneath 4,500 m a.s.l.. The changes in the debris-cover are presented in more detail in the section 5.4.

In Figure 5.8a, a scatter plot of the mean slope and the area of the glaciers for the year 2002 and 2013 are displayed. It can be seen, that small glaciers are distributed over a great range of slope inclination, while larger glaciers are found often in flatter terrain. Although in the scatter plot of the year 2002 several outliers of large glaciers are on a steeper slope inclination. The investigation of some of these outliers shows large accumulation areas at steep inclinations while the glacier tongues do not reach far down into the valley and the resulting mean slope of the glaciers is due to this lack of the flat valley inclination rather high. This may indicate a recent recession of the glaciers, and the glaciers are not yet in balance. In Figure 5.8b the mean elevation of the glaciers compared to the aspect of the glaciers is illustrated. The mean elevation of all glaciers in 2002 was situated on 4962.36 m a.s.l.. In 2013, the mean elevation was slightly higher on 4988.42 m a.s.l.. In the year 2013 the distribution was more even than in 2002.

In Figure 5.8c, scatter plots of the elevation (m a.s.l.) and the glacier area for the years of 2002 and 2013 are illustrated. One can see the tendency of large glaciers to range over a larger elevation belt. Glaciers larger than 1 km² show different minimum and maximum elevation values, whereas glaciers smaller than 1 km² show overlapping minimum and maximum elevations. A correlation between the mean elevations of the glacier size cannot be derived.

To sum up, the overall characteristics of small glaciers having a lower minimal and maximal elevation, respectively large glaciers having their origin at high elevation and reaching to a lower elevation into the valley, can be seen.
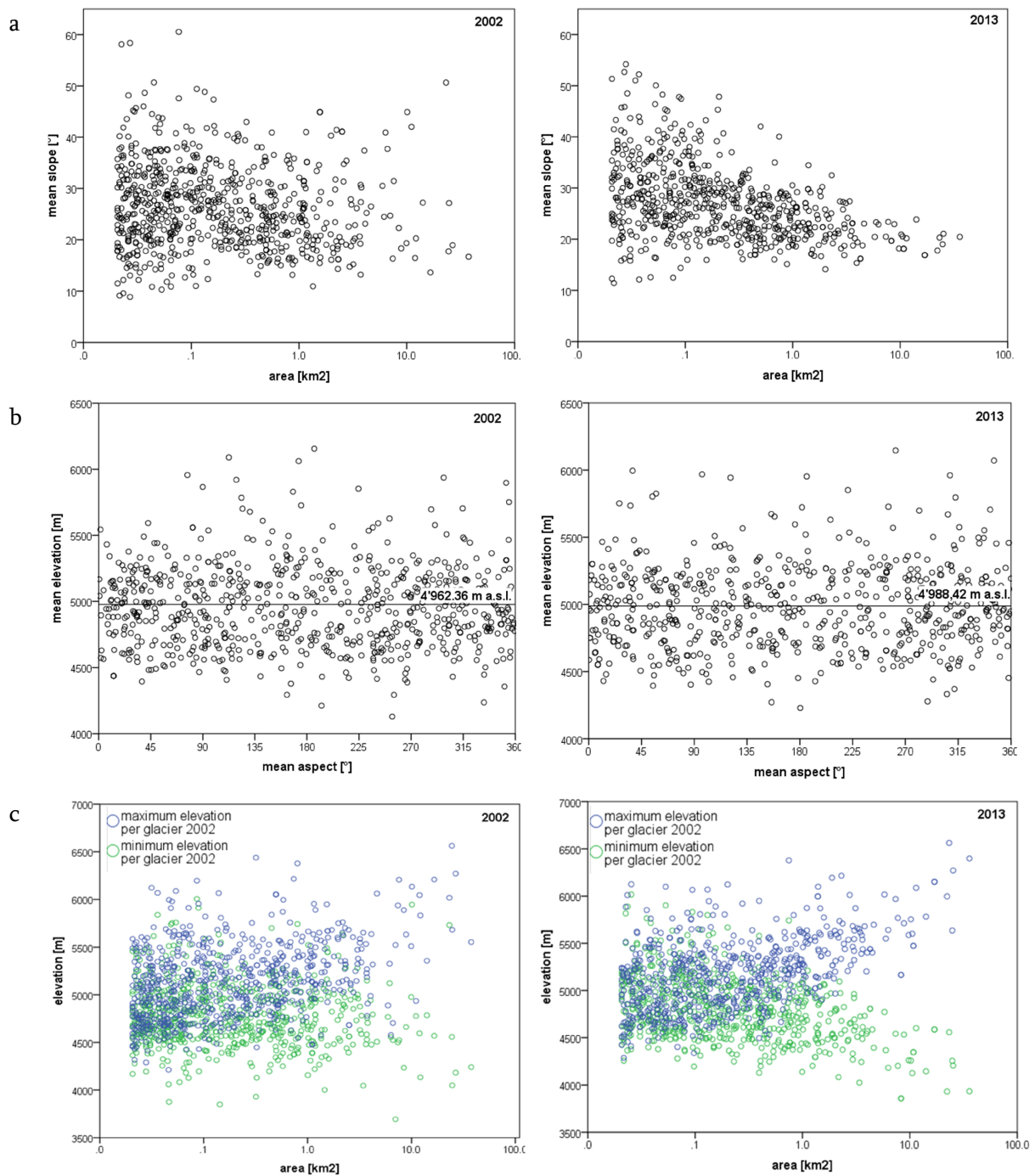
Figure 5.8: Comparison between the inventories of 2002 and 2013 considering (a) the mean glacier slope related to the glacier area, (b) the mean glacier elevation related to the aspect for all individual glaciers and (c) the minimum (green) and maximum (blue) elevation related to the glacier area for the entire sample.

5.3 Ice thickness distribution and total ice volume for the Kullu glaciers

The ice volume was calculated based on the ice thickness distribution output of GlabTop. GlabTop generated a raster file containing the values of the ice thickness distribution per glacier (Figure 5.9). With the mean thickness values and the area of the glaciers, the overall volume of all glaciers was calculated. The total glacier volume of all glaciers in the Kullu District in the year 2002 amounted to 27.82 km³.
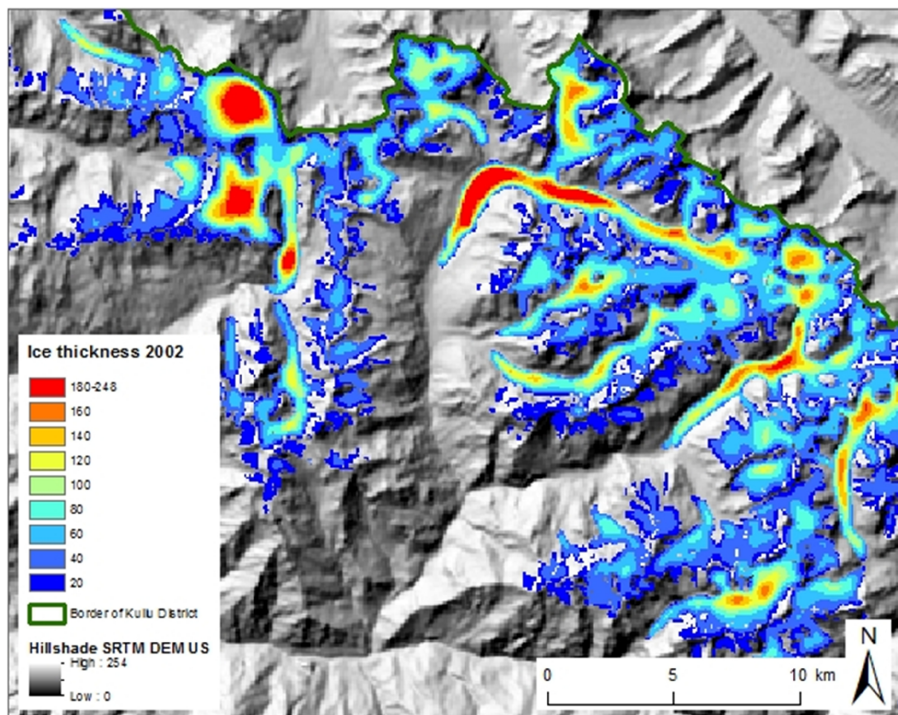
Figure 5.9: ice thickness distribution of the year 2002 modeled with GlabTop. Input parameters were the SRTM DEM US, the digitalized branchlines and the outlines of the inventory of the year 2002.

As comparison, the glacier volume in the Swiss Alps was estimated to 74±9km³ after Farinotti et al. (2009a). The 1483 glaciers cover an area of 1063±10km². The glaciated area of the Kullu District corresponds to 55.5% of the glaciated area of the Swiss Alps and the volume in the Kullu District account for 37.6% to the Swiss Alps.

As input parameters to GlabTop, the SRTM DEM US, the digitalized branchlines and the glacier outlines were used. The SRTM DEM US describes the situation of the year 2000 and is therefore reasonably representative for the inventory of 2002.

The volume of 2013 could not be modeled realistically with the same DEM; hence, a more recent DEM was necessary. A potential DEM from a later time period was the ASTER GDEM2, generated out of stereo images, taken between 2005 and 2009 (section 3.2.1). Unfortunately, the ASTER GDEM2 differs considerably from the SRTM DEM US (section 5.1); thereby a GlabTop run with this DEM would lead to too many uncertainties. Due to the large differences of the two DEMs, it was decided to co-register the ASTER GDEM2 to the SRTM DEM US, in order to reduce the discrepancies out of the different acquisition methods, instruments and georeferencing. This was done by means of the co-registration method, described by Nuth and Kääb (2011). For a proper assessment of the co-registration, only stable terrain areas (no glaciers, no rivers, no artefacts) should be selected and analyzed by the iterative method (Nuth and Kääb, 2011). The co-registration of the elevation data sets, was only partly successful. Nevertheless, it was possible to reduce the bias to some degree and thereby achieve an improvement. In Figure 5.10, the comparison between the two difference images before the co-registration (a) and after the coregistration (b) of the ASTER GDEM2 can be seen. In Figure 5.10a, the voids of the SRTM DEM, filled with the ASTER GDEM2 data in de US version are clearly visible. These areas appear yellow (no difference), because the values in these areas of both datasets, are the same (section 5.1). In Figure 5.10b, the voids are no longer visible as areas of no difference. After the co-registration, the Figure 5.10b showed a greater homogeneity. In addition to that, the relief, which was easily recognizable in the image Figure 5.10a, disappeared to a certain degree in the Figure 5.10b. During this process, the mean of the difference of the pixel between the two DEMs changed from -4.4 to -3.8 m, while the standard deviation remained almost the same (Table 5.3). Despite efforts, no complete satisfying result was achieved with the performance of the co-registration.
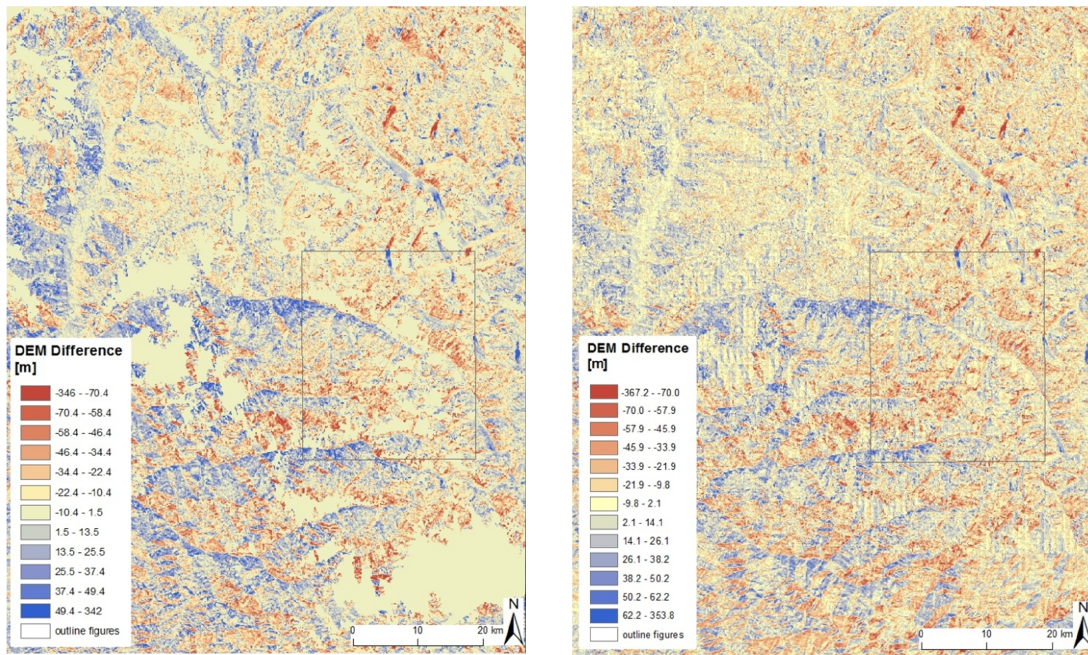
Figure 5.10: DEM difference image of (a) SRTM DEM US and ASTER GDEM2 and (b) SRTM DEM US and co-registered ASTER GDEM2. The rectangles show the location of the Figure 5.2 and the Figure 5.3.

Table 5.3: Statistic values of the difference images before and after the co-registration of the ASTER GDEM2.

	Before co-registration	After co-registration
min	-346	-367.2
max	342	353.8
mean	-4.47	-3.88
Std dev	23.98	24.05

The total ice volume change between the glacier outlines of 2002 and a state between 2005 and 2013 (see section 6.4 for the detailed explanation for this time span) was on the one hand estimated out of the subtraction of the co-registered ASTER GDEM2 from the SRTM DEM

US. The glacier volume change, received out of the subtraction of the two DEMs is –3.73 km³.

And on the other hand the glacier volume change generated out of the GlabTop modeling with the co-registered ASTER GDEM2 as input data, resulted in –2.62 km³. These different values, respectively the used methods are discussed in detail in the section 6.4.

Here, it has to be again mentioned, that the difference images in section 5.1 were made with the SRTM DEM US, without a special void filling with the co-registered ASTER GDEM2.

As one can see in Figure 5.11a, there is a correlation between the glacier size and their mean ice thickness. With a significance level of 0.01 the parameter mean area and mean thickness show a positive correlation (R=0.86). So with an increase in glacier size, the mean glacier thickness increases as well. The Figure 5.11b depicts the relation between the mean ice thickness and the aspect of the glaciers. The statistical evaluation of these parameters resulted in no correlation (R=-0.089)

In the northern sectors of the glaciers the median of the ice thickness was the highest (10.08 m), followed by the glaciers of the south-western sectors (7.42 m), and the southern sectors (7.17 m). The thinnest glaciers were found in the north-western sectors (5.53 m). In all ordinal direction there is a large scattering of the ice thickness values and for the sake of clarity some outliers had to be cut off.

The volume values used in the Figure 5.11d origin from the mean ice thickness values per glacier out of the GlabTop output (with SRTM DEM US). No clear relationship is visible between the mean volume of a glacier and their ordinal direction and a statistic test demonstrated the lack of the correlation between the two parameters (R=-0.094). The median of the glacier volumes in the northern sector shows a significant peak. This is consistent with the largest glacier thickness in the northern sector (Figure 5.11b), as the mean thickness is integrated in the mean volume.
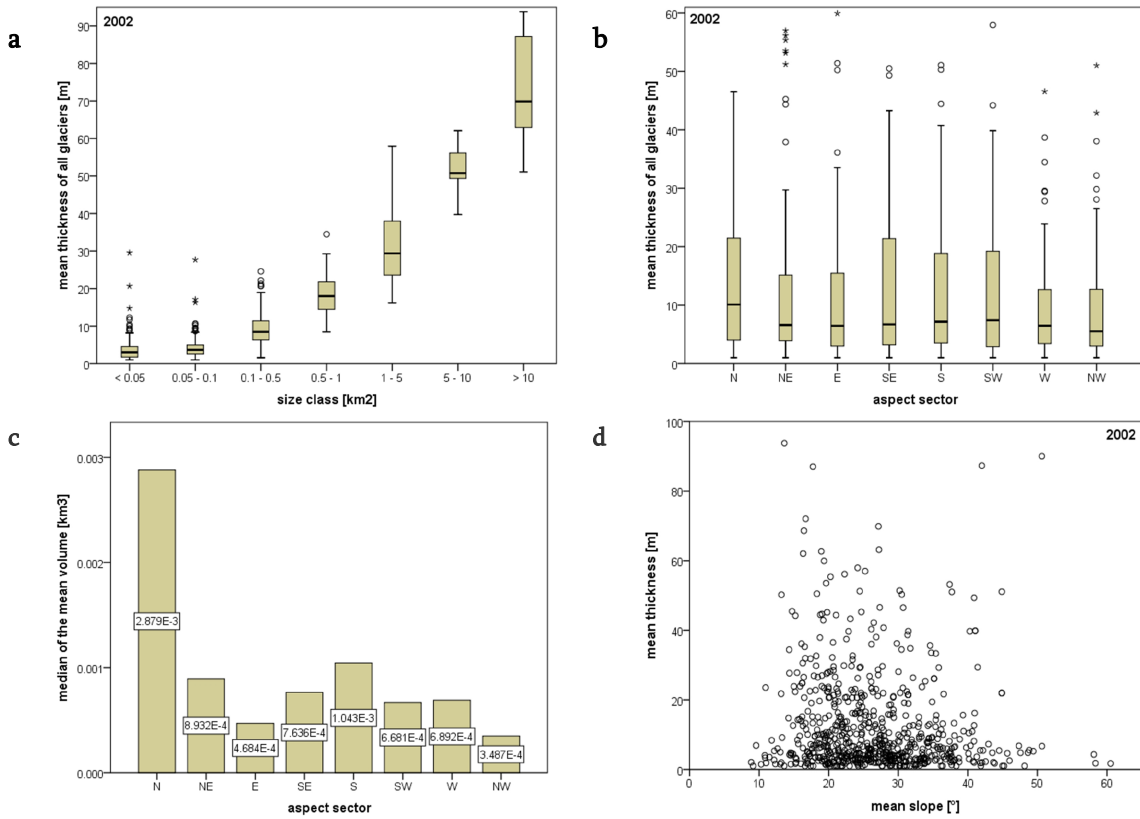
Figure 5.11: Mean ice thickness [m] per size class (a) and aspect sector (b) in the year 2002. (c) mean volume [km³] per aspect sector and (d) mean thickness [m] related to the mean glacier slope [°], 2002.

Figure 5.11d shows the mean thickness in relationship to the mean slope of the glaciers. Thick glaciers tend to be situated in smaller slope inclination, while thin glaciers can also be situated in steep slope. This correlation could be expected to higher (section 6.4). Similarly to small glaciers, thin glaciers are neither linked to a certain slope (compare with Figure 5.8a).

In this section the glacier changes concerning the ice thickness and the total ice volume were treated and discussed in section 6.3. The results of all other changes are shown in section 5.4.

5.4   Glacier changes between 2002 and 2013

As already mentioned in chapter 5.2 the total area of the glaciers in the Kullu District decreased from 2002 to 2013 by around 9.17 km² from 590.04 km² to 581.78 km². In this section a special focus is placed on the area and the debris-cover change between the two inventories. The Figure 5.7 shows that the glacier changes took place below an elevation of 5'200 m a.s.l. and the glaciated area stayed equal above this elevation, due to furthermore optimal climatic conditions for glaciers.

The mean elevation of the glaciers in the Kullu District increased by around 26 m from the year 2002 (4962.4 m a.s.l.) to the year 2013 (4988.4 m a.s.l.). As well as the mean minimal elevation of the glaciers increased by around 160 m between the two investigated years. In the year 2002 the mean minimal elevation was 3694 m a.s.l., in the year 2013 it was 3858 m.a.s.l. The mean maximal glaciated elevation (highest level of the accumulation zone) was on 6563 m a.s.l. in both years.

The Figure 5.12 illustrates the changes in glaciations between the year 2002 and 2013 in the Kullu District. The outlines of the glaciers, shown in the Figure 5.12, Figure 5.13 and Figure 5.15, resulted out of the combination of the glacier outlines of the year 2002 and the outlines of 2013. This is the maximum extension of the overlay of the two inventories and is called the "pseudo outlines" hereafter. Owing to this overlay of the two points in time, one can see the areas of glacier loss as well as areas of glacier growth.
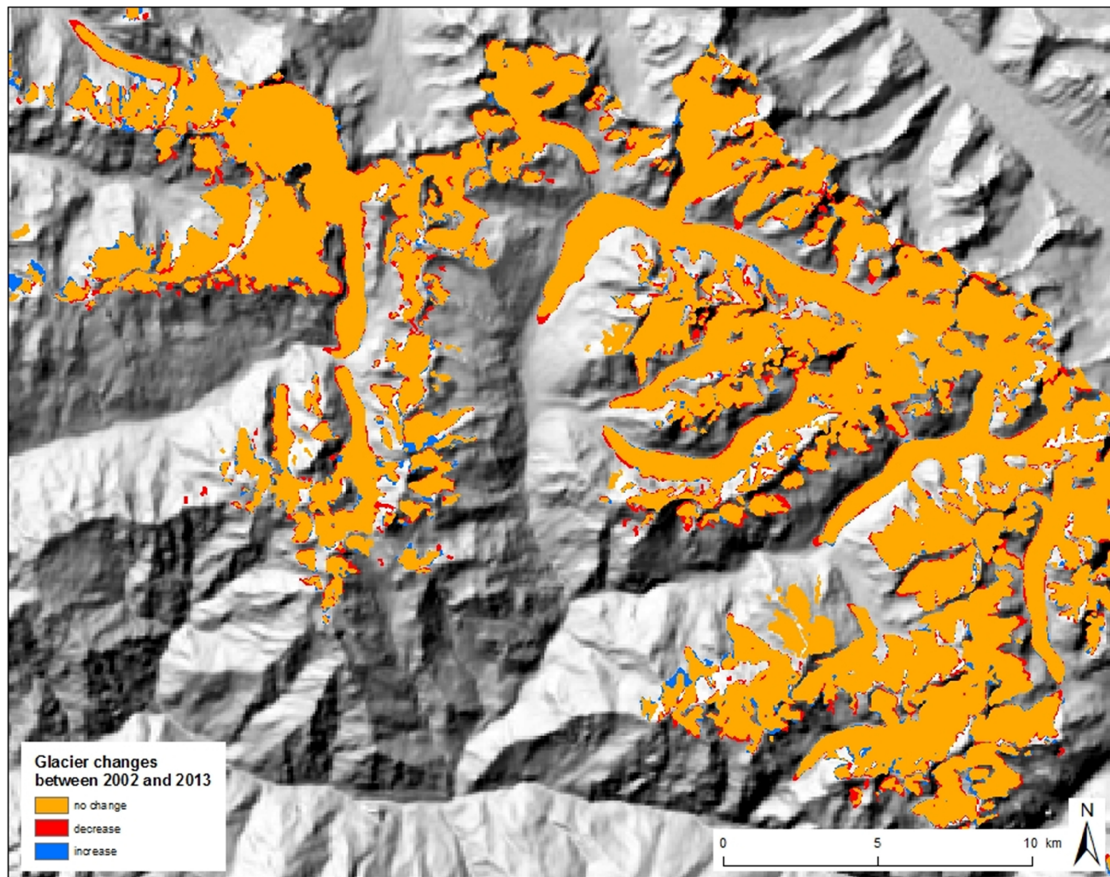
Figure 5.12: Glacier changes between 2002 and 2013.

The Figure 5.12 shows the region of the outline 3 shown in Figure 5.1. The glacier retreat is marked in a red color and is mainly located at the glacier tongues. Areas of glacier growth can be detected as well; these areas are colored blue. The locations of the area increase are rather arbitrary and without any regularity. The orange colored glacier parts have not changed in the period of the years 2002 and 2013.

The Figure 5.13 displays the changes in debris-cover between the years of 2002 and 2013. The areas with a decrease in debris-cover between 2002 and 2013 are marked in red. The areas of increase are colored blue. The orange zones are debris-cover in both years. The areas with a decrease in debris-cover are relatively large. This is consistent with the previous findings described in section 5.2 respectively the Figure 5.7.
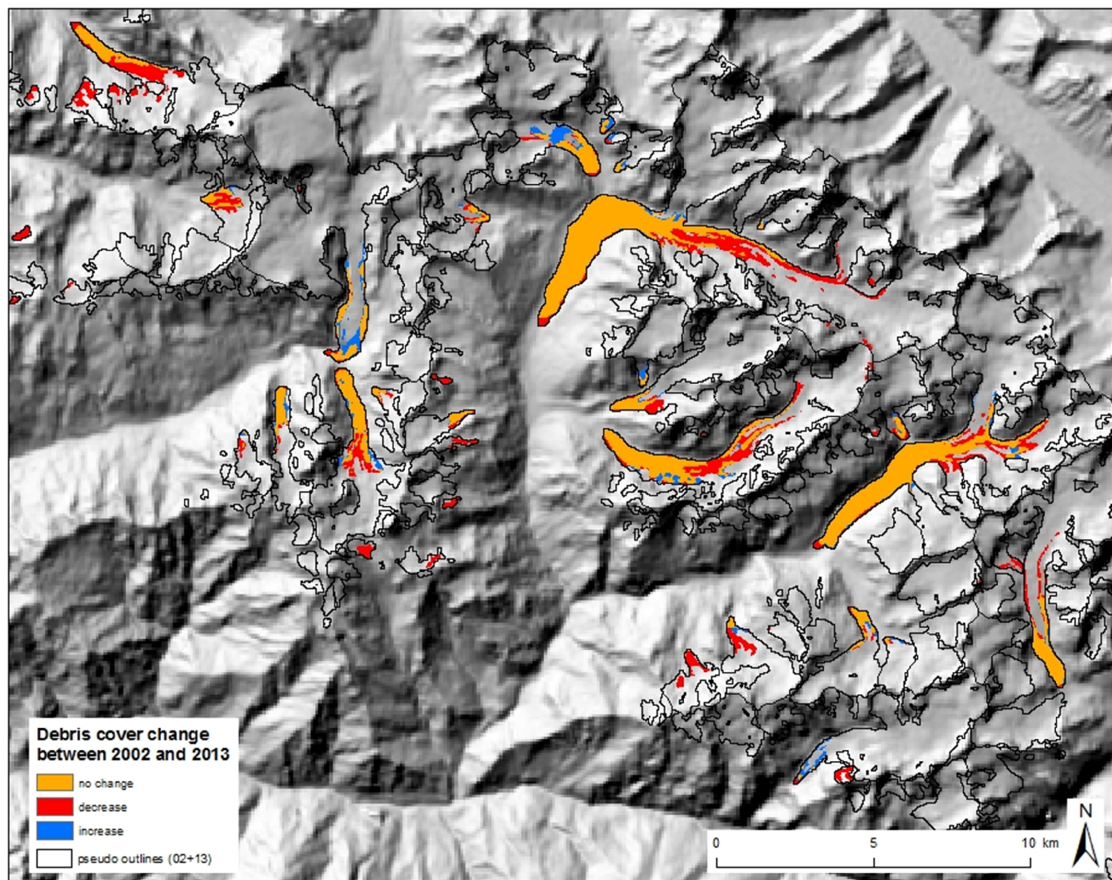
Figure 5.13: Debris-cover change between 2002 and 2013.

The areas of decreased debris-cover at the glacier tongues are mostly congruent with the decrease of the total glacier area in Figure 5.12. The rest of the area with decreased debris-cover is located at the margins to the clean ice. This large change in debris-cover is rather suspicious and was not expected in this magnitude. The possible reason for this debris decrease is discussed in section 6.3.

Figure 5.14 gives a closer look to the hypsometry of the debris-covered glacier areas. The curves are also shown in Figure 5.7, but here, the hypsometry curve of the debris-cover is represented alone. The large difference between the years 2002 and 2013 from 4300 m a.s.l. to 5500 m a.s.l. is obvious. The hypsometry of the glaciers is already described in the section 5.2 and Figure 5.14 is shown as addition concerning the debris-cover in detail.
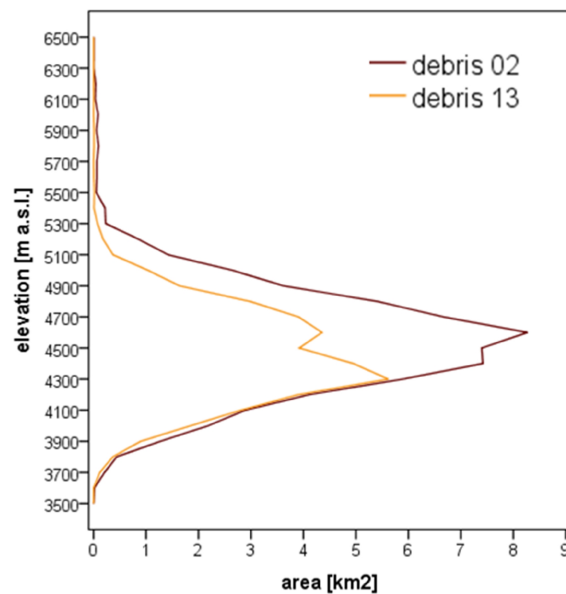
Figure 5.14: Hypsometry of the debris-covered area of all glaciers in the study region.

It is also interesting to have a look at the distribution of the debris in relation to the accumulation and the ablation zones of the glaciers (Figure 5.15). The Figure 5.15 shows the distribution of the debris-cover of the year 2002. The equivalent figure of the year 2013 is added in the appendix. The boundary between the accumulation and the ablation zone is drawn at the mean elevation of the individual glacier, as an approximation to the equilibrium line altitude (ELA) (Bakke and Nesje, 2011). Another method to approximate the ELA of an individual glacier would be the division of the total area of the glacier into 3 parts. The accumulation zone is twice as big as the ablation zone and consists out of two parts. The majority of the debris is situated in the ablation zones. The total debris-covered area reaches 73.16 km² in the year 2002; this were 12.43% of the total glaciated area. In the year 2013 an area of 13.4 km² was debris-covered; this was only 2.3%. In 2002 only 7.81% (5.6 km²) were found in the accumulation zones, while the other 92.19% (66.52 km²) were situated in the ablation zones of the glaciers. In the year 2013 only 1.94% (0.26 km²) of the debris was situated in the accumulation zones, while the majority of 98.06% (13.14 km²) was found in the ablation zones. This large difference of the debris-covered areas between the year 2002 and 2013 is seen in Figure 5.13 and Figure 5.14.
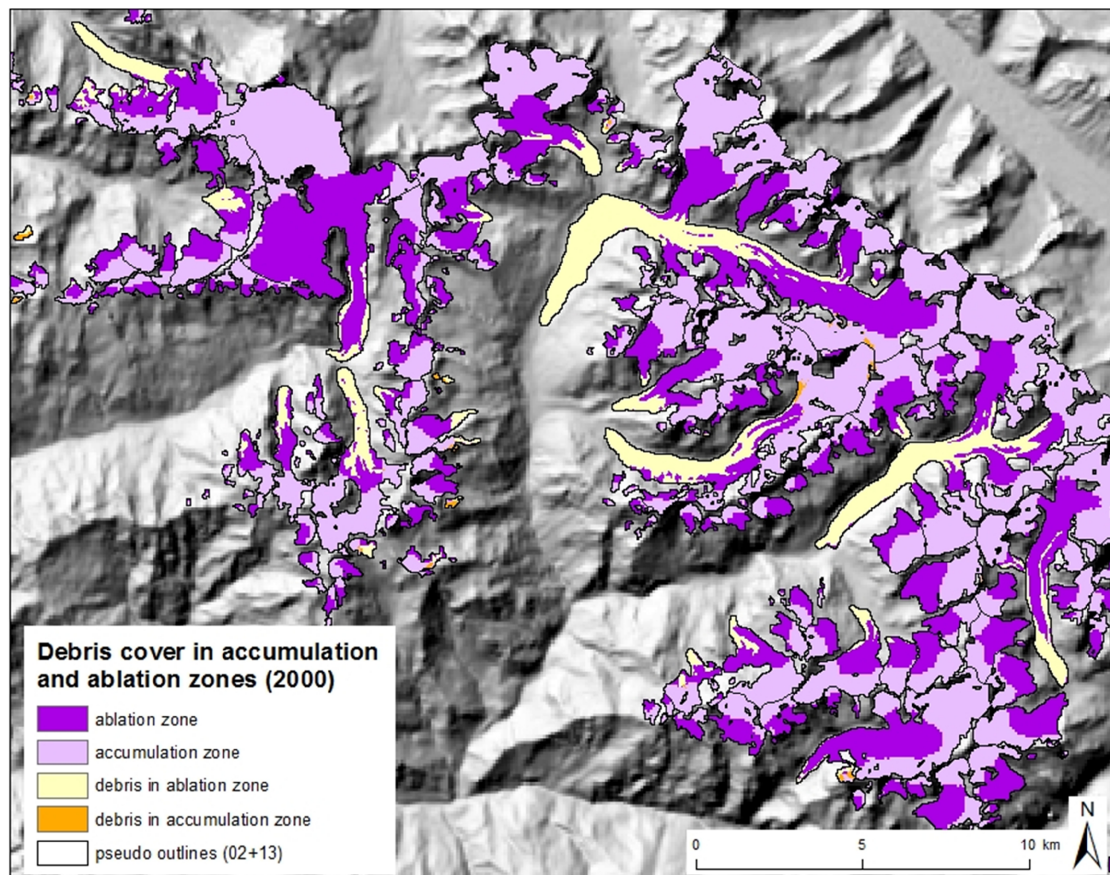
Figure 5.15: Debris-cover in relation to the accumulation and ablation zones of the glaciers (2002).

The debris-covered part of the glaciers is visualized in Figure 5.16a per size class and also shows the larger debris-cover in the year 2002. In both years the glaciers of the two largest size classes (5-10 km² and >10 km²) show the most debris-cover. The relation between the glacier size and the percentage of debris-cover shows no clear correlation. The correlation coefficient for the year 2002 is R=0.339 and for the year 2013 R=0.405, while the null hypothesis is accepted. A relationship between the debris-covered area and the aspect sector in the years 2002 and 2013 cannot be detected and is therefore not shown.
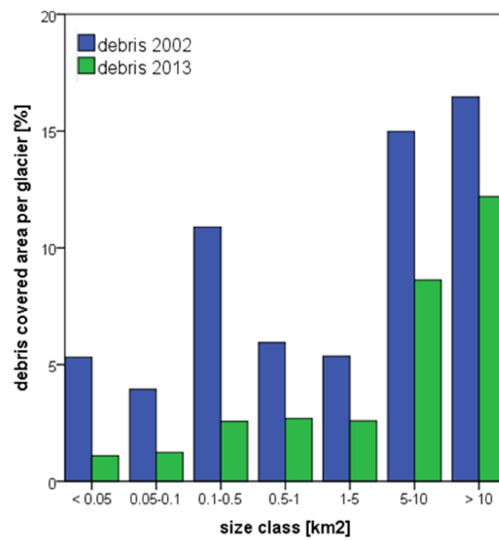
Figure 5.16: Debris-covered area per glacier in percent (a) per size class [km²].

The mean area per size class of the years 2002 and 2013 can be seen in the Figure 5.17a. The figure shows the logical growth in area with increasing size class, because both axes represent the same parameter (self-correlation). The reasons to display this figure are the differences between the mean glaciated areas per size class for the years 2002 and 2013. The changes between the two years are rather small, and the two largest size classes, 5-10 km² and >10 km², were the only two classes with mentionable changes. The second largest size class lost one glacier (10, 9) from the year 2002 to the year 2013 and decreased from a mean area per glacier of 7.43 km² to 6.78 km² (-0.64 km²). The largest size class gained one glacier (11, 12) but decreased from 19.29 km² to 18.72 km² (-0.57 km²) as well. This decrease is also seen in the Figure 5.18a.
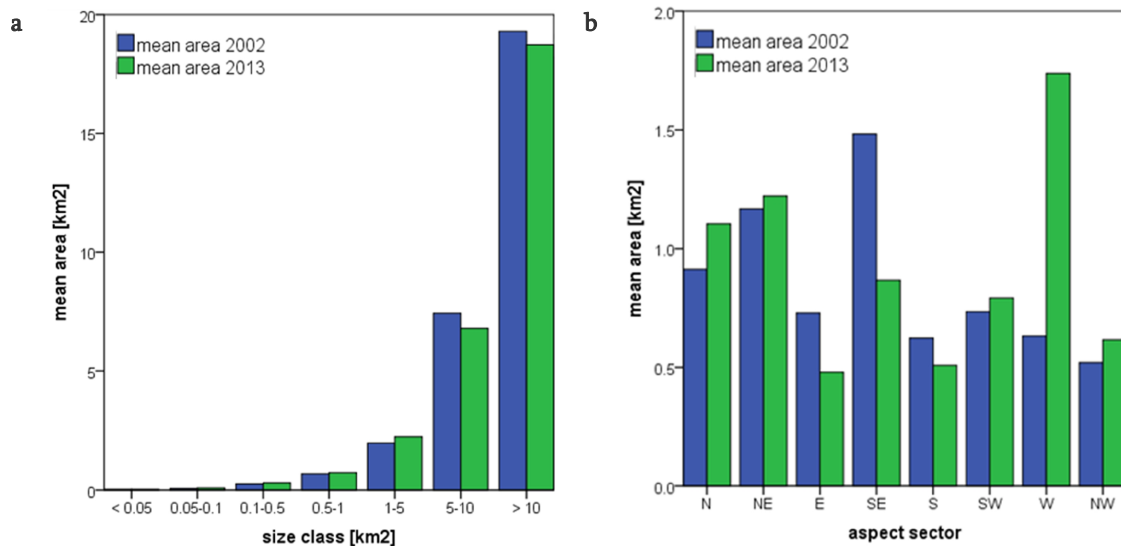
Figure 5.17: mean glacier area of 2002 and 2013 (a) per size classes and (b) per aspect sector.

Figure 5.17b shows in the year 2002, a mean area in the south-eastern sector which is significantly higher than in the other sectors (1.48 km²). The mean glacier area in this sector in 2013 is only 0.86 km², but therefore the western sector shows a significantly increase in from 0.63 to 1.73 km² from 2002 to 2013. The other sectors have the same order of magnitude in both inventories. And the north-eastern sector shows a relatively large mean area in both years.

It has not yet been looked at the absolute changes between the years 2002 and 2013 concerning the area of the glaciers and the debris-cover changes. To get the absolute change, the year 2002 was taken as the reference year. This means that all the changes were calculated relative to the state of the glaciers in the year 2002. In the Figure 5.18a, the absolute changes of the mean glacier area between the years 2002 and 2013 per size class are shown. The change of the mean glacier area within the smallest size class is zero, while the second, third and fourth size class depict a small increase. The glaciers of the size class 1-5 km² show an increase in 0.26 km² on average. The glaciers in the two largest size classes depict a decrease in -0.64 and -0.57 km² on average. It was already addressed to this decrease in Figure 5.17a. Figure 5.18b represents the changes of the mean area per glacier compared to

their aspect sector. In the western sector the mean area increased by 1.11 km² per glacier. In the eastern, south-eastern and southern sectors the glaciers decreased by -0.25, -0.62 and -0.11 km². The northern sector shows a small increase in 0.19 km², while the changes in the other sectors are negligible. The bar graph in Figure 5.18c depicts the percentage change in debris-covered glacier area per size classes of the glaciers. The overall decrease between the year 2002 and 2013, mentioned before, appears at first sight. The glaciers of a size between 0.1 and 0.5 km² lost the most of debris-cover (-8.33%). The second most debris-cover decrease is found in the size class 5 – 10 km² (–6.37%), followed by the smallest size class < 0.05 km² (–4.23%).
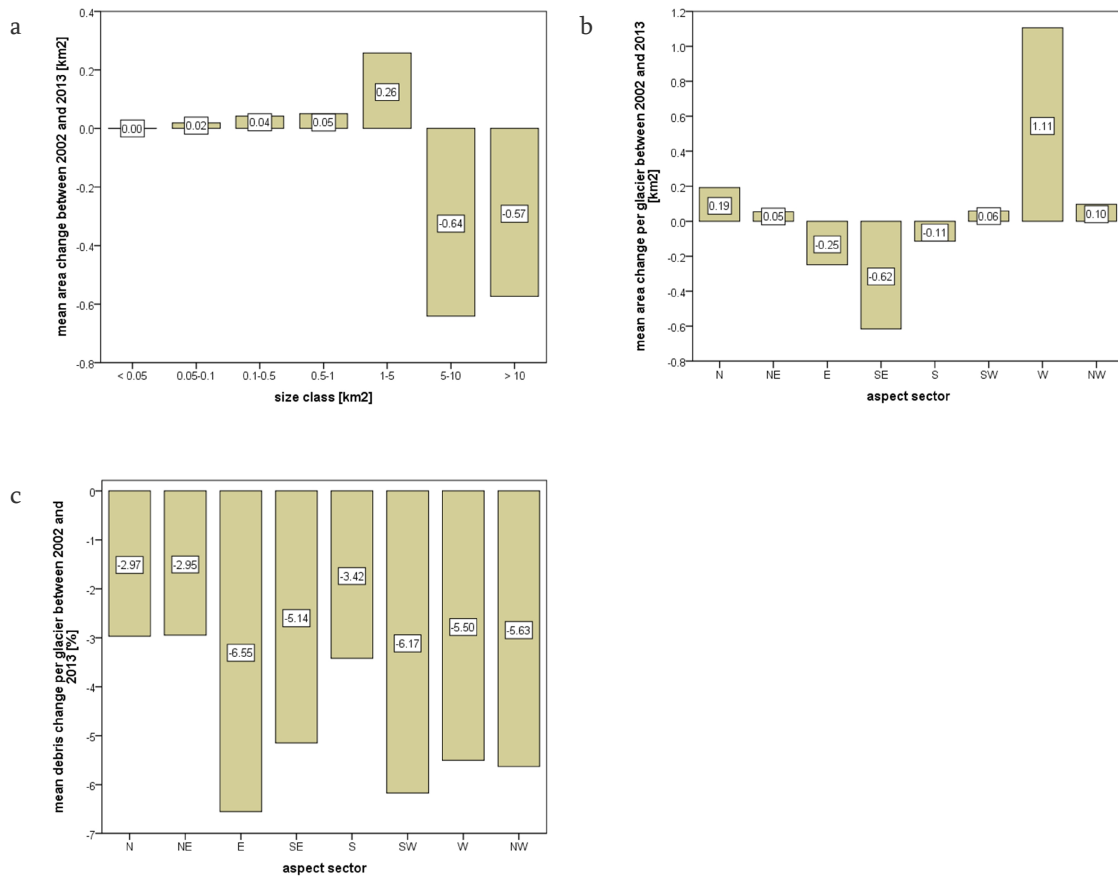
Figure 5.18: (a) Mean area and (b) debris change between 2002 and 2013 per size classes and aspect sectors and (c) mean debris changes per size classes.

6. Discussion

6.1   Comparison of the different DEMs

Because the SRTM DEM has a clear recording date (February 2000), close to the first inventory of 2002, this DEM was preferred over the ASTER GDEM2, even though the resolution of 90 m is not as good as the one of the ASTER GDEM2 with a 30 m resolution. As in section 3.2.2 mentioned, the SRTM has data voids over a large part of the Himalayas and there already exist different void-filled versions. The fact is that the SRTM DEM void filled version of CGIAR, with its crater-like depressions in the filled voids (Figure 3.4), is relatively poor and not suitable for further studies and calculations in the region of the Kullu District. Compared to the void-filled version of CGIAR (Figure 3.4), the version of USGS (Figure 3.5) does not show such a crater-like landscape. Therefore, the filling appears more reliable. The idea to fill the voids in the context of this study with data of the ASTER GDEM2 (e.g. Kääb, 2005) arose even before the other existing void-filled version of USGS (Figure 3.5) was downloaded.

The comparison with the GPR profiles of the Chhota Shigri showed that the GlabTop ice thickness with the SRTM DEM US was more accurate than the SRTM DEM USGS (Figure 5.4). A closer consideration of the Figure 3.5 showed as well some fuzziness in the area of the data voids of the SRTM DEM USGS, so the filling with the ASTER GDEM2 delivered clearer results. Based on the comparisons with the GPR profiles, it was decided to do the further investigations with the SRTM DEM US.

Another advantage of the usage of the improved void-filled version generated in this study, was the fact, that the void interpolating methods of the other two versions (CGIAR, USGS) were only poorly documented (Burns and Nolin, 2014).

One has to be kept in mind, that the comparisons of all these different DEMs just allow a relative statement concerning their accuracy, because none of them can be taken as an absolute reference DEM (Kääb, 2005). It was decided to generate difference images between

Discussion

the SRTM DEM US and the other relevant DEMs to make statements concerning their usability for compiling glacier inventories and the determination of the glacier volumes.

The deviations in the difference image between the SRTM DEM US and the ASTER GDEM2 (Figure 5.2) were more diverse than in the image of the subtraction of SRTM DEM CGIAR from SRTM DEM US (Figure 5.3a) or the difference image between SRTM DEM US and SRTM DEM USGS (Figure 5.3b). The cause therefore was, that the ASTER GDEM2 has been acquired in other years and with other techniques than the SRTM DEM (Rexer and Hirt, 2014). A reason for the visibility of the relief in the difference image of ASTER GDEM2 and SRTM DEM US in Figure 5.2 was a slight shift between the two datasets, which caused that one valley site appeared red (negative) and the other blue (positive) (Racoviteanu et al., 2009). As mentioned in the section 5.1, glaciers show yellow to blue colors in the difference image (Figure 5.2), and the blue color could indicate the lowering of the glacier surface between the two acquisition years. The SRTM was collected in February 2000 while the ASTER is compiled of various images taken between 2005 and 2009. In the section 6.4, the topic of the difference between the two SRTM DEMs and the ASTER GDEM2, respectively the co-registered ASTER mentioned below, is discussed in more detail, also with regard to the ice volume estimation based on the surface lowering between the datasets.

Additional to the comparisons with the GPR profiles (Figure 5.4), the decision to work with the SRTM DEM US was also based on the parallel comparison of the difference images (Figure 5.2 and Figure 5.3a,b) and the hillshades (Figure 3.4, Figure 3.5 and Figure 3.7). The SRTM DEM US shows a relatively even course of the terrain and all the other investigations showed also a good suitability for the planned aims.

The co-registration of the ASTER GDEM2 described in section 5.3, was partly successful. For a future use, the SRTM DEM with voids should be filled with a co-registered ASTER GDEM2 dataset from beginning onwards (Kääb, 2005). In this study, the co-registration was done only within the framework of the thickness modeling and volume estimation, which will be discussed in the section 6.4. Because the SRTM DEM US was also a basis for the generation of the glacial parameters of the inventories, it can be concluded that the results may had been a

little bit different, if the co-registration of the ASTER GDEM2 would had been done before the void-filling process of the SRTM DEM. However, because the main focus of this study was on the compilation of the glacier inventories and the need of the co-registration got obvious only in the course of the work, it was decided to use the co-registered ASTER GDEM2 only for the mentioned volume change between the two inventories. The topic of the glacier volume and ice thickness distribution estimations is treated in the section 6.4.

6.2 Challenges and findings of the compilation of a glacier inventory

In this study the glacier mapping was done with Landsat data. The first time-consuming and challenging step in order to compile a glacier inventory was the selection of appropriate Landsat satellite scenes. The oldest found scene in the GLOVIS catalogue was one from the 15th of November in 1972 of Landsat 1 MSS. Unfortunately, the scene showed an insufficient quality due to seasonal snow coverage and a resolution of 79m. Since 1998 the region of Himachal Pradesh was covered form Landsat 5 TM in more or less regular intervals. In 1999 Landsat 7 ETM+ was launched and covered the region as well. But the scan-line corrector (SLC) failure of Landsat 7 ETM+ in May 2003 caused data gaps in the scenes and they were not suitable anymore for glacier mapping.

The requirements to be fulfilled of the satellite scene, in order to compile a glacier inventory, are firstly, a minimal cloud cover. This because the passive optical sensor is not able to penetrate through cloud cover, unlike radar is (Rosenfeld, 1984). Secondly, the snow cover should be as low as possible (Le Bris et al., 2011), because the sensor cannot distinguish between seasonal snow and snow-covered ice. Therefore, it is important, that the glacier mapping is based on a scene taken at the end of the ablation period with no or at least little seasonal snow and no snowfields connected to the glaciers (Paul, 2006).

It was set as target to elaborate one inventory for the year 2013 with data from the Landsat 8 OLI sensor, which was launched in February 2013. The scene in the year 2013, which fulfilled the criteria mentioned the best possible, was acquired the 27th October 2013. Because

the ultimate goal of this study was a change assessment between the two compiled inventories, it was strived for a time span as big as possible between them. The satellite scene which fulfilled the criterion of the recording date, and met the above mentioned conditions as well, was a scene of the second of August 2002. This scene showed optimal weather conditions with few clouds over the glaciated areas in the Kullu District and a marginal seasonal snow coverage.

It was accepted that the two chosen scenes were recorded once in August and once in October. This difference was not optimal because of the seasonality. It can falsify the interpretation of the change assessment, but this could not be prevented.

To generate two inventories which are appropriate for a change assessment, it is important, that they are elaborated by meeting particular criteria. The importance of taking into account these certain factors turned out in this study during the compilation of the inventories. In the following, the important points are mentioned and their relevance for the change assessment is discussed. As already mentioned at the beginning, the satellite scenes should be taken around the same date in year and show little snow and cloud cover. But there are some other factors which must be considered during the generation of an inventory. The glacier delineation has to be built on the same glacier basins as former inventories (Svoboda and Paul, 2009). If they are not identical, the glacier polygons get divided at a different position and the individual glaciers will have various areas, without any real glacier change. For the basin generation, the semi-automatic approach described by e.g. Bolch et al. (2010) or Schiefer et al. (2008) was attempted in this study. The results were not satisfying due to large errors in the accumulation regions (e.g. sliver polygons along the glacier divides) (Figure 4.4). These discrepancies date from the inaccuracies of the DEMs in the regions of steep topography. Because of the useless results, it was decided to work with the basins from Frey et al. (2012). Firstly, they tried the described semi-automatic approach as well, but were neither satisfied, so they corrected the basins manually. For this study, their dataset was taken and adapted to the inventories of 2002 and 2013. With this way of proceeding, the comparability of the two inventories concerning their drainage divides was ensured. Many of

the individual and independently compiled inventories do not fulfill this criterion, and should be excluded from the use for change assessments or at least any changes in the regions of the ice divides ignored (Paul et al., 2007; Racoviteanu et al., 2008a). For the compilation of a single new inventory of a region, for which already a former glacier inventory exists, it is recommended to adapt the divides to the older ones, so nohting would stop the potential future comparison (Racoviteanu et al., 2009).

The best way to prevent potential inaccuracies is, when the same person compiles the inventories, which shall be compared with each other (Racoviteanu et al., 2009). As Andreassen et al. (2008) and Paul et al. (2013) describe, that small glacier changes from 2 to 5% may result from differences in snow conditions at the acquisition time or from the interpretation of the operator and not from real changes. The differences in area tend to be larger by glaciers with debris-cover than by such without debris-cover. The differences can be reduced by a comparison with some high-resolution data from e.g. GoogleEarth (Paul et al., 2013). Raup et al. (2007) found also inaccuracies by working with different analysts trying to analyze non-uniform glacier outlines. This highlights the importance of the careful interpretation of inventories done by different experts out of non-comparable data.

Human inspection is also required by to control the automated mapping of the clean glacier ice, where the threshold, applied on the ratio image, has to be determined (Paul and Andreassen, 2009). This potential difference of interpretation was accepted in this study. The thresholds of the inventory of the year 2002 were indirectly assumed from Frey et al. (2012) by working with their dataset. This difference is estimated to be rather small, and because of the revision of the outlines of the total glaciers, the difference out of the thresholds should be eliminated concerning the area of the total glaciers. The probable residual difference regarding the debris-covered glacier area is treated in the section 6.3.

For an easy comparison the glaciers should have the same identification numbers in both inventories – this was the case in this study. All glaciers that disappeared in the study, their numbers also disappeared. And all glaciers which have newly formed, for example through glacier fragmentation, got a new identification number. With this numbering system it is not

possible to keep track on the "parent glacier relations" when glaciers got split off. The numbers were called individual identification numbers (IID) in this study. The numbering of the glaciers is also seen as a big challenge for the comparison of different inventories by Andreassen et al. (2008). To ensure this criterion, some investment in time is essential, but it is worth it in any case.

The topographic glacier parameters were calculated based on DEM, in this study of the SRTM DEM US. The quality of the glacier parameters are just as accurate as the DEM they are based on (Frey and Paul, 2012; Paul et al., 2009). In this study, for both inventories the same DEM was used, in order to avoid the inaccuracies of using different DEM references. The topographic parameters were stored in the attribute tables of the inventories, together with the IID of the glaciers. Such attribute tables form the heart of glacier inventories and contain much important and useful information and build the base of the followed change assessments.

6.3 Change assessment

To calculate the changes of the glacier area and the debris-cover illustrated in Figure 5.18, the inventory of 2002 was taken as reference year. This means that, the differences of the inventory of the year 2013 were calculated relatively to the inventory of the year 2002. It is demonstrated numerically, that the total glaciated area decreased from 2002 (590.04 km³) to 2013 (581.78 km³) but also visually in the Figure 5.12 and Figure 5.18a. Concerning the glacier area the main change was found in the size class 5-10 km² (-0.64 km³ on average). Let there be no confusion on the fact that this size class shows an area increase from the year 2002 to 2013 in Figure 5.5. This contradiction dates from the different units on the axes of the figures. In Figure 5.18a the mean area change per size class [km²] between the years is shown and in the Figure 5.5 the part on the total area [%] per year can be seen. The total area loss of 8.22 km² ice in the eleven years from 2002 to 2013 corresponds to a decrease in 1.042%, means 0.13% year $^{-1}$. The glacier area changes found in this study are consistent with

other studies carried out in the Himalayas. Bhambri et al. (2011) examined the glacier changes in the Garwahl Himalaya and found an area decrease in $0.12 \pm 0.07\%$ year $^{-1}$. Kulkarni et al. (2011) as well wrote of a glacier retreat in the Indian Himalaya of 0.2-0.7% year $^{-1}$. Bolch et al. (2012) summed up the results of various studies in the Himalayas and conclude that there is, notwithstanding the huge regional variability and uncertainties, a uniform picture of net area loss in the most parts of the Himalayas.

The glacier hypsometry in Figure 5.7 and in Figure 5.15 show a significant deviation of the areas covered with debris. While the debris-cover decreased from the year 2002 to the year 2013, the part covered by clean ice relatively increased. The increase in clean ice (+2.14 km² per 100 m elevation band) from the year 2002 to 2013 between an elevation of 4,400 and 4,700 m a.s.l. and the slight increase in the total glacier (+1.11 km² per 100 m elevation band) compensate the decrease in the debris-cover in this elevation range (-3.15 km² per 100 m elevation band). The reason for the debris-cover decrease has therefore mainly to be identified in the mapping process or the quality of the input data and not in a real decrease, due to an environmental change.

In 2002 12.43% of the glaciated areas were covered with debris. In the year 2013 only 2.3% debris-cover was mapped. The percentage of the year 2002 (12.43%) is consistent with the findings of Frey et al. (2012), which found debris-covered parts slightly below 15% in the western Himalayas. The debris investigated in this study was supraglacial debris-cover. The debris affecting glaciers can also be inside the ice (englacial) or below the glacier (subglacial), as well as beside the glaciers. The debris-cover notably influences the glaciers in respect of the melting or the movement process (Bolch, 2011; Kirkbride, 2011). The sources of the debris are e.g. rock falls, ice, snow or rock avalanches or debris flows and the amount of the debris depends on the weathering and the erosion rate of the surrounding rock walls (Bolch, 2011; Hambrey et al., 2008; Maisch et al., 1999). The debris found in the Kullu District is mostly covering the whole or substantial parts of the glacier tongued, due to the low surface slope values (Paul et al., 2004). That the majority of the debris-cover is found in the ablation zones of the glaciers (Figure 5.15), quite likely has the reason that debris deposited in the

accumulation zones of the glaciers gets covered with snow and is incorporated into the glacier (englacial debris). The debris deposited in the ablation zones remains in contrast on the glacier surface (Bolch, 2011). The development of the typical moraines (side-, medial-, end-) out of the transported respectively deposited debris was not investigated in this study.

Bolch and Kamp (2006) stated that a glacier retreat often causes a relative increase in debris-covered areas. This criterion was definitely not fulfilled for the glacier retreat between 2002 and 2013 in the Kullu District. The large debris-cover decrease cannot be realistic and is explained by the different snow cover on the satellite images the inventories were based on. The image of the year 2013 shows as stronger snow cover and a lot of the debris at the higher glacier parts probably was covered with snow. This was a cause of the different recording dates of the two satellite scenes (August and October). In the Figure 5.13 is seen, that the changes in debris-cover took place on the one hand at the glacier tongue, which is assumed as real glacier retreat. And the other hotspot of decrease was found at the transition to clean ice. In October, the glaciers might have been snow covered again at these elevations and these parts therefore were mapped as clean ice. This fact underlines the importance of a satellite image with preferably no seasonal snow coverage. Another fact which could have influenced the different debris-cover in the inventories of the year 2002 and 2013 was the chosen threshold of the ratio images. This threshold was chosen individually for the different satellite scenes and influenced the glacier part mapped as clean ice and depending on this the manually added debris-covered parts (section 4.2.1).

As already mentioned before, the debris-cover of a glacier influences as well the melting regime. Depending on the debris thickness, it reduces or enhances the ablation process. A very thin debris-cover enhances the ablation rate, due to the low albedo of the debris and the resulting increased absorption of shortwave radiation, which is energy for the melting process (Kirkbride, 2011; Tangborn and Rana, 2000). More than 2cm debris on the ice normally acts as thermal barrier and has an insulating effect which reduces the melting (Adhikary et al., 2000; Benn and Evans, 2010). Therefore, a thick debris-cover can lead to a delayed reaction of the glaciers to climate fluctuations (Bolch, 2011) and has to be taken into

account by interpreting glacier receding. In this study, no investigations concerning the debris thickness were done, and no statements to the above mentioned effects can be made.

The fact that small glaciers are distributed over a large range of slopes is presented in Figure 5.8a. In return, the large glaciers are found especially between slope inclinations of 15-25°. The figures look similar for both years, with the exception of some outliers in the year 2002. Paul and Svoboda (2009) describe the same relationship. The large scatter towards the small glaciers, having low mean slopes as well, can be explained with the location of these glaciers in e.g. topographic depressions (Svoboda and Paul, 2009). A similar pattern of a slope-dependence is seen in the Figure 5.11d, which shows the relationship between the mean thickness and the slope (section 6.4).

The mean elevation is a good approximation to make statements concerning the climatic conditions (e.g. Bolch et al., 2012; Braithwaite and Raper, 2010; Le Bris et al., 2011). The ELA, where the accumulation and the ablation of the glaciers are in balance, was approximated by the mean elevation in this study (Figure 5.15) (Bakke and Nesje, 2011). The increase of the mean elevation (Figure 5.8b) therefore can be interpreted as increase of the ELA and this implies a negative mass balance of the glaciers (Benn and Evans, 2010). The mean elevation of the entire sample in the Kullu District rose from the year 2002 to the year 2013 by 16 meters (section 5.2).The mass balance of the glaciers in the Kullu District was not investigated and the connection of this mean elevation rise with the mass balance is a presumption only. In further research, with the aid of climate data as temperature and precipitation, such an investigation of the mass balance of the glaciers in the Kullu District could be done.

6.4   Uncertainties related to the ice thickness modeling

The uncertainties related to the GlabTop method were already mentioned in the section 4.3.1 and the alternative methods to estimate the glacier volume out of the DEM-subtraction was shortly described in the section 5.3 and discussed here in detail. The glacier volume of the

year 2002 was calculated based on the GlabTop modeling using the SRTM DEM US (27.82 km³).

The method to derive the volume change, based on the subtraction of the co-registered ASTER GDEM2 from the SRTM DEM US was not ideal because of the mentioned DEM differences. Firstly, the exact recording date of the ASTER GDEM2 is not defined and therefore the time span between the two DEMs is unknown (Frey and Paul, 2012). Secondly, the differences between the SRTM DEM US and the ASTER GDEM2 were not completely removed by the co-registration and there remained differences which are not fully negligible. As the co-registration was only applied on stable terrain, the changes over the glacier surfaces were thought to demonstrate the volume change. As already mentioned the SRTM DEM US and the ASTER GDEM2 were not at all congruent – neither after the co-registration; they differed not only over glaciated terrain, but also over the landscape, that was assumed to be stable terrain. The temporal difference to the SRTM DEM US should be eleven years (2002-2013). But due to the unclear acquisition date of the DEM and the outlines of the year 2013, the volume change generated with the co-registered ASTER GDEM2 refers to a point between 2005 and 2013. Further corrections and adaptions of the DEM differences were not possible, hence the change was perceived with caution as a volume loss. The subtraction resulted in the surface elevation difference over the glaciers between the two DEMs (converted into a volume loss of -3.73 km³).

The second approach to derive the volume change based on the GlabTop model with the co-registered ASTER GDEM2, suffered as well from various inaccuracies due to the DEM differences as mentioned before (e.g. shift, unclear recording date, and different acquisition techniques) and resulted in a volume loss of –2.62 km³. Additional to the differences in the input DEMs, the GlabTop approach is accompanied with uncertainties as well (Paul and Linsbauer, 2012). These uncertainties can be neglected in the relative comparison of the volume change generated out of the GlabTop outputs (also the one for 2002) because both calculations (SRTM DEM US and co-registered ASTER GDEM2) are influenced equally. The

ice thickness distribution was not determined for the inventory of the year 2013 due to the known issues.

It was difficult to decide, which of the two methods, that work with the co-registered ASTER GDEM2 and the SRTM DEM US, were more reliable to estimate the volume change. Nevertheless it can be said, that the DEM subtraction has to be described as more reliable, because it is not affected of the errors out of the GlabTop calculation. The results of the two methods differ by only 1.11 km^3. Both results were taken as information about the approximation of the volume change and not as absolute volume change. This was also the reason why it was decided to not insert any information in the column "mean_thickness" in the attribute table of the inventory of 2013.

The correlation between the ice thickness and the glacier area found in this study (Figure 5.11a) was also mentioned by Frey et al. (2013), even if they found a rather weak correlation. For example Bahr et al. (1997), Chen and Ohmura (1990) and Cogley (2012) dealt as well with the proportionality between the ice thickness and the glacier area, respectively the resulting proportionality between the volume (volume as product of mean thickness and area) and the area. This relationship is the basis of the "volume-area scaling" method, it is shortly addressed to it in section 4.3 as an alternative method to derive the glacier volume/thickness (e.g. Bahr et al., 1997; Chen and Ohmura, 1990; Haeberli and Hoelzle, 1995). This is a common method in ice thickness and ice volume estimations of glaciers (e.g. Bolch et al., 2012; Frey et al., 2013; Paul and Linsbauer, 2012; Paul and Svoboda, 2009). The GlabTop approach, used in this study, has integrated this relation in his algorithm as well to estimate the mean ice thickness (Linsbauer et al., 2012).

The investigation of the ice thickness per glacier relative to their mean slope in Figure 5.11d reflect the statement found in Cuffey and Paterson (2010). Although, a higher correlation between glacier thickness and slope could be expected, since the mean thickness is calculated with GlabTop and this model is basically based on the parameters slope (α) and shear stress (τ), while the other parameters are fix (see formula 1 in section 4.3.1). Nevertheless, there is a dependency between the thickness and the inclination of a glacier. Mostly, thick

glaciers/glacier parts are situated at flat areas, while thin glaciers/glacier parts are found at steep positions in the terrain.

6.5   Comparison to other studies

Particular attention was given to the glacial situation in the HK region due to the controversial statement by Cruz et al. (2007) in the 4th IPCC report, that the glaciers of the Himalayas will have been decreased to one-fifth of its today's volume by the year 2035. This statement was incorrect and leaded to fierce discussions and provoked many further studies covering the HK (Cogley et al., 2010).

The results of these many studies that dealt with the glacier mass changes and their contribution to sea level rise of the Himalayan glaciers stated an overall mass loss (Bolch et al., 2012; Gardelle et al., 2012; Gardner et al., 2013; Kääb et al., 2012). The study of Jacob et al. (2012) stands in contrast to the aforementioned studies, because he found no net mass change of the glaciers in the greater Himalayas, when compared with other regions of the world.

The publication of Kääb et al. (2012) reported from an overall mass loss in the Hindu-Kush-Karakoram Himalayas of -210±50 kg/m²/y between 2003 and 2008. The studies were based on repeated measurements of the glacier surface elevation with Ice, Cloud and Land Elevation Satellite (ICESat) (Kääb et al., 2012).

The field-based estimates of Bolch et al. (2012) were more negative than the estimations of Kääb et al. (2012). In the study of Bolch et al. (2012) a quarter of the glaciers in the Hindu-Kush and the western Karakoram showed a stable or advancing behavior between 1971 and 2007, while in the northern Karakoram the glaciers retreated in the same period. Gardner et al. (2013) found the glaciers in the HK to be near a balanced state and they refer to Gardelle et al. (2012) that found the glaciers decreased in HK by –0.12 to –0.16m year^{-1}.

As introduced, Jacob et al. (2012) found almost no net mass change in the greater Himalayas, in HK they recorded a shrinkage rate of -5 ± 6 Gty^{-1} from 2003 to 2010. They worked with Gravity Recovery and Climate Experiment (GRACE) satellite measurements.

Because all these studies were conducted independently and with different methods, and because the investigated regions were chosen differently, a direct comparison without further evaluations and conversions is not readily possible. And for a comparison with my results of retreat a conversion to the same area would be required.

7. Conclusions and perspectives

7.1   Major findings and conclusions

To sum up the findings of this study the research questions were listed once again and are shortly answered in the following.

RQ 1: Is it possible to compile an improved void-filled SRTM DEM version for the region of the Kullu District?

This second research question can be answered with a restrained yes. It was possible to compile a void-filled SRTM DEM for the Kullu region. It was not too difficult to achieve an improvement on the SRTM DEM version of the CGIAR, because of their crater-like depressions in the interpolated voids. The filling of the voids of the SRTM DEM version of the USGS in contrary seemed much more accurate. The disadvantage of the available void-filled versions was the poor and opaque documentation of the applied algorithms and interpolation methods used to fill the voids. The really simple method, maybe oversimplified, which was used in this study, delivered nevertheless results which could keep up with the available versions. As mentioned in section 6.1 the void-filling in this study was done with resampled ASTER GDEM2 data.

A co-registration before the void-filling process would have resulted quite likely in better results. This is because the co-registration was done much later in the context of the volume change estimation; it was decided to do the void-filling process and all the following processing steps not once again from the beginning with the adapted ASTER GDEM2.

The comparison of the GlabTop output carried out with the three SRTM versions (CGIAR, USGS and US) with the GPR profiles from the Chhota Shigri showed the best fit to the profile curve with the void-filled version compiled in this study (SRTM DEM US). Therefore

the topographic parameters of the compiled inventories of the years 2002 and 2013 were based on the SRTM DEM US.

RQ 2: Compilation of glacier inventories for 2002 and 2013: What must be considered compiling glacier inventories of two different years, when we like to do a change assessment with them?

As already discussed in the section 6.2, during the compilation of the glacier inventories some criteria must be considered in order to reduce the following workload and to ensure a meaningful change assessment. To answer this first research question, the important points are summed up and listed below. It has to be mentioned, that this list is only designed for the glacier mapping method with band ratios. Of course, there would be also other algorithms to map glaciers (semi-)automatically, but the subsequent points focus on the band ratio approach.

Careful selection of the satellite scene; recorded at the end of the ablation season.

Avoid scenes with seasonal snow outside the glaciers.

Select scenes with low cloud cover over the glaciated areas.

Invest enough time in the iterative selection of the image threshold for the band ratios; this reduces the workload needed for post-processing (manual editing).

The threshold should be selected based on the shadowed regions, which are most sensitive for the threshold value.

If a former glacier inventory exists, the drainage divides should be placed at the same locations to ensure a realistic change assessment.

To minimize inconsistency, the inventories should be compiled by the same surveyor. This guarantees the same interpretation of the different settings.

The glacier numbering in the two inventories should be the same (IID); this enables a comparison without any problems.

These conditions are never all fulfilled, and sometimes it is necessary to compromise. The above listed points may appear impossible to fulfill completely, and were not entirely fulfilled in this study either.

RQ 3: How did the glaciers in the Kullu District change in the examined time span (2002-2013) concerning their area and also their debris-cover extent?

The total glacier area in the region of the Kullu District decreased in the examined eleven year time span by 8.22 km^2 (590.04-581.78 km^2) (section 5.2.1 and 5.4), respectively 0.13%y^{-1} and was consistent with findings in other studies in the Himalayas.

The debris-cover was considerably different in the two inspected years. The total debris-cover decreased from 12.43% in 2002 to only 2.3% in 2013. Because the change of the total area was not as large, this negative development can be attributed to the suboptimal seasonal snow cover on the satellite scene of the year 2013. The snow covered large parts of the debris-cover. This fact shows clearly a negative consequence of seasonal snow cover on the satellite scenes as well as the influence of the manual mapping.

RQ 4: What were the volume and the ice thickness distribution changes of the glaciers in the Kullu District between the years 2002 and 2013?

At the beginning the study, among others, was supposed to estimate the volume and the glacier ice thickness distribution for the two compiled glacier inventories with the GlabTop model. This was planned to be able to make statements concerning changes in volume and ice thickness. The glacier volume of all glaciers in the Kullu District for the year 2002, based on the GlabTop model run with SRTM DEM US, resulted in 27.82 km^3. The ice thickness distribution for 2002 is readable out of the raster file. The ice volume for the year 2013 was not possible to determine, because of the lack of a DEM from this state at that time. As an approximation two approaches were tried; these were based on the co-registered ASTER

GDEM2. One has to keep in mind that the volume changes estimated with these methods refer to a point between 2005 and 2013 (sections 3.2.1 and 5.3), because of the unclear acquisition date of the ASTER GDEM2 scenes.

One attempt has been made to calculate the volume change out of the subtraction of the co-registered ASTER GDEM2 from the SRTM DEM US. The second attempt tried to provide the volume change out of the GlabTop modeling with the co-registered ASTER GDEM2.

The volume change gained out of the subtraction of the SRTM DEM US and the co-registered ASTER GDEM2 resulted in –3.73 km³. The volume change calculated based on the GlabTop modeling using the co-registered ASTER GDEM2 resulted in –2.62 km³. But consequently the ice thickness distribution of the glaciers in the Kullu District in the year 2013 was not determined due to the large inaccuracies that would result out of the GlabTop run with one of the available DEMs. The ice thickness distribution was just estimated for the inventory of 2002.

Because the accompanying errors and the uncertainties of both methods were relatively large and no data was available to validate the results, the delivered estimates were not interpreted as absolute change but at least served for having an idea of the scale of the volume loss.

To conclude: The aim of this research question was not completely achieved as initially planned, because the volume and the ice thickness was not determined for the state of the year 2013, due to the aforementioned difficulties and inaccuracies.

7.2   Outlook and further research

The two compiled glacier inventories for Kullu District recorded the state of the glaciers at the beginning of the 21ᵗʰ century. The trend of the glacier decrease shown will continue in future and there is no evidence that this trend would change in the next decades because of the persistent global warming (Bahadur, 2004). As the focus of this study was the compilation of the inventories; limited time was spent on the assessment of potential natural hazards in context of the glacier changes. Based on the GlabTop modeling of the year 2002 it would be

possible to locate overdeependings under the ice and predict future development of glacier lakes. Such glacier lakes hold a high hazard potential of glacier lake outburst floods (GLOFs) (Huggel et al., 2002) and these risks alter due to glacial changes (Bolch et al., 2012). Frey et al. (2010) presented an approach to detect future glacier lakes and Bajracharya et al. (2007) investigated the impact of the Climate Change on the glaciers and glacier lakes in Nepal and Bhutan with particular focus on GLOFs and other hazards with the aid of glacier inventories. Other natural hazards are e.g. debris flows (e.g. Clague et al., 2012; Stoffel and Huggel, 2012), ice avalanches (e.g. Salzmann et al., 2004), rock and snow avalanches etc. These hazards are often the cause or the consequence of a GLOF (Richardson and Reynolds, 2000). Such detailed studies of the various natural hazards could be done for the Kullu District building on the inventories compiled in this study.

Based on temperature data of meteorological stations in the Kullu District, glacier shrinkage could be modeled. To model the retreat of the glaciers it would be possible to work with a temperature-index model; a so called degree-day model (Hock, 2003; Pellicciotti et al., 2005). Temperature-index models are the most common approach for modeling the melt of snow and ice. The degree-day model is based on the relationship between the ablation and the air temperature – the so called degree-day factor (DDF) – expressed in the sum of positive temperatures (Braithwaite, 2008). This relationship between the ablation and the air temperature is reflected in the mass balance. The mass balance of some glaciers in the region of Himachal Pradesh were investigated by Azam et al. (2014), Azam et al. (2012), Berthier et al. (2007) and Wagnon et al. (2007) among others. These studies could be used as basis for such a DDF-approach to conduct glacier shrinkage of the Kullu District. Based on the knowledge of the future glacier retreat the water storage capacity of the glaciers could be evaluated and the impacts and the consequences for the population in the valleys could be predicted. The forecast of the glacier shrinkage could be used for predictions of the water sources in the Himalayas. Therefore, the availability of a current and local DEM would improve the accuracy of the actual volume and ice thickness distribution determinations.

The inventories compiled in this study could establish the basis for such further investigations and studies in the region of the Kullu District.

8. Bibliography

Abrams, M., Bailey, B., Tsu, H., Hato, M. (2010): The ASTER Global DEM. Photogrammetric Engineering and Remote Sensing 76, 344–348.

Adhikary, S., Nakawo, M., Katsumoto, S., Shakya, B. (2000): Dust influence on the melting process of glacier ice: experimental results from Lirung Glacier, Nepal Himalayas, in: Nakawo, M., Raymond, C.F., Fountain, A. (Eds.), Debris-Covered Glaciers. IAHS Publication 264, pp. 43–52.

Andreassen, L.M., Paul, F., Kääb, a., Hausberg, J.E. (2008): The new Landsat-derived glacier inventory for Jotunheimen, Norway, and deduced glacier changes since the 1930s. The Cryosphere Discussions 2, 299–339. doi:10.5194/tcd-2-299-2008.

Azam, M.F., Wagnon, P., Ramanathan, A., Vincent, C., Sharma, P., Arnaud, Y., Linda, A., Pottakkal, J.G., Chevallier, P., Singh, V.B., Berthier, E. (2012): From balance to imbalance: a shift in the dynamic behaviour of Chhota Shigri glacier, western Himalaya, India. Journal of Glaciology 58, 315–324. doi:10.3189/2012JoG11J123.

Azam, M.F., Wagnon, P., Vincent, C., Ramanathan, A., Linda, A., Singh, V.B. (2014): Reconstruction of the annual mass balance of Chhota Shigri glacier, Western Himalaya, India, since 1969. Annals of Glaciology 55, 69–80. doi:10.3189/2014AoG66A104.

Bahadur, J. (2004): Himalayan Snow and Glaciers. Associated Environmental Problems, Progress and Prospects, Concept Pu. ed. New Delhi, India.

Bahr, D., Meier, M., Peckham, S. (1997): The physical basis of volume-area scaling. Journal of Geophysical Research 102, 20355–20362.

Bajracharya, S.R., Mool, P.K., Shrestha, B.R. (2007): Impact of Climate Change on Himalayan Glaciers and Glacial Lakes. Case Studies on GLOF and Associated Hazards in Nepal and Bhutan.

Bakke, J., Nesje, A. (2011): Equilibrium-line altitude (ELA), in: Singh, V.P., Singh, P., Haritashya, U.K. (Eds.), Encyclopedia of Snow, Ice and Glaciers. Springer Publications, Utrecht, the Neterlands, pp. 268–277.

Baviskar, A. (2003): Conservation: The Practice of Ecodevelopment in the Great Himalayan National PArk, in: Saberwal, V., Rangarajan, M. (Eds.), Battles over Nature. Permanent Black, Delhi, pp. 267–299.

Benn, D.I., Evans, D.J.A. (2010): Galciers&Glaciation, 2nd ed. Hodder Education, London.

Berthier, E., Arnaud, Y., Kumar, R., Ahmad, S., Wagnon, P., Chevallier, P. (2007): Remote sensing estimates of glacier mass balances in the Himachal Pradesh (Western Himalaya, India). Remote Sensing of Environment 108, 327–338. doi:10.1016/j.rse.2006.11.017.

Bhambri, R., Bolch, T., Chaujar, R.K. (2011): Mapping of debris-covered glaciers in the Garhwal Himalayas using ASTER DEMs and thermal data. International Journal of Remote Sensing 32, 8095–8119. doi:10.1080/01431161.2010.532821.

Bolch, T. (2011): Debris, in: Singh, V.P., Singh, P., Haritashya, U.K. (Eds.), Encyclopedia of Snow, Ice and Glaciers. Springer Publications, Utrecht, the Neterlands, pp. 186–188.

Bolch, T., Kamp, U. (2006): Glacier Mapping in High Mountains Using DEMs , Landsat and ASTER Data. Grazer Schriften der Geographie und Raumforschung 41, 37–48.

Bolch, T., Kulkarni, A., Kääb, A., Huggel, C., Paul, F., Cogley, J.G., Frey, H., Kargel, J.S., Fujita, K., Scheel, M., Bajracharya, S., Stoffel, M. (2012): The state and fate of Himalayan glaciers. Science (New York, N.Y.) 336, 310–314. doi:10.1126/science.1215828.

Bolch, T., Menounos, B., Wheate, R. (2010): Landsat-based inventory of glaciers in western Canada, 1985–2005. Remote Sensing of Environment 114, 127–137. doi:10.1016/j.rse.2009.08.015.

Braithwaite, R.J. (2008): Temperature and precipitation climate at the equilibrium-line altitude of glaciers expressed by the degree-day factor for melting snow. Journal of Glaciology 54, 437–444. doi:10.3189/002214308785836968.

Braithwaite, R.J., Raper, S.C.B. (2010): Estimating equilibrium-line altitude (ELA) from glacier inventory data. Annals of Glaciology 50, 127–132. doi:http://dx.doi.org/10.3189/172756410790595930.

Burns, P., Nolin, A. (2014): Using atmospherically-corrected Landsat imagery to measure glacier area change in the Cordillera Blanca, Peru from 1987 to 2010. Remote Sensing of Environment 140, 165–178. doi:10.1016/j.rse.2013.08.026.

CGIAR-CSI (2008): SRTM 90m Digital Elevation Data. http://srtm.csi.cgiar.org/SELECTION/inputCoord.asp Access:06/02/2014.

Chen, J., Ohmura, A. (1990): Estimation of Alpine glacier water resources and their change since the 1870s., in: Lang, H., Musy, A. (Eds.), Hydrology in Mountain Regions. I-

Bibliography

Hydrological Measurements; the Water Cycle, Proceedings of Two Lausanne Symposia, August 1990. IAHS Publications, pp. 127–136.

Clague, J.J., Huggel, C., Korup, O., Mcguire, B. (2012): Climate Change and Hazardous Processes in High Mountains. Revista de la Asociación Geológica Argentina 69, 328–338.

Cogley, G. (2012): The future of the world's glaciers, in: Henderson-Sellers, A. and McGuffie, K. (Ed.), The Future of the Worlds Climate. Elsevier, pp. 197–222.

Cogley, J.G. (2011): Present and future states of Himalaya and Karakoram glaciers. Annals of Glaciology 52, 69–73. doi:10.3189/172756411799096277.

Cogley, J.G., Kargel, J.S., Kaser, G., van der Veen, C.J. (2010): Tracking the Source of Glacier Misinformation. Science 327, 522.

Cruz, R.V., Harasawa, H., Lal, M., Wu, S., Anokhin, Y., Punsalmaa, B., Honda, Y., Jafari, M., Li, C., Ninh, N.H. (2007): Asia, in: Parry, M.., Canziani, O.F., Palutikof, J.P., van der Linden, P.J., Hansen, C.E. (Eds.), Climate Change 2007: Impacts, Adaptation and Vulnerability. Contribution of Working Group II to the Fourth Assessment Report of the Intergovernmental Panel on Climate Change. Cambridge University Press, Cambrige etc., pp. 469–506.

Cuffey, K.M., Paterson, W.S.B. (2010): The Physics of Glaciers, 4th revise. ed. Academic Press.

Dutta, S., Ramanathan, A.L., Linda, A. (2012): Glacier fluctuation using Satellite Data in Beas basin , 1972 – 2006 , Himachal Pradesh , India. Journal of Earth System Science 121, 1105–1112.

Evans, I.S. (2006): Local aspect asymmetry of mountain glaciation: A global survey of consistency of favoured directions for glacier numbers and altitudes. Geomorphology 73, 166–184. doi:10.1016/j.geomorph.2005.07.009.

Farinotti, D., Huss, M., Bauder, A., Funk, M. (2009a): An estimate of the glacier ice volume in the Swiss Alps. Global and Planetary Change 68, 225–231. doi:10.1016/j.gloplacha.2009.05.004.

Farinotti, D., Huss, M., Bauder, A., Funk, M., Truffer, M. (2009b): A method to estimate the ice volume and ice-thickness distribution of alpine glaciers. Journal of Glaciology 55, 422–430. doi:10.3189/002214309788816759.

Farr, T.G., Rosen, P.A., Caro, E., Crippen, R., Duren, R., Hensley, S., Kobrick, M., Paller, M., Rodriguez, E., Roth, L., Seal, D., Shaffer, S., Shimada, J., Umland, J., Werner, M., Oskin, M., Burbank, D., Alsdorf, D. (2007): The shuttle radar topography mission. Reviews in Geophysics 45, 1–33. doi:10.1029/2005RG000183.1.

Frey, H. (2011): Compilation and Application of Glacier Inventories using Satellite Data and Digital Terrain Information. Schriftenreihe Physische Geographie Glaziologie und Geomorphodynamik.

Frey, H., Haeberli, W., Linsbauer, A., Huggel, C., Paul, F. (2010): A multi-level strategy for anticipating future glacier lake formation and associated hazard potentials. Natural Hazards and Earth System Science 10, 339–352.

Frey, H., Machguth, H., Huss, M., Huggel, C., Bajracharya, S., Bolch, T., Kulkarni, a., Linsbauer, a., Salzmann, N., Stoffel, M. (2013): Ice volume estimates for the Himalaya–Karakoram region: evaluating different methods. The Cryosphere Discussions 7, 4813–4854. doi:10.5194/tcd-7-4813-2013.

Frey, H., Paul, F. (2012): On the suitability of the SRTM DEM and ASTER GDEM for the compilation of topographic parameters in glacier inventories. International Journal of Applied Earth Observation and Geoinformation 18, 480–490. doi:10.1016/j.jag.2011.09.020.

Frey, H., Paul, F., Strozzi, T. (2012): Compilation of a glacier inventory for the western Himalayas from satellite data: methods, challenges, and results. Remote Sensing of Environment 124, 832–843. doi:10.1016/j.rse.2012.06.020.

Gardelle, J., Berthier, E., Arnaud, Y. (2012): Slight mass gain of Karakoram glaciers in the early twenty-first century. Nature Geoscience 5, 322–325. doi:10.1038/ngeo1450.

Gardner, A.S., Moholdt, G., Cogley, J.G., Wouters, B., Arendt, A. a, Wahr, J., Berthier, E., Hock, R., Pfeffer, W.T., Kaser, G., Ligtenberg, S.R.M., Bolch, T., Sharp, M.J., Hagen, J.O., van den Broeke, M.R., Paul, F. (2013): A reconciled estimate of glacier contributions to sea level rise: 2003 to 2009. Science (New York, N.Y.) 340, 852–7. doi:10.1126/science.1234532.

Gardner, J.S. (2002): Natural Hazards Risk in the Kullu District, Himachal Pradesh, India. Geographical Review 92, 282–306.

GHNP (2014): Great Himalayan National Park. http://www.greathimalayannationalpark.com/index.html Access:01/12/2013.

Bibliography

Global Administrative Areas. Boundaries without limits: http://gadm.org/country
    Access:09/16/2014.

Haeberli, W., Hoelzle, M. (1995): Application of inventory data for estimating characteristics
    of and regional climate-change effects on mountain glaciers: a pilot study with the
    European Alps. Annals of Glaciology1 21, 206–212.

Haeberli, W., Hohmann, R. (2008): Climate , glaciers and permafrost in the Swiss Alps 2050:
    scenarios , consequences and recommendations, in: Proceedings of the 9th International
    Conference on Permafrost. Fairbanks, Alaksa, USA, pp. 607–612.

Hall, D.K., Ormsby, J.P., Bindschadler, R.A., Siddalingaiah, H. (1987): Characterization of
    snow and ice reflectance zones on glaciers using Landsat Thematic Mapper data. Annals
    of 9, 104–108.

Hambrey, M.J., Quincey, D.J., Glasser, N.F., Reynolds, J.M., Richardson, S.J., Clemmens, S.
    (2008): Sedimentological, geomorphological and dynamic context of debris-mantled
    glaciers, Mount Everest (Sagarmatha) region, Nepal. Quaternary Science Reviews 27,
    2361–2389. doi:10.1016/j.quascirev.2008.08.010.

Hock, R. (2003): Temperature index melt modelling in mountain areas. Journal of Hydrology
    282, 104–115. doi:10.1016/S0022-1694(03)00257-9.

Huggel, C., Kääb, A., Haeberli, W., Teysseire, P., Paul, F. (2002): Remote sensing based
    assessment of hazards from glacier lake outbursts: a case study in the Swiss Alps.
    Canadian Geotechnical Journal 39, 316–330. doi:10.1139/t01-099.

Huss, M., Farinotti, D. (2012): Distributed ice thickness and volume of all glaciers around the
    globe. Journal of Geophysical Research 117, 1–10. doi:10.1029/2012JF002523.

IHCAP (2013): Indian Himalayas Climate Adaption Programme. http://ihcap.in/ Access:
    09/11/2013.

Immerzeel, W.W., van Beek, L.P.H., Bierkens, M.F.P. (2010): Climate change will affect the
    Asian water towers. Science (New York, N.Y.) 328, 1382–1385.
    doi:10.1126/science.1183188.

Jacob, T., Wahr, J., Pfeffer, W.T., Swenson, S. (2012): Recent contributions of glaciers and ice
    caps to sea level rise. Nature 482, 514–8. doi:10.1038/nature10847.

Kääb, A. (2005): Combination of SRTM3 and repeat ASTER data for deriving alpine glacier flow velocities in the Bhutan Himalaya. Remote Sensing of Environment 94, 463–474. doi:10.1016/j.rse.2004.11.003.

Kääb, A., Berthier, E., Nuth, C., Gardelle, J., Arnaud, Y. (2012): Contrasting patterns of early twenty-first-century glacier mass change in the Himalayas. Nature 488, 495–8. doi:10.1038/nature11324.

Kääb, A., Paul, F., Maisch, M., Hoelzle, M., Haeberli, W. (2002): The new remote-sensing-derived Swiss glacier inventory: II. First results. Annals of Glaciology 34, 362–366. doi:10.3189/172756402781817473.

Kienholz, C., Hock, R., Arendt, A. a. (2013): A new semi-automatic approach for dividing glacier complexes into individual glaciers. Journal of Glaciology 59, 925–937. doi:10.3189/2013JoG12J138.

Kirkbride, M.P. (2011): Debris-covered glaciers, in: Singh, V.P., Singh, P., Haritashya, U.K. (Eds.), 2Encyclopedia of Snow, Ice and Glaciers. Utrecht, the Neterlands, pp. 190–192.

Klimadaten Simla / Himachal Pradesh (n.d.):http://www.wetter.net/klimadaten/klima-simla--himachal-pradesh.html Access:05/22/2014.

Kulkarni, A. V, Rathore, B.P., Mahajan, S., Mathur, P. (2005): Alarming retreat of Parbati glacier, Beas basin, Himachal Pradesh. Current Science 88, 1844–1850.

Kulkarni, A. V., Rathore, B.P., Singh, S.K., Bahuguna, I.M. (2011): Understanding changes in the Himalayan cryosphere using remote sensing techniques. International Journal of Remote Sensing 32, 601–615. doi:10.1080/01431161.2010.517802.

Kuniyal, J.C., Vishvakarma, S.C.R., Badola, H.K., Jain, A.P. (2004): Tourism in Kullu Valley. An Environmental Assessment. G.B. Pant Institute of Himalayan Environment and Development.

Le Bris, R., Paul, F., Frey, H., Bolch, T. (2011): A new satellite-derived glacier inventory for western Alaska A new satellite-derived glacier inventory for western Alaska. Annals of Glaciology 52, 135–143.

Lillesand, T.M., Kiefer, R.W., Chipman, J.W. (2008): Remote Sensing and Image Interpretation, 6th ed. John Wiley & Sons, Inc.

Linsbauer, A. (2014): Personal Communication. Zürich.

Bibliography

Linsbauer, A., Paul, F., Haeberli, W. (2012): Modeling glacier thickness distribution and bed topography over entire mountain ranges with GlabTop: Application of a fast and robust approach. Journal of Geophysical Research 117, 1–17. doi:10.1029/2011JF002313.

Linsbauer, A., Paul, F., Hoelzle, M., Frey, H., Haeberli, W. (2009): The Swiss Alps Without Glaciers – A GIS-based Modelling Approach for Reconstruction of Glacier Beds. Proceedings of Geomorphometry 243–247.

LPDAAC (2014): Global Data Explorer. http://gdex.cr.usgs.gov/gdex/ Access:11/20/2013.

Maisch, M., Haeberli, W. (1982): Interpretation geometrischer Parameter von Spätglazial-Gletschern im Gebiet Mittelbünden, Schweizer Alpen. Physische Geographie 1, 111–126.

Maisch, M., Haeberli, W., Hoelzle, M., Wenzel, J. (1999): Occurrence of rocky and sedimentary glacier beds in the Swiss Alps as estimated from glacier-inventory data. Annals of Glaciology 28, 231–235. doi:http://dx.doi.org/10.3189/172756499781821779.

Manley, W.F. (1980): Geospatial inventroy and analysis of glaciers: a case study for the eastern Alaska Range, in: Williams, R.S., Ferrigno, J.G., Ferrigno, J. (Eds.), Satellite Image Atlas of Glaciers Wof the World. United States Geologicals Survey, Denver, pp. K424–439.

Marzeion, B., Cogley, J.G., Richter, K., Parkes, D. (2014): Attribution of global glacier mass loss to anthropogenic and natural causes. Science 345, 919–921. doi:10.1126/science.1254702.

Molden, D. (2012): New Studies Provide Insights on Glaciers in the Greater Himalayan Region. ICIMOD 30.http://www.icimod.org/?q=8249 Access:09/19/2014.

Moors, E.J., Groot, A., Biemans, H., van Scheltinga, C.T., Siderius, C., Stoffel, M., Huggel, C., Wiltshire, A., Mathison, C., Ridley, J., Jacob, D., Kumar, P., Bhadwal, S., Gosain, A., Collins, D.N. (2011): Adaptation to changing water resources in the Ganges basin, northern India. Environmental Science & Policy 14, 758–769. doi:10.1016/j.envsci.2011.03.005.

NSIDC (2014): GLIMS Glacier Database. http://nsidc.org/glims/ Access:11/03/2013.

Nuth, C., Kääb, a. (2011): Co-registration and bias corrections of satellite elevation data sets for quantifying glacier thickness change. The Cryosphere 5, 271–290. doi:10.5194/tc-5-271-2011.

Paul, F. (2006): The New Swiss Glacier Inventory 2000 Application of Remote Sensing and GIS. Schriftenreihe Physische Geographie 52, University of Zurich.

Paul, F., Andreassen, L.M. (2009): A new glacier inventory for the Svartisen region, Norway, from Landsat ETM+ data: challenges and change assessment. Journal of Glaciology 55, 607–618. doi:10.3189/002214309789471003.

Paul, F., Barrand, N.E., Baumann, S., Berthier, E., Bolch, T., Casey, K., Frey, H., Joshi, S.P., Konovalov, V., Bris, R. Le, Mölg, N., Nosenko, G., Nuth, C., Pope, a., Racoviteanu, a., Rastner, P., Raup, B., Scharrer, K., Steffen, S., Winsvold, S. (2013): On the accuracy of glacier outlines derived from remote-sensing data. Annals of Glaciology 54, 171–182. doi:10.3189/2013AoG63A296.

Paul, F., Barry, R., Cogley, G., Frey, H., Haeberli, W., Ohmura, A., Ommanney, S., Raup, B., Rivera, A., Zemp, M. (2009): Recommendations for the compilation of glacier inventory data from digital sources. Annals of Glaciology 51, 1–8.

Paul, F., Frey, H., Le Bris, R. (2011): A new glacier inventory for the European Alps from Landsat TM scenes of 2003: challenges and results A new glacier inventory for the European Alps from Landsat TM scenes of 2003: challenges and results. Annals of Glaciology 52, 144–152.

Paul, F., Huggel, C., Kääb, A. (2004): Combining satellite multispectral image data and a digital elevation model for mapping debris-covered glaciers. Remote Sensing of Environment 89, 510–518. doi:10.1016/j.rse.2003.11.007.

Paul, F., Kääb, A. (2005): Perspectives on the production of a glacier inventory from multispectral satellite data in Arctic Canada: Cumberland Peninsula, Baffin Island. Annals of Glaciology 42, 59–66.

Paul, F., Kääb, A., Haeberli, W. (2007): Recent glacier changes in the Alps observed by satellite: Consequences for future monitoring strategies. Global and Planetary Change 56, 111–122. doi:10.1016/j.gloplacha.2006.07.007.

Paul, F., Kääb, A., Kellenberger, T., Haeberli, W. (2002): The new remote-sensing-derived Swiss glacier inventory: I . Methods. Annals of Glaciology 34, 355–361.

Paul, F., Linsbauer, A. (2012): Modeling of glacier bed topography from glacier outlines, central branch lines, and a DEM. International Journal of Geographical Information Science 26, 1173–1190. doi:10.1080/13658816.2011.627859.

Bibliography

Paul, F., Svoboda, F. (2009): A new glacier inventory on southern Baffin Island , Canada , from ASTER data: II. Data analysis , glacier change and applications. Annals of Glaciology 50, 22–31.

Pellicciotti, F., Brock, B., Strasser, U., Burlando, P., Funk, M., Corripio, J. (2005): An enhanced temperature-index glacier melt model including the shortwave radiation balance : development and testing for Haut Glacier d ' Arolla, Switzerland. Journal of Glaciology 51, 573–587. doi:10.3189/172756505781829124.

Rabus, B., Eineder, M., Roth, A., Bamler, R. (2003): The shuttle radar topography mission—a new class of digital elevation models acquired by spaceborne radar. ISPRS Journal of Photogrammetry and Remote Sensing 57, 241–262. doi:10.1016/S0924-2716(02)00124-7.

Racoviteanu, A.E., Arnaud, Y., Williams, M.W., Ordon, J. (2008a): Decadal changes in glacier parameters in the Cordillera Blanca , Peru , derived from remote sensing. Journal of Glaciology 54, 499–510.

Racoviteanu, A.E., Paul, F., Raup, B., Jodha, S., Khalsa, S., Armstrong, R. (2009): Challenges and recommendations in mapping of glacier parameters from space: results of the 2008 Global Land Ice Measurements from Space (GLIMS) workshop, Boulder, Colorado, USA. Annals of Glaciology 50, 53–69.

Racoviteanu, A.E., Williams, M.W., Barry, R.G. (2008b): Optical Remote Sensing of Glacier Characteristics: A Review with Focus on the Himalaya. Sensors 8, 3355–3383. doi:10.3390/s8053355.

Raup, B., Kääb, A., Kargel, J.S., Bishop, M.P., Hamilton, G., Lee, E., Paul, F., Rau, F., Soltesz, D., Khalsa, S.J.S., Beedle, M., Helm, C. (2007): Remote sensing and GIS technology in the Global Land Ice Measurements from Space (GLIMS) Project. Computers & Geosciences 33, 104–125. doi:10.1016/j.cageo.2006.05.015.

Reuter, H.I., Nelson, a., Jarvis, a. (2007): An evaluation of void-filling interpolation methods for SRTM data. International Journal of Geographical Information Science 21, 983–1008. doi:10.1080/13658810601169899.

Rexer, M., Hirt, C. (2014): Comparison of free high resolution digital elevation data sets (ASTER GDEM2, SRTM v2.1/v4.1) and validation against accurate heights from the Australian National Gravity Database. Australian Journal of Earth Sciences 61, 213–226. doi:10.1080/08120099.2014.884983.

Richards, J.A. (2013): Remote Sensing Digital Image Analysis. An Introduction., 5th ed. Springer. doi:10.1007/978-3-642-30062-2.

Richardson, S.D., Reynolds, J.M. (2000): An overview of glacial hazards in the Himalayas. Quaternary Invernational 65, 31–47.

Rosenfeld, C.L. (1984): Remote Sensing Techniques for Geomorphologists, in: Costa, J.E., Fleisher, R.J. (Eds.), Developments and Applications of Geomorphology. Springer, Berlin, p. 372. doi:10.1007/978-3-642-69759-3_1.

Salzmann, N., Kääb, A., Huggel, C., Allgöwer, B., Haeberli, W. (2004): Assessment of the hazard potential of ice avalanches using remote sensing and GIS-modelling. Norsk Geografisk Tidsskrift - Norwegian Journal of Geography 58, 74–84. doi:10.1080/00291950410006805.

Scherler, D., Bookhagen, B., Strecker, M.R. (2011): Spatially variable response of Himalayan glaciers to climate change affected by debris cover. Nature Geoscience 4, 156–159. doi:10.1038/ngeo1068.

Schiefer, E., Menounos, B., Wheate, R. (2008): An inventory and morphometric analysis of British Columbia glaciers, Canada. Journal of Glaciology 54, 551–560. doi:10.3189/002214308785836995.

Shroder, J.F., Bishop, M.P., Copland, L., Sloan, V.F. (2000): Debris-covered glaciers and rock glaciers in the Nanga Parbat Himalaya, Pakistan. Geografiska Annaler 17–31.

Soot (2013): Climate Change in the Kullu Valley. A Scoping Study. Indian Himalayan Climate Adaption Programme IHCAP.

Stoffel, M., Huggel, C. (2012): Effects of climate change on mass movements in mountain environments. Progress in Physical Geography 36, 421–439. doi:10.1177/0309133312441010.

Svoboda, F., Paul, F. (2009): A new glacier inventory on southern Baffin Island , Canada , from ASTER data: I. Applied methods , challenges and solutions. Annals of Glaciology 50, 11–21.

Tachikawa, T., Kaku, M., Iwasaki, A., Gesch, D., Oimoen, M., Zhang, Z., Danielson, J., Krieger, T., Curtis, B., Haase, J., Abrams, M., Crippen, R., Carabajal, C. (2011): ASTER Global Digital Elevation Model Version 2 - Summary of Validation Results .http://www.jspacesystems.or.jp/ersdac/GDEM/ver2Validation/Summary_GDEM2_valid ation_report_final.pdf Access:05/30/2014.

Bibliography

Tangborn, W., Rana, B. (2000): Mass balance and runoff of the partially debris-covered Langtang Glacier, Nepal, in: Nakawa, M., Raymond, C., Fountain, A. (Eds.), Debris-Covered Glaciers. IAHS Publication 264, pp. 99–108.

Toutin, T. (2008): ASTER DEMs for geomatic and geoscientific applications: a review. International Journal of Remote Sensing 29, 1855–1875. doi:10.1080/01431160701408477.

Urai, M., Tachikawa, T., Fujisada, H. (2012): Data acquisition strategies for aster global dem generation, in: ISPRS Annals of the Photogrammetry, Remote Sensing and Spatial Information Sciences. Melbourne, Australia, pp. 199–202.

USGS (2014a): Band Designations Landsat Satellites. http://landsat.usgs.gov/band_designations_landsat_satellites.php Access:07/10/2014.

USGS (2014b): Earth Explorer. http://earthexplorer.usgs.gov/ Access:05/14/2014.

Wagnon, P., Linda, A., Arnaud, Y., Kumar, R., Sharma, P., Vincent, C., Pottakkal, J.G., Berthier, E., Ramanathan, A., Hasnain, S.I., Chevallier, P. (2007): Four years of mass balance on Chhota Shigri Glacier, Himachal Pradesh, India, a new benchmark glacier in the western Himalaya. Journal of Glaciology 53, 603–611. doi:10.3189/002214307784409306.

Watson, R.T., Haeberli, W. (2004): Environmental threats, mitigation strategies and high-mountain areas. Ambio Spec No 13, 2–10.

9. Appendix
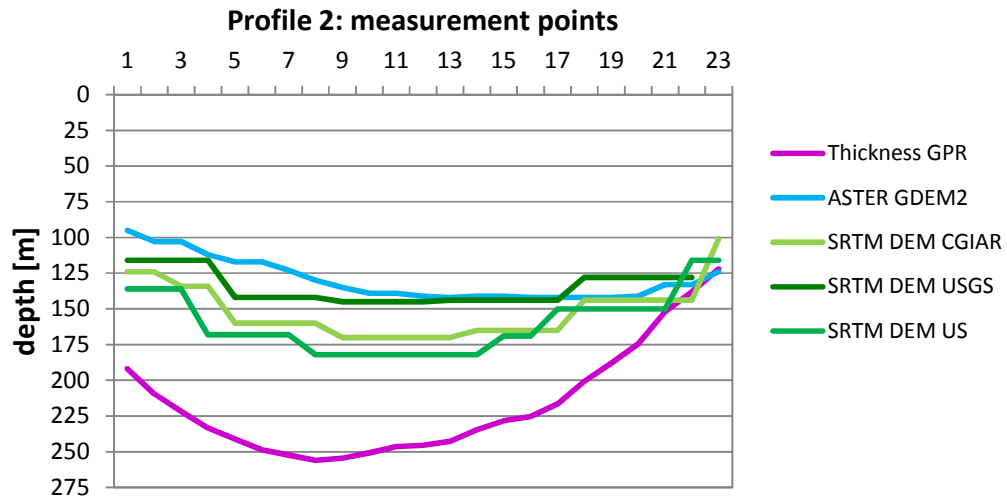
Figure 9.1: Ice thickness outputs from GlabTop modeling with different DEMs compared with the ground truth of the GPR profile 2 at Chhota Shigri.
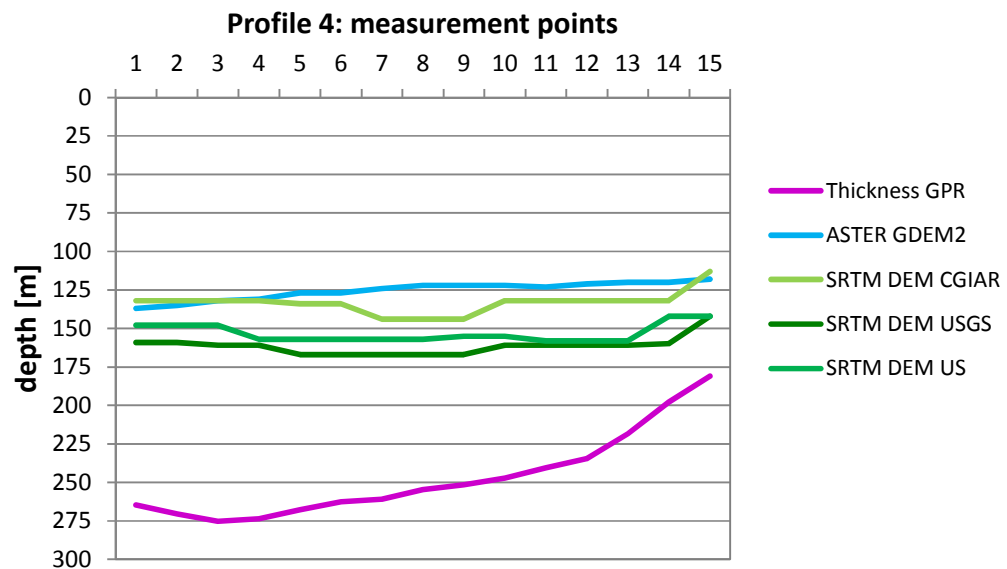
Figure 9.2: Ice thickness outputs from GlabTop modeling with different DEMs compared with the ground truth of the GPR profile 4 at Chhota Shigri.

Profile 5: measurement points
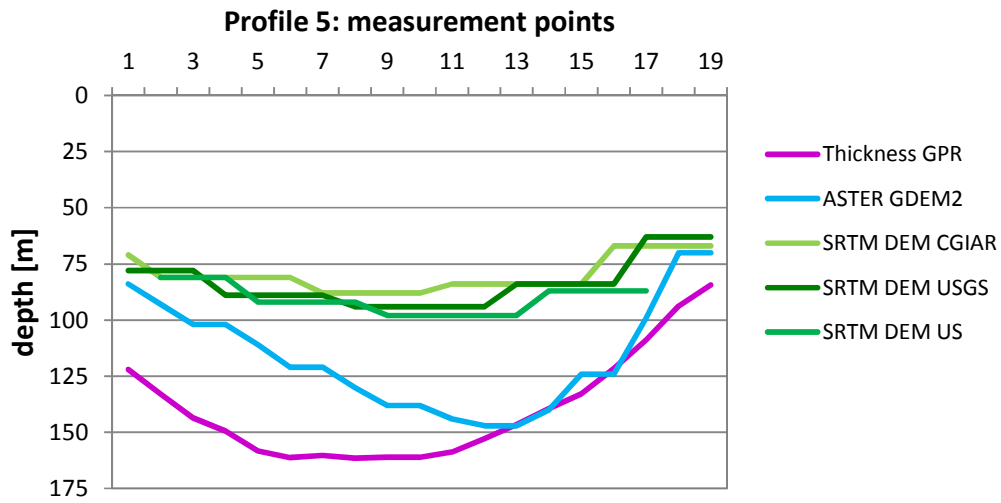
Figure 9.3: Ice thickness outputs from GlabTop modeling with different DEMs compared with the ground truth of the GPR profile 5 at Chhota Shigri.

Table 9.1: Area and count of glaciers per size class in 2002 and 2013.

Size class	2002 Number		2013 Number		2002 Area		2013 Area	
	N	%	N	%	km²	%	km²	%
< 0.05	203.00	29.12	144.00	22.97	6.53	1.11	4.64	0.80
0.05-0.1	113.00	16.21	109.00	17.38	7.84	1.33	9.65	1.66
0.1-0.5	194.00	27.83	208.00	33.17	48.26	8.18	60.41	10.38
0.5-1	67.00	9.61	68.00	10.85	45.31	7.68	49.37	8.49
1-5	99.00	14.20	77.00	12.28	195.50	33.13	171.88	29.54
5-10	10.00	1.43	9.00	1.44	74.31	12.59	61.11	10.50
> 10	11.00	1.58	12.00	1.91	212.29	35.98	224.71	38.62
Total	697.00	100.00	627.00	100.00	590.04	100.00	581.78	100.00

Table 9.2: Area and count of glaciers per aspect sector in 2002 and 2013.

Aspect sector	2002 Number		2013 Number		2002 Area		2013 Area	
	N	%	N	%	km²	%	km²	%
N	95.00	13.63	96.00	15.31	86.77	14.71	106.05	18.23
NE	99.00	14.20	82.00	13.08	115.59	19.59	98.91	17.00
E	92.00	13.20	83.00	13.24	67.03	11.36	39.78	6.84
SE	75.00	10.76	69.00	11.00	111.20	18.85	59.83	10.28
S	86.00	12.34	64.00	10.21	53.59	9.08	32.58	5.60
SW	76.00	10.90	58.00	9.25	55.79	9.46	45.98	7.90
W	86.00	12.34	81.00	12.92	54.34	9.21	140.69	24.18
NW	88.00	12.63	94.00	14.99	45.73	7.75	57.94	9.96
Total	697.00	100.00	627.00	100.00	590.04	100.00	581.75	100.00
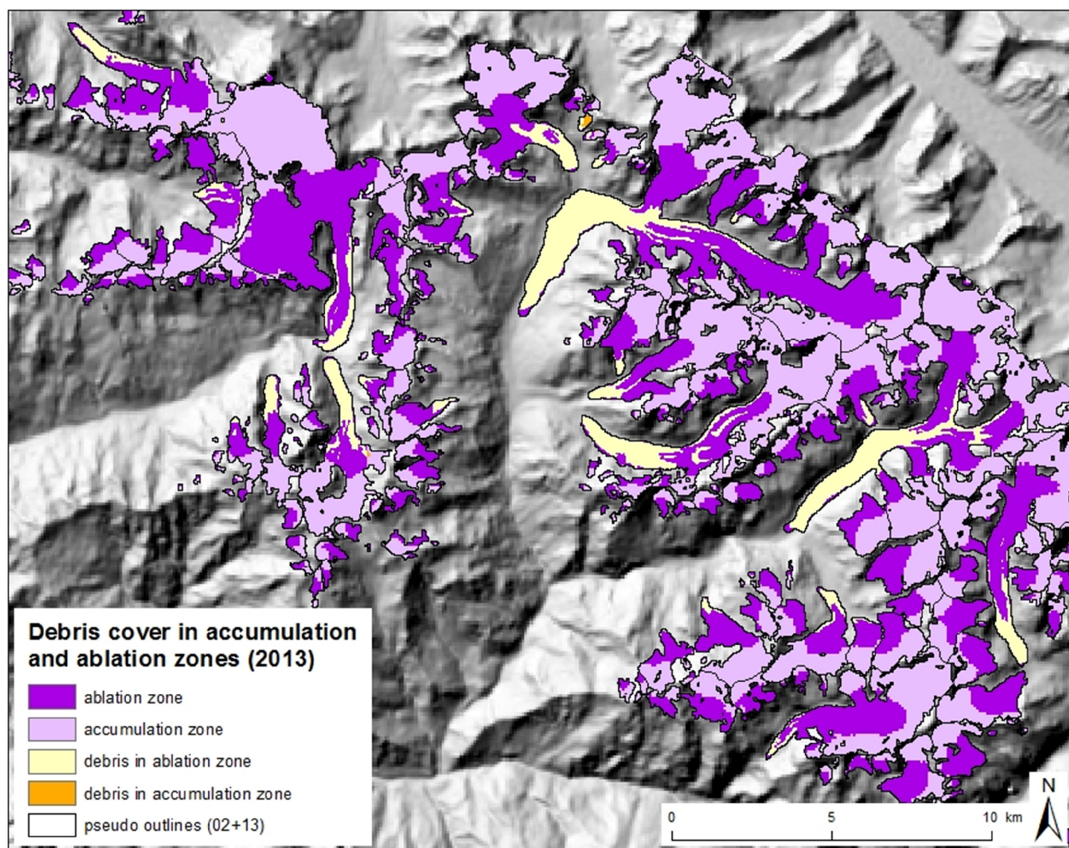
Figure 9.4: Debris-cover in relation to the accumulation and ablation zones of the glaciers (2013)

10.   Personal Declaration

«I hereby declare that the submitted thesis is the result of my own, independent, work. All external sources are explicitly acknowledged in the thesis.»

City, Date: Signature:

                                               Ursina Stoll